The IAGOS-Core Greenhouse Gas package: a CO_2, CH_4, CO and H_2O measurement system for deployment on board commercial airliners

Dissertation

zur Erlangung des akademischen Grades doctor rerum naturalium

(Dr. rer. nat)

vorgelegt dem Rat der Chemisch-Geowissenschaftlichen Fakultät der

Friedrich-Schiller-Universität Jena

von Dipl.-Phys. Annette Filges

geboren am 16. August 1984 in Jena

Gutachter:

1. Prof. Dr. Wolfgang Weigand, Friedrich-Schiller-Universität Jena

2. Dr. habil. Christoph Gerbig, Max-Planck-Institut für Biogeochemie, Jena

Tag der Verteidigung: 28.10.2020

Contents

Abstract

Reliable measurement systems are the basis for investigating the temporal and spatial atmospheric distribution of the most significant greenhouse gases and for understanding their budgets, trends and connection to global climate change. Within the framework of the IAGOS project (In-service Aircraft for a Global Observing System) an analyser for the autonomous measurement of the greenhouse gases (GHGs) CO_2 and CH_4, as well as CO and water vapour was designed, tested and qualified for deployment aboard passenger aircrafts. It is based on a commercial cavity ring-down spectroscopy (CRDS) instrument which has been modified to meet the specific requirements regarding physical dimensions, automatic and long-term operation and safety issues on board commercial airliners.

The analyser components are mounted into a frame suitable for integration in the avionics bay of the Airbus A330 and A340 series. An inlet system was designed to eliminate sampling of larger aerosols, ice particles and water droplets, and to provide additional positive ram pressure to ensure operation throughout an aircraft altitude operating range up to 12.5 km without an upstream sampling pump. A two-standard calibration system, that allows for in-flight and on ground calibrations during each 6-month deployment period, ensures the traceability of the CO_2, CH_4 and CO measurements to the World Meteorological Organization primary scales. No sample drying is required as the simultaneously measured water vapour mole fraction is used to correct for dilution and spectroscopic effects of water vapor on CO_2, CH_4 and CO. This simplifies maintenance considerably and enables measurements of water vapour throughout the atmosphere.

Various laboratory tests of the prototype instrument regarding stability, sensitivity to pressure changes, the calibration system and airworthiness were successfully conducted and confirmed the great potential of the device. During test flights of the measurement system on a research aircraft the analyser demonstrated very good performance, long-term stability and measurement quality. Analysis of the sample cell pressure stability at altitudes up to 14 km and during ascents and descents showed that sample cell pressure issues are not expected to have a great impact on the measurements within IAGOS. An estimate of the overall uncertainty of the measurements, mainly based on laboratory tests and accounting for uncertainties of the calibration and wet to dry correction and the 0.4 Hz measurement repeatability, resulted in <0.13 ppm for CO_2, <1.3 ppb for CH_4 and <4 ppb for CO. A less conservative assumption of instrument drift, as suggested by the flight test, reduces the overall uncertainties to <0.10 ppm for CO_2, <1.3 ppb for CH_4 and <3.4 ppb for CO.

The participation of the analyser in an inter-comparison flight campaign for airborne hygrometers allowed for an initial validation of the water vapour measurements against reference instruments with a long performance record, since the quantitative capabilities of the CRDS water vapor measurements have never been evaluated and reviewed in detail before. In addition to the standard calibration method, which is the comparison against a dew point mirror or a frost point hygrometer, a newly developed, independent calibration based on the measurement of the dilution effect of water vapour on the CO_2 mole fraction was tested. It could be shown that the

new method is statistically consistent with the standard calibrations, which allows the method to be considered as a possible calibration not only for H_2O but also for other gas species. Comparison of the in-flight data against the reference instruments proved that the analyser is reliable and has a good time response and long-term stability. An upper limit of the measurement precision was determined as 4 ppm for H_2O <10 ppm, 20 % or 10 ppm (whichever is smaller) for 10 ppm < H_2O < 100 ppm, and 5 % or 30 ppm (whichever is smaller) for water vapour >100 ppm. Accuracy of the CRDS instrument was estimated, based on laboratory calibrations, as 1 % for the water vapor range from 25000 ppm down to 7000 ppm, increasing to 5 % at 50 ppm water vapor. Accuracy at water vapor mole fractions below 50 ppm was difficult to assess, as the reference systems suffered from lack of data availability.

The first of the IAGOS-core GHG packages was successfully deployed aboard a passenger aircraft as part of the IAGOS project in 2017. The aim is to have five systems operational within the next few years, providing regular, long-term observations of the most important GHGs covering major parts of the globe, which can be utilized for the validation of remote sensing based observations, inverse modelling of GHG fluxes, process studies and the improvement of regional and global climate models.

Zusammenfassung

Zuverlässige Messsysteme sind die Grundlage für die Untersuchung der zeitlichen und räumlichen Verteilung wichtiger Treibhausgase in der Atmosphäre und für das Verständnis ihrer Budgets, Trends und ihrer Bedeutung für den globalen Klimawandel. Im Rahmen des IAGOS-Projekts (In-service Aircraft for a Global Observing System) wurde ein Gerät zur Messung der Treibhausgase CO_2 und CH_4, sowie CO und Wasserdampf entwickelt, getestet und für den Einsatz an Bord von Passagierflugzeugen vorbereitet. Es basiert auf einem kommerziellen Cavity Ring-Down Spektroskopie Instrument (CRDS), welches so modifiziert wurde, dass es die besonderen Anforderungen hinsichtlich der Größe, des Gewichts, des automatischen und langfristigen Betriebs und der Sicherheit an Bord von Verkehrsflugzeugen erfüllt.

Die einzelnen Gerätekomponenten wurden in ein spezielles Gehäuse integriert, das in der Avionics Bay der Airbus A330- und A340-Serie eingebaut werden kann. Es wurde ein System zur Zuführung der Außenluft entworfen, dass das Eindringen größerer Aerosole, Eispartikel und Wassertröpfchen in die Ansaugleitung verhindert. Außerdem erzeugt es genügend zusätzlichen Staudruck, um auch bei Flughöhen von bis zu 12,5 km auf eine vorgeschaltete Pumpe verzichten und trotzdem einen ausreichend hohen Durchfluss gewährleisten zu können. Durch ein Kalibriersystem mit zwei Referenzgasstandards, das während jedes sechsmonatigen Einsatzes des Messgeräts im Flugzeug regelmäßige Kalibrierungen während der Flüge und am Boden ermöglicht, wird die Rückführbarkeit der CO_2-, CH_4- und CO-Messungen auf die Primärskalen der World Meteorological Organization gesichert. Da die Messung des Wasserdampfs genutzt werden kann, um den Verdünnungseffekt und die spektroskopischen Einflüsse des Wassers auf die CO_2-, CH_4- und CO-Messungen zu korrigieren, ist keine Trocknung der Probenluft nötig, was die Gerätewartung erheblich vereinfacht und auch Wasserdampfmessung in der gesamten Atmosphäre ermöglicht.

Verschiedene Labortests eines Prototyps des Geräts zur Stabilität, Empfindlichkeit gegenüber Druckänderungen, sowie des Kalibriersystems und der Flugtauglichkeit konnten erfolgreich durchgeführt werden und bestätigten das große Potential des Messsystems. Bei Testflügen auf einem Forschungsflugzeug bestätigte sich die sehr gute Funktionalität, Langzeitstabilität und Messqualität des Geräts. Die Analyse der Stabilität des Drucks in der Probenzelle in Flughöhen bis zu 14 km und während der Steig- und Sinkflüge zeigte, dass aufgrund der innerhalb von IAGOS-Einsätzen auftretenden Luftdruckänderungen der Atmosphäre keine großen Beeinträchtigungen der Messungen zu erwarten sind. Eine Schätzung der Gesamtunsicherheit der Messdaten, die hauptsächlich auf Labortests basiert und die Unsicherheiten der Kalibrierung und der Wasserkorrektur, sowie die 0,4 Hz-Messwiederholbarkeit berücksichtigt, ergab für CO_2 <0,13 ppm, für CH_4 <1,3 ppb und <4 ppb für CO. Durch eine weniger konservative Abschätzung der Drift des Messgeräts, wie es die Ergebnisse der Testflüge nahelegen, können die Gesamtunsicherheiten auf <0,10 ppm für CO_2, <1,3 ppb für CH_4 und <3,4 ppb für CO reduziert werden.

Der Einsatz des IAGOS-Instruments in einer Flugkampagne zum Vergleich verschiedener flugzeuggestützter Hygrometer ermöglichte eine erste Validierung der CRDS-Wasserdampf-messungen, deren Genauigkeit nie zuvor ausführlich quantifiziert und bewertet wurde. Zusätzlich

zur Standardkalibrierung, dem Vergleich gegen einen Taupunktspiegel oder ein Gefrierpunkthygrometer, wurde hier auch eine neu entwickelte, unabhängige Kalibrierungsmethode getestet, die auf der Messung des Verdünnungseffekts von Wasserdampf auf den CO_2-Anteil in der Luft basiert. Es konnte gezeigt werden, dass das neue Verfahren funktioniert und statistisch mit den Standardkalibrierungen konsistent ist, was die Methode auch als mögliches Kalibrierverfahren anderer Gase interessant macht. Der Vergleich der Flugdaten des Messgeräts mit bewährten Referenzgeräten bestätigte die Zuverlässigkeit, schnelle Reaktionszeit und gute Langzeitstabilität des Instruments. Als obere Grenze der Wiederholbarkeit wurden 4 ppm für H_2O <10 ppm, 20 % oder 10 ppm (je nachdem, welcher Wert kleiner ist) für 10 ppm < H_2O < 100 ppm und 5 % oder 30 ppm (je nachdem, welcher Wert kleiner ist) für Wasserdampf >100 ppm ermittelt. Die Messgenauigkeit, basierend auf den Laborkalibrierungen, beträgt 1 % für den Wasserdampfbereich von 25000 ppm bis 7000 ppm und steigt dann auf 5 % bei 50 ppm Wasserdampf an. Die Genauigkeit bei Wasserdampfkonzentrationen unter 50 ppm konnte nicht bewertet werden, da nicht genügend Vergleichsdaten der Referenzmesssysteme zur Verfügung standen.

Das erste IAGOS-Core GHG Instrument wurde 2017 erfolgreich an Bord eines Passagierflugzeugs als Teil des IAGOS-Projekts eingesetzt. Innerhalb der nächsten Jahre sollen fünf weitere Systeme in Betrieb genommen werden und weltweit regelmäßige und langfristige Messungen der wichtigsten Treibhausgase liefern, welche zur Validierung von Fernerkundungsdaten, zur inversen Modellierung von Treibhausgasflüssen, für Prozessstudien und zur Verbesserung regionaler und globaler Klimamodelle genutzt werden können.

List of Figures

List of Tables

List of abbreviations, acronyms and symbols

AC	alternating current
AGGI	Annual Greenhouse Gas Index
AIMS	Atmospheric Ionization Mass Spectrometer
CA	California
CAMS	Copernicus Atmospheric Monitoring Service
CARIBIC	Civil Aircraft for Remote Sensing and In Situ Measurements in Troposphere and Lower Stratosphere Based on the Instrumentation Container Concept, or Civil Aircraft for the Regular Investigation of the atmosphere Based on an Instrument Container
CCL	Central Calibration Laboratory
CHARM-F	CO_2 and CH_4 Atmospheric Remote Monitoring – Flugzeug
CONTRAIL	Comprehensive Observation Network for Trace gases by Airliner
CRDS	cavity ring-down spectroscopy
DC	direct current
DENCHAR	Development and Evaluation of Novel Compact Hygrometers for Airborne Research
DLR	German Aerospace Centre
EMI	electromagnetic interference
ENVISAT	Environmental Satellite
EUFAR	European Facility for Airborne Research
FEP	Fluorinated Ethylene Propylene
FISH	Fast In situ Stratospheric Hygrometer
FPM	fluororubber
GASP	Global Atmospheric Sampling Program
GAW	Global Atmosphere Watch
GCOS	Global Climate Observing System
GHG	greenhouse gas
GMES	Global Monitoring for Environment and Security
GOSAT	Greenhouse Gases Observing Satellite
GRUAN	GCOS Reference Upper-Air Network
HAI	Hygrometer for Atmospheric Investigations
HALO	High Altitude and Long Range Research Aircraft
HWV	Harvard Water Vapour instrument
IAGOS	In-service aircraft for a global observing system
IAGOS-ERI	IAGOS - European Research Infrastructure
ICOS	Integrated Cavity output Spectrometer
ID	inner diameter
IGAS	IAGOS for the GMES Atmospheric Service

I/O	input/output
IPCC	Intergovernmental Panel on Climate Change
IPDA	Integrated Path Differential Absorption
JLH	Jet Propulsion Laboratory Laser Hygrometer
LIDAR	Light Detection and Ranging
MACPEX	Mid-latitude Airborne Cirrus Properties Experiment
MD	Maryland
MERLIN	Methane Remote Sensing Lidar Mission
MIPAS	Michelson Interferometer for Passive Atmospheric Sounding
MOZAIC	Measurements of Ozone and water vapour by in-service Airbus aircraft
MPI-BGC	Max Planck Institute for Biogeochemistry
NDIR	nondispersive infrared spectroscopy
NIST	National Institute of Standards and Technology
NOAA	National Oceanic and Atmospheric Administration
NOAA-ESRL	NOAA Earth System Research Laboratory
NOXAR	Measurements of Nitrogen Oxides and ozone along Air Routes
OCO-2	Orbiting Carbon Observatory 2
OD	outer diameter
P2d	IAGOS-Core Package 2d (GHG Instrument)
QA/QC	quality assurance and quality control
SAGE	Stratospheric Aerosol and Gas Experiment
SCIAMACHY	Scanning Imaging Absorption Spectrometer for Atmospheric Chartography
SEALDH	Selective Extractive Airborne Laser Diode Hygrometer
SOA	Semiconductor Optical Amplifier
SSD	solid state drive
STE	stratosphere-troposphere exchange
TAT	Total Air Temperature
TGI	Trace Gas Inlet
TROPOMI	TROPOspheric Monitoring Instrument
UK	United Kingdom of Great Britain and Northern Ireland
US	United States of America
UTLS	upper troposphere and lowermost stratosphere
VURF	vacuum ultraviolet resonance fluorescence
WIS	WMO Information System
WMO	World Meteorological Organization
WoW	Weight-on-Wheels

@	at
A	peak area
^{13}C	a carbon isotope
CH_4	methane

CO	carbon monoxide
CO_2	carbon dioxide
Δ	delta
δx_{VPDB}	isotopic signature with respect to Vienna Pee Dee Belemnite standard
H_2O	water vapour
$Mg[ClO_4]_2$	magnesium perchlorate
n	number of samples
NO	nitrogen monoxide
NO_x	nitrogen oxides
OH	hydroxyl radical
p	pressure
σ	*s*igma
t	time
T	temperature
X	mole fraction

Foreword

Main parts of this work are also reflected in two scientific articles:

- Filges, A., Gerbig, C., Chen, H., Franke, H., Klaus, C., and Jordan, A.: The IAGOS-core greenhouse gas package: a measurement system for continuous airborne observations of CO_2, CH_4, H_2O and CO, Tellus B, 67,27989, doi:10.3402/tellusb.v67.27989, 2015.

- Filges, A., Gerbig, C., Rella, C. W., Hoffnagle, J., Smit, H., Krämer, M., Spelten, N., Rolf, C., Bozóki, Z., Buchholz, B., and Ebert, V.: Evaluation of the IAGOS-Core GHG package H_2O measurements during the DENCHAR airborne inter-comparison campaign in 2011, Atmos. Meas. Tech., 11, 5279-5297, https://doi.org/10.5194/amt-11-5279-2018, 2018.

1 Introduction

Never has the climate debate been discussed as seriously as it has been in 2019. The question of how we want to live in the future and what we have to do for it today has arrived the everyday life of the people. Especially the younger generation is afraid of the consequences of a 'business as usual', with increasing fossil fuel emissions and environmental degradation, and wants to change our lifestyles. According to a special report of the Intergovernmental Panel on Climate Change (IPCC) from 2018 global warming would have to be limited to 1.5°C above pre-industrial level in order to prevent the most devastating effects of climate change, like sea level rise, heat waves, more extreme weather, and disruption to marine and land ecosystems (IPCC, 2018). To achieve this, the leading industrial nations would need to operate climate neutrally within the next two to three decades (IPCC, 2018), something we are still a long way from achieving, as the newest United Nations Environment Programmes Emissions Gap Report (2019) shows. Furthermore, there is a risk that the global warming will be even faster, and stronger, as irreversible climate tipping points could be reached earlier than expected and lead to chain reactions (Lenton et al., 2019). That it is so difficult to make precise predictions and scenarios on climate change, to give concrete figures and simple answers, is due to the complexity of the topic, which involves an endless number of processes in the Earth system, from micro to global scale. One of the key elements is the carbon cycle.

1.1 Carbon cycle

Carbon occurs nearly everywhere in the Earth system. In various chemical compounds it is found in the atmosphere, lithosphere, hydrosphere, and in the biosphere, where it is an important element of life on Earth. The carbon cycle describes the exchange of carbon in its different forms between these reservoirs. As can be seen in Figure 1.1 by the red arrows and figures the reservoirs and the corresponding fluxes between them were changed compared to the natural carbon cycle due to human interventions since the industrial revolution. The burning of fossil fuels and land use changes (e.g. deforestation) releases carbon into the atmosphere. About a quarter of this carbon is absorbed by each the biosphere and the ocean through various processes on different time and spatial scales, while the rest (around 45 %) stays in the atmosphere. Figure 1.2 shows the timeseries of the estimated sources and sinks of anthropogenic carbon since 1850. The remaining difference between the total emissions (pink line) and total sinks indicates an imbalance, that can't be explained by our current knowledge and understanding of the carbon cycle (Friedlingstein et al., 2019). Therefore, further research is necessary, especially regarding the prediction and estimation of future reactions of the carbon cycle to human perturbations.

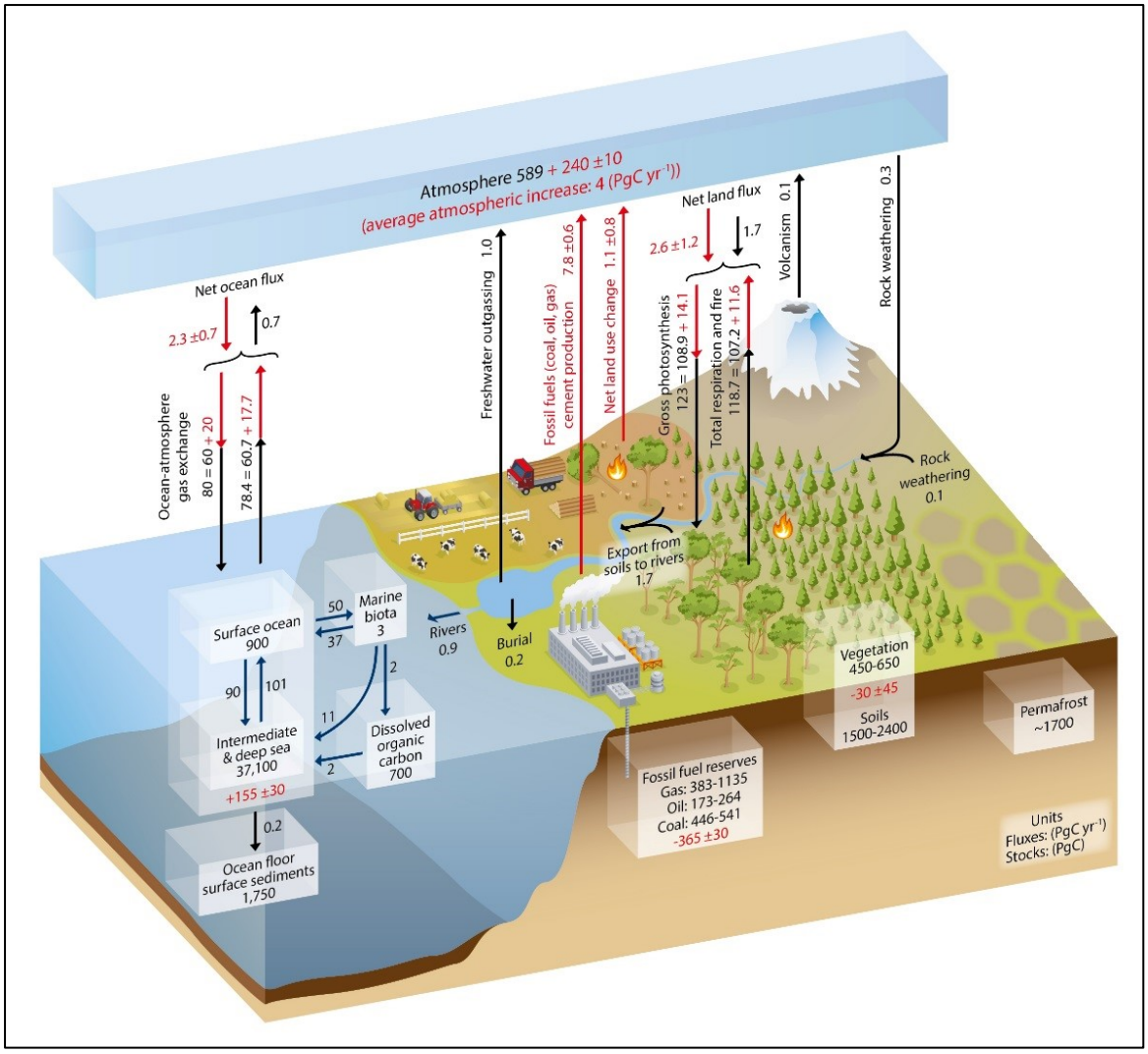

Figure 1.1: Simplified overview of the global carbon cycle. Numbers indicate the reservoir masses ('carbon stocks') in Petagram Carbon (1 PgC = 10^{15} gC) and the annual carbon exchange fluxes in PgC/yr between the reservoirs. Black numbers and arrows represent mass and flux estimates of the pre-industrial era (about 1750), red arrows represent annual anthropogenic fluxes (averaged over the time period 2000-2009), and red numbers show the net increase (+) or decrease (-) of carbon in the reservoirs due to anthropogenic activities in the industrial period from 1750 to 2011. Figure taken from IPCC (2013, p. 471).

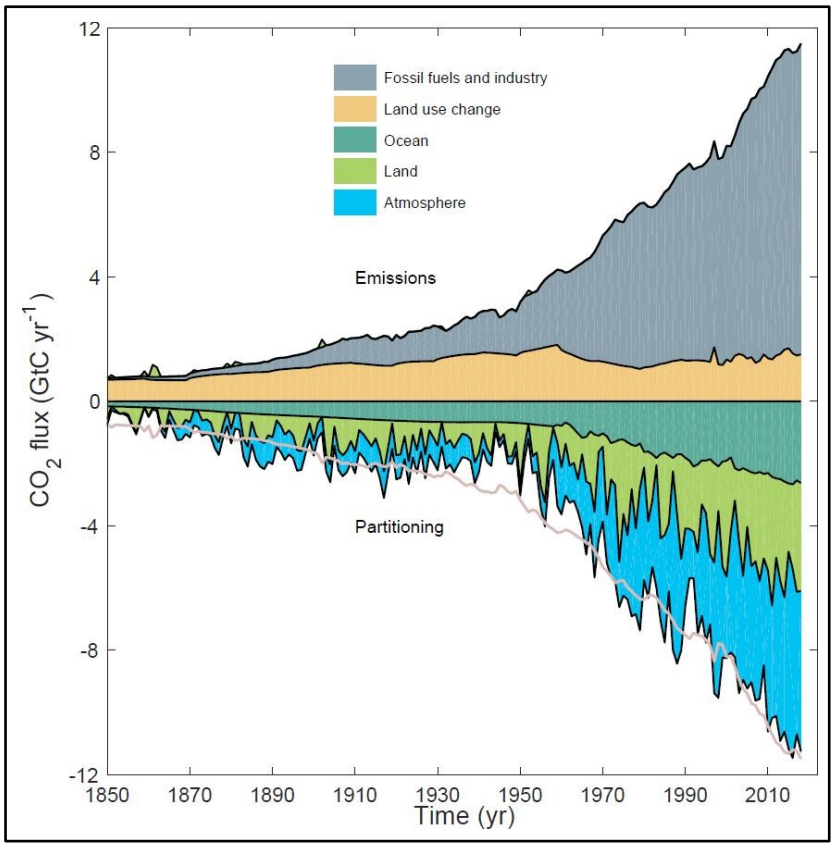

Figure 1.2: Timeseries of the annual anthropogenic carbon emissions (due to burning of fossil fuels and industry in grey, due to land use changes in yellow) in the upper part of the graph and the carbon sinks (ocean in turquoise, land in green, and atmosphere in blue) in the bottom part of the graph. The bottom pink line represents the total emissions. All fluxes are in gigatonnes of carbon per year. Figure taken from Friedlingstein et al. (2019).

1.1.1 Atmospheric part

The topic of this thesis contributes to the study of the atmospheric part. In contrast to the determination of the oceanic and land sink, which are largely based on models, atmospheric carbon can be constrained mainly by observations. Carbon occurs in the atmosphere as gaseous CO_2, CH_4, CO, and in very small amounts as Hydrocarbons, black carbon aerosols and organic compounds.

Carbon dioxide is the most abundant of these gases and is closely linked to human activities. While the largest natural source is respiration, significant anthropogenic emissions from combustion of fossil fuels, cement production, deforestation and biomass burning have been added since industrialization. Through photosynthesis, CO_2 from the atmosphere is taken up again by the biosphere, just as the oceans absorb CO_2 through gas exchange. However, the imbalance due to the anthropogenic emissions has led to such a strong increase in atmospheric carbon dioxide that it cannot be fully compensated by the removal processes and a large amount of CO_2 will remain in the atmosphere for centuries. In 2018 the level of CO_2 increased up to 147 % of the pre-industrial level of 278 ppm (parts per million). The globally averaged concentration reached 407.8 ppm and is forecast to average 410 ppm in 2019. The yearly growth was on average 2.26 ppm/yr

in the past ten years, which is higher than ever before since the beginning of direct CO_2 measurements. (IPCC, 2103; Friedlingstein et al., 2019; WMO, 2019)

Methane concentrations have also risen strongly over the last century due to anthropogenic emissions, reaching 1869 ppb (parts per billion) in 2018, which is 259 % of the pre-industrial level of around 722 ppb. Anthropogenic CH_4 originates primarily from agriculture (e.g. ruminant livestock farming, rice paddies, biomass burning), fossil fuel exploitation, and waste treatment. Only 40 % of the total CH_4 emissions come from natural processes like wetlands, termites, biomass burning and geological sources. The predominant sink of atmospheric methane is the photochemical reaction with the hydroxyl radical OH. In contrast to CO_2 the atmospheric lifetime of CH_4 is short, less than 10 years. Hence, the concentration of methane in the atmosphere would react quickly to a stabilization or reduction of emissions. The atmospheric growth rate of CH_4 varied strongly in the last decades, with periods of nearly zero growth to rates of more than 10 ppb/yr, which is still not fully understand. (IPCC, 2013; Saunois et al., 2019; WMO, 2019)

CO, the third most abundant carbon-containing gas, is released by incomplete combustion of fossil fuels as well as natural and anthropogenic fires. It is also formed during oxidation of CH_4 and plays itself an important role in atmospheric chemistry, for example as chemical reactant of OH and as a precursor of ozone. Atmospheric carbon monoxide has a short lifetime of 2 to 3 month and its concentration showed a slight decreasing trend in the last decades, but with large uncertainties and high interannual variability, mainly due to year to year changing fire emissions. (IPCC, 2013)

1.1.2 Greenhouse gas effect

The special importance of the atmospheric part of the carbon cycle for the climate is due to the greenhouse gas (GHG) effect. As first described in 1896 by Svante Arrhenius, the greenhouse gas effect is that atmospheric gases absorb long-wave (infrared) radiation emitted by the Earth and thereby trap a significant part of the energy and thus heat (Arrhenius, 1896). The natural GHG effect, which is mainly driven by the water vapour in the atmosphere, ensures that the global mean surface temperature is about 15°C. However, the effect is reinforced by the anthropogenic emissions of specifically CO_2 and CH_4, which is the direct and most important link of human activities to global warming and climate change. Currently the global mean surface temperature is around 1°C warmer than in pre-industrial times and is rising at a rate of 0.2°C per decade, with the largest contribution coming from the increase in GHG emissions (IPCC, 2018). As a measure of the warming or cooling effects on climate the concept of radiative forcing is commonly used, which quantifies the ‘net change in the energy balance of the Earth system in response to some external perturbation’, like the human influence on the GHG budgets (IPCC, 2013). Figure 1.3 shows the radiative forcing of the major five long-lived greenhouse gases relative to 1750 and on the right scale the Annual GHG Index, which is a measure for the relative radiative forcing compared to the value of 1990. The increase in CO_2, due to anthropogenic emissions, clearly has the largest impact: 81 % of the 43 % increase in radiative forcing by long-lived GHGs from 1990 to 2018 are caused by CO_2 (WMO, 2019). Methane, as the second most important of the gases, is responsible for 17 %. In order to prevent a further increase in radiative forcing due to anthropogenic GHGs, and thus in global warming, emissions would have to be cut.

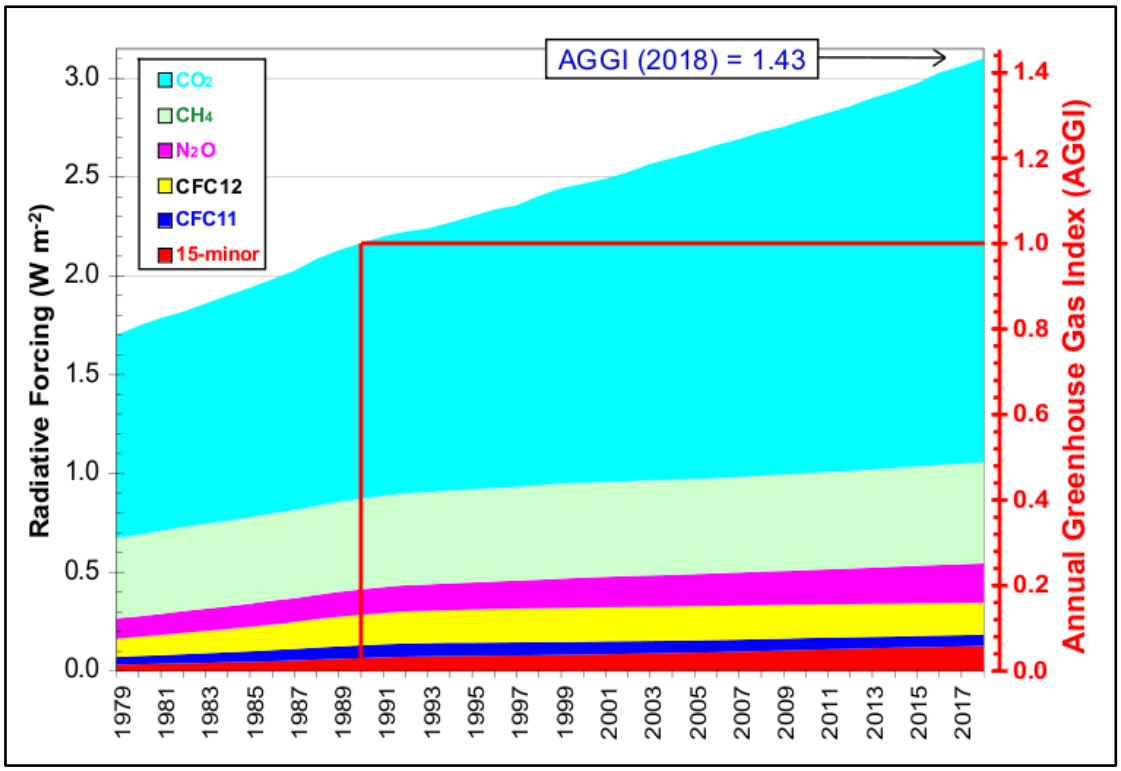

Figure 1.3: Radiative forcing of long-lived greenhouse gases from 1979 to 2018 relative to 1750. The Right axis shows the NOAA Annual Greenhouse Gas Index, a measure for the relative radiative forcing compared to 1990, which is set to 1. Figure taken from Butler and Montzka (2019).

1.2 Atmospheric observations

Observing atmospheric concentrations of carbon-containing gases is the most direct way to quantify the amount of carbon in the atmosphere, and thus is essential for the understanding of the global carbon cycle and its changes over time. The most famous observation series is the CO_2 monitoring on Mauna Loa in Hawaii. It was started at the end of the 1950s and has been measuring atmospheric CO_2 concentrations continuously and with high quality ever since. Figure 1.4 shows the whole measurement series until today. Since local sources and sinks at Mauna Loa are negligible, the curve shows very nicely the steady increase of the global background concentration of CO_2 in the atmosphere over the last 60 years.

Today there is a global network of such measurements, which helps to monitor the concentrations of important greenhouse gases and other carbon-containing gases from local to global scale. The measurements are no longer limited to surface stations, but can be performed from various platforms, such as tall towers, ships, balloons, aircraft, and satellites, as in situ or remote sensing data, or as air samples. An important application of the thus obtained concentration data is the so-called 'top-down approach': In combination with atmospheric models and inverse methods the sources and sinks of the gases can be quantified and localized (e.g. Bousquet et al., 2006; Ciais et al., 2010; Gurney et al., 2002; Rödenbeck et al., 2003). In order to achieve the best results with this method, data of different measurement methods are combined to complement their respective advantages and compensate for disadvantages. For example, the high precision but spatially limited in situ measurements on ground and remote sensing data from satellites with

high spatial coverage but lower precision and temporal resolution. A big challenge in this process is to trace the data of different measurement methods back to common calibration scales, since biases in the atmospheric gas concentrations also lead to biases in the inferred sources and sinks.

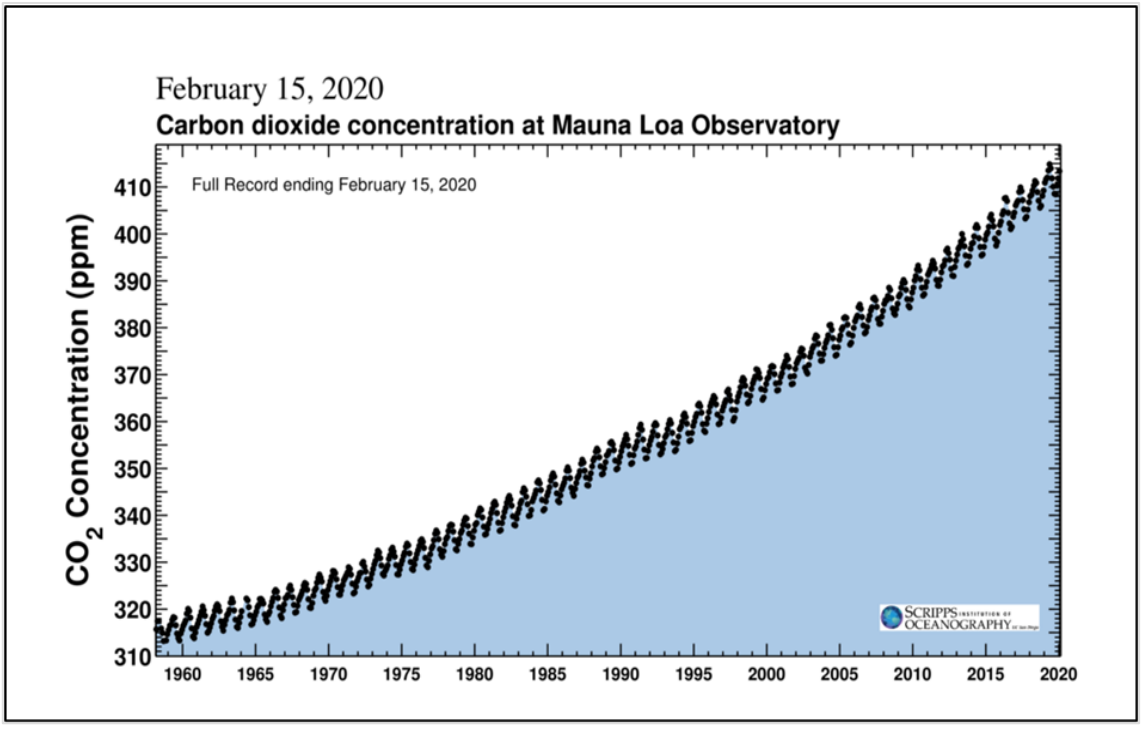

Figure 1.4: Atmospheric monthly in situ CO_2 data measured at Mauna Loa Observatory, Hawaii, from 1958 to 2020 (https://scripps.ucsd.edu/programs/keelingcurve, Keeling and Keeling (2017)).

1.2.1 Aircraft as measurement platform

Aircraft play an important role as measuring platform. They help to bridge the gap between ground and satellite observations and provide valuable atmospheric data from the troposphere and lower parts of the stratosphere (e.g. Sweeney et al., 2015; Wofsy, 2011). The vertical profile measurements are essential for the validation of remote sensing data, both from satellites and from ground. They help to link the remote sensing measurements to the same scales as the in situ ground and aircraft data, and thus to trace them back to common standards (e.g. Wunch et al., 2010; Maddy et al., 2008; Xiong et al., 2008; de Laat et al., 2012; Inoue et al., 2016; Frankenberg et al., 2016). As mentioned above, the alignment of data from different measurement methods is a key point for atmospheric inversions. Another important application of aircraft data is the evaluation and improvement of atmospheric transport and chemistry models. Tests against tracer data, like long-living GHGs, help to improve the representation and parameterization of transport processes, such as convection, turbulent mixing, or stratosphere-troposphere exchange (STE), in the models (e.g. Stephens et al., 2007; Yang et al., 2007; Nakatsuka and Maksyutov, 2009; Patra et al., 2011; Wofsy, 2011).

Due to the great disadvantage of aircraft measurements - their relatively large effort and very high costs - the temporal and spatial coverage of the data is limited. The few regular measurements

with aircraft over fixed sites, mostly restricted to the northern hemisphere, can at best be performed once or twice per week. Special campaigns with research aircraft can provide data with higher temporal and spatial coverage for a short time period, but only take place sporadically. As an interesting and cost-efficient alternative, commercial aircraft were therefore already being considered as measurement platforms in the 1960s (Bolin and Bischof, 1970). They fly the same routes on a regular and long-term basis, spanning almost the entire globe. In this way even poorly monitored regions, such as the tropics, can be better covered. And since the main flight path is in the upper troposphere and lowermost stratosphere (UTLS) they are also the crucial data source for this region. The UTLS is one of the most climate sensitive parts of the atmosphere and hence it is very important to study and better understand its chemistry, particle and gas concentrations, and transport processes (Riese et al., 2012; Solomon et al., 2010). While the first large routine projects with passenger aircraft, such as GASP (Global Atmospheric Sampling Program; e.g. Falconer, 1978 and Dudzinski, 1979), MOZAIC (Measurements of Ozone and water vapour by in-service Airbus aircraft; Marenco et al., 1998), CARIBIC (Civil Aircraft for Remote Sensing and In Situ Measurements in Troposphere and Lower Stratosphere Based on the Instrumentation Container Concept; Brenninkmeijer et al., 1999) and NOXAR (Measurements of Nitrogen Oxides and ozone along Air Routes; Brunner et al., 2001), mainly focused on the measurements of ozone, nitrogen oxides, carbon monoxide, water vapour, and particles, there were early efforts in Japan and Australia to analyse CO_2 and later also CH_4 from air samples (Pearman and Beardsmore, 1984; Nakazawa et al., 1991; Matsueda and Inoue, 1996). In the end, however, it took until 2006 before the first in situ measurement systems for CO_2 were installed on board commercial aircraft to obtain regular and continuous atmospheric CO_2 concentration data. As part of the Japanese CONTRAIL project (Comprehensive Observation Network for Trace gases by Airliner; Machida et al., 2008), they have since been providing measurements with nearly global coverage, particularly the northern hemisphere, but also of the interesting north-south route between Japan and Sydney (Australia), which covers the tropical region and crosses the tropopause.

On European side, the first in situ CO_2 concentration measurements were carried out within the second phase of the CARIBIC project (Civil Aircraft for the Regular Investigation of the atmosphere Based on an Instrument Container; Brenninkmeijer et al., 2007) since the end of 2004. However, because of its special concept of a cargo container equipped with a variety of instruments, the deployment is limited to four long-haul flights per month. Moreover, the CO_2 device was found to be unreliable and not sufficiently accurate.

Due to the great response of researchers worldwide to the datasets of MOZAIC and CARIBIC, which was reflected in hundreds of scientific publications in atmospheric research (www.iagos.org/scientific-publications; www.caribic-atmospheric.com/Publications.php), IAGOS (In-service aircraft for a global observing system; Volz-Thomas et al., 2009; Petzold et al., 2015) was established in 2005 as a follow-up project to continue and expand the measurements based on the scientific and technological experience gained within the two projects. One objective of IAGOS was the development, certification and finally deployment of a new measuring system for CO_2 mixing ratios for continuous operation on a fleet of long-haul passenger aircraft.

1.2.2 The IAGOS-Core GHG Instrument

Within the IAGOS - Design Study from 2005 to 2010 a suitable CO_2 measuring device was to be selected or developed. The demands on the instrument were very high: Size and weight were limited to 30 cm x 35 cm x 53 cm and 30 kg due to the conditions in the aircraft. Replacement and maintenance intervals of the measurement system are linked to the routine aircraft checks, so that it must be able to operate unattended for up to half a year. Furthermore, the instrument should of course fulfil the scientific requirements and meet the compatibility goals recommended by the World Meteorological Organization (WMO) of 0.1 ppm for atmospheric CO_2 measurements in the northern hemisphere (0.5 ppm in the southern hemisphere) (WMO, 2018). The selection and testing of suitable analysers is described in detail in Chen (2010). First, an instrument based on the nondispersive infrared (NDIR) technique was considered, as it is a proven method, which is also used for the CONTRAIL in situ CO_2 measurements. However, laboratory tests of the corresponding system with regard to its possible use for IAGOS showed that the stability of the analyser is not sufficient, requiring frequent calibration and sample drying, all of which could not be implemented within the IAGOS project. More promising proved to be a just newly developed instrument based on the cavity ring-down technique (CRDS), which had already been successfully tested and used for ground-based applications (Crosson, 2008). In addition to its very good stability, low maintenance needs and linearity, it offered the great advantage of being able to measure not only CO_2 mole fractions, but also other gas species such as CH_4 and water vapour simultaneously. This also makes it possible to convert the measured wet air mole fractions, with the aid of the water vapour measurements, to dry air mole fractions and thereby rendering drying of the air unnecessary, which significantly simplifies maintenance. Consequently, a new analyser was developed, which was adapted to the special requirements and environmental conditions for flight operations by minor modifications of the original ground-based device. After successful test flights and validation against an established NDIR measuring system the analyser was found to be suitable for the IAGOS project and shall henceforth be used with some necessary modifications as 'IAGOS-Core GHG package' for the measurement of CO_2, CH_4, CO and water vapour.

1.3 Thesis outline

This work presents the development of the IAGOS-Core GHG package and the results of various laboratory and flight tests of the instrument, which were performed to qualify the device for successful use within the IAGOS project. Chapter 2 introduces the measurement system and describes its design and functions, which meet the specific requirements regarding physical dimensions, performance and safety issues on board commercial aircraft. It presents the calibration strategy, that allows the measurements to be fully traceable to WMO scales and shows the results of several laboratory experiments and a test flight, which document the performance of the CO_2, CH_4, CO and water vapour measurements. Furthermore, it gives an overview of the uncertainty budget estimates of the measurement data. Chapter 3 focuses on the water vapour measurements of the instrument. Different calibration methods are presented and tested, including a new, independent approach based on the dilution effect of water vapour on CO_2.

Comparison against reference instruments with a long performance record during a flight campaign allowed for an initial assessment of the water vapour measurements, since the quantitative capabilities of the CRDS water vapour measurements were never evaluated and reviewed in detail before. Chapter 4 presents the first flight tests of the IAGOS-core GHG package prototype, in the exact status as it will be deployed within IAGOS, on a research aircraft. It describes the analysis and evaluation of the instrument operation and performance, the calibration procedures and the atmospheric measurement data. Chapter 5 concludes the thesis with a summary and an outlook.

1.4 References

Arrhenius, S.: On the influence of carbonic acid in the air upon the temperature of the ground, Philosophical Magazine and Journal of Science, 41, 237-276, 1896.

Bolin, B. and Bischof, W.: Variations of the carbon dioxide content of the atmosphere in the northern hemisphere, Tellus, 22:4, 431-442, https://doi.org/10.3402/tellusa.v22i4.10236, 1970.

Bousquet, P., Ciais, P., Miller, J., Dlugokencky, E. J., Hauglustaine, D. A., Prigent, C., Van der Werf, G. R., Peylin, P., Brunke, E.-G., Carouge, C., Langenfelds, R. L., Lathière, J., Papa, F., Ramonet, M., Schmidt, M., Steele, L. P., Tyler, S. C., and White, J.: Contribution of anthropogenic and natural sources to atmospheric methane variability, Nature, 443, 439–443, https://doi.org/10.1038/nature05132, 2006.

Brenninkmeijer, C. A., Crutzen, P. J., Fischer, H., Güsten, H., Hans, W., Heinrich, G., Heintzenberg, J., Hermann, M., Immelmann, T., Kersting, D., Maiss, M., Nolle, M., Pitscheider, A., Pohlkamp, H., Scharffe, D., Specht, K., and Wiedensohler, A.: CARIBIC—Civil Aircraft for Global Measurement of Trace Gases and Aerosols in the Tropopause Region, J. Atmos. Oceanic Technol., 16, 1373–1383, https://doi.org/10.1175/1520-0426(1999)016<1373:CCAFGM>2.0.CO;2, 1999.

Brenninkmeijer, C. A. M., Crutzen, P., Boumard, F., Dauer, T., Dix, B., Ebinghaus, R., Filippi, D., Fischer, H., Franke, H., Frieß, U., Heintzenberg, J., Helleis, F., Hermann, M., Kock, H. H., Koeppel, C., Lelieveld, J., Leuenberger, M., Martinsson, B. G., Miemczyk, S., Moret, H. P. Nguyen, H. N., Nyfeler, P., Oram, D., O'Sullivan, D., Penkett, S., Platt, U., Pupek, M., Ramonet, M., Randa, B., Reichelt, M., Rhee, T. S., Rohwer, J., Rosenfeld, K., Scharffe, D., Schlager, H., Schumann, U., Slemr, F., Sprung, D., Stock, P., Thaler, R., Valentino, F., van Velthoven, P., Waibel, A., Wandel, A., Waschitschek, K., Wiedensohler, A., Xueref-Remy, I., Zahn, A., Zech, U., and Ziereis, H.: Civil Aircraft for the regular investigation of the atmosphere based on an instrumented container: The new CARIBIC system, Atmos. Chem. Phys., 7, 4953-4976, https://doi.org/10.5194/acp-7-4953-2007, 2007.

Brunner, D., Staehelin, J., Jeker, D., Wernli, H., and Schumann, U.: Nitrogen oxides and ozone in the tropopause region of the Northern Hemisphere: Measurements from commercial aircraft in 1995/1996 and 1997, J. Geophys. Res., 106, 27,673– 27,699, https://doi.org/10.1029/2001JD900239, 2001.

Butler, J. H. and Montzka, S. A.: The NOAA Annual Greenhouse Gas Index (AGGI), http://www.esrl.noaa.gov/gmd/aggi/aggi.html, 2019.

Chen, Huilin: Development of a high-accuracy continuous CO_2/CH_4/H_2O analyser for deployment on board a commercial airliner, https://www.db-thueringen.de/receive/dbt_mods_00017276, 2010.

Ciais, P., Rayner, P., Chevallier, F., Bousquet, P., Logan, M., Peylin, P., and Ramonet, M.: Atmospheric inversions for estimating CO_2 fluxes: methods and perspectives, Climatic Change, 103, 69–92, https://doi.org/10.1007/s10584-010-9909-3, 2010.

Crosson, E. R.: A cavity ring-down analyser for measuring atmospheric levels of methane, carbon dioxide, and water vapour, Applied Physics B - Lasers and Optics, 92(3), 403-408, https://doi.org/10.1007/s00340-008-3135-y, 2008.

De Laat, A. T. J., Dijkstra, R., Schrijver, H., Nédélec, P., and Aben, I.: Validation of six years of SCIAMACHY carbon monoxide observations using MOZAIC CO profile measurements, Atmos. Meas. Tech., 5, 2133–2142, https://doi.org/10.5194/amt-5-2133-2012, 2012.

Dudzinski, T. J.: Carbon monoxide measurement in the Global Atmospheric Sampling Program, NASA technical paper, 1526, Washington, 1979.

P. Falconer: Global Atmospheric Sampling Program: Prospects for Establishing a Tropospheric Ozone Budget from Commercial Aircraft Data, Air Quality Meteorology and Atmospheric Ozone, ed. A. Morris and R. Barras, West Conshohocken, PA: ASTM International, 479-490, https://doi.org/ 10.1520/STP36602S, 1978.

Frankenberg, C., Kulawik, S. S., Wofsy, S. C., Chevallier, F., Daube, B., Kort, E. A., O'Dell, C., Olsen, E. T., and Osterman, G.: Using airborne HIAPER Pole-to-Pole Observations (HIPPO) to evaluate model and remote sensing estimates of atmospheric carbon dioxide, Atmos. Chem. Phys., 16, 7867–7878, https://doi.org/10.5194/acp-16-7867-2016, 2016.

Friedlingstein, P., Jones, M. W., O'Sullivan, M., Andrew, R. M., Hauck, J., Peters, G. P., Peters, W., Pongratz, J., Sitch, S., Le Quéré, C., Bakker, D. C. E., Canadell, J. G., Ciais, P., Jackson, R. B., Anthoni, P., Barbero, L., Bastos, A., Bastrikov, V., Becker, M., Bopp, L., Buitenhuis, E., Chandra, N., Chevallier, F., Chini, L. P., Currie, K. I., Feely, R. A., Gehlen, M., Gilfillan, D., Gkritzalis, T., Goll, D. S., Gruber, N., Gutekunst, S., Harris, I., Haverd, V., Houghton, R. A., Hurtt, G., Ilyina, T., Jain, A. K., Joetzjer, E., Kaplan, J. O., Kato, E., Klein Goldewijk, K., Korsbakken, J. I., Landschützer, P., Lauvset, S. K., Lefèvre, N., Lenton, A., Lienert, S., Lombardozzi, D., Marland, G., McGuire, P. C., Melton, J. R., Metzl, N., Munro, D. R., Nabel, J. E. M. S., Nakaoka, S.-I., Neill, C., Omar, A. M., Ono, T., Peregon, A., Pierrot, D., Poulter, B., Rehder, G., Resplandy, L., Robertson, E., Rödenbeck, C., Séférian, R., Schwinger, J., Smith, N., Tans, P. P., Tian, H., Tilbrook, B., Tubiello, F. N., van der Werf, G. R., Wiltshire, A. J., and Zaehle, S.: Global Carbon Budget 2019, Earth Syst. Sci. Data, 11, 1783–1838, https://doi.org/10.5194/essd-11-1783-2019, 2019.

Gurney, K. R., Law, R. M., Denning, A. S., Rayner, P. J., Baker, D., Bousquet, P., Bruhwiler, L., Chen, Y.-H., Ciais, P., Fan, S., Fung, I. Y., Gloor, M., Heimann, M., Higuchi, K., John, J., Maki, T., Maksyutov, S., Masarie, K., Peylin, P., Prather, M., Pak, B. C., Randerson, J., Sarmiento, J., Taguchi, S., Takahashi, T., and Yuen, C.-W.: Towards robust regional estimates of CO_2 sources and sinks using atmospheric transport models, Nature, 415, 626–630, https://doi.org/10.1038/415626a, 2002.

Inoue, M., Morino, I., Uchino, O., Nakatsuru, T., Yoshida, Y., Yokota, T., Wunch, D., Wennberg, P. O., Roehl, C. M., Griffith, D. W. T., Velazco, V. A., Deutscher, N. M., Warneke, T., Notholt, J., Robinson, J., Sherlock, V., Hase, F., Blumenstock, T., Rettinger, M., Sussmann, R., Kyrö, E., Kivi, R., Shiomi, K., Kawakami, S., De Mazière, M., Arnold, S. G., Feist, D. G., Barrow, E. A., Barney, J., Dubey, M., Schneider, M., Iraci, L. T., Podolske, J. R., Hillyard, P. W., Machida, T., Sawa, Y., Tsuboi, K., Matsueda, H., Sweeney, C., Tans, P. P., Andrews, A. E., Biraud, S.C., Fukuyama, Y., Pittman, J.V., Kort, E.A., and Tanaka, T.: Bias corrections of GOSAT SWIR XCO_2 and XCH_4 with TCCON data and their evaluation using aircraft measurement data, Atmos. Meas. Tech., 9, 3491–3512, https://doi.org/10.5194/amt9-3491-2016, 2016.

IPCC: Climate Change 2013: The Physical Science Basis. Contribution of Working Group I to the Fifth Assessment Report of the Intergovernmental Panel on Climate Change [Stocker, T.F., D. Qin, G.-K. Plattner, M. Tignor, S.K. Allen, J. Boschung, A. Nauels, Y. Xia, V. Bex and P.M. Midgley (eds.)], Cambridge University Press, Cambridge, United Kingdom and New York, NY, USA, 1535 pp, https://www.ipcc.ch/report/ar5/wg1, 2013.

IPCC: Summary for Policymakers. In: Global Warming of 1.5°C. An IPCC Special Report on the impacts of global warming of 1.5°C above pre-industrial levels and related global greenhouse gas emission pathways, in the context of strengthening the global response to the threat of climate change, sustainable development, and efforts to eradicate poverty [Masson-Delmotte, V., P. Zhai, H.-O. Pörtner, D. Roberts, J. Skea, P.R. Shukla, A. Pirani, W. Moufouma-Okia, C. Péan, R. Pidcock, S. Connors, J.B.R. Matthews, Y. Chen, X. Zhou, M.I. Gomis, E. Lonnoy, T. Maycock, M. Tignor, and T. Waterfield (eds.)], In Press., https://www.ipcc.ch/sr15, 2018.

Keeling, R. F. and Keeling, C. D.: Atmospheric Monthly In Situ CO_2 Data - Mauna Loa Observatory, Hawaii, In Scripps CO_2 Program Data, UC San Diego Library Digital Collections, https://doi.org/10.6075/J08W3BHW, Accessed on 18.02.2020, https://scripps.ucsd.edu/ programs/ keelingcurve, 2017.

Lenton, T. M., Rockström, J., Gaffney, O., Rahmstorf, S., Richardson, K., Steffen, W., Schellnhuber, H. J.: Climate tipping points — too risky to bet against, Nature, 575 (7784), 592-595, https://doi.org/10.1038/d41586-019-03595-0, 2019.

Machida, T., Matsueda, H., Sawa, Y., Nakagawa, Y., Hirotani, K., Kondo, N., Goto, K., Nakazawa, T., Ishikawa, K., and Ogawa, T.: Worldwide Measurements of Atmospheric CO_2 and Other Trace Gas Species Using Commercial Airlines, J. Atmos. Oceanic Technol., 25(10), 1744–1754, https://doi.org/10.1175/2008JTECHA1082.1, 2008.

Maddy, E. S., Barnet, C. D., Goldberg, M., Sweeney, C., and Liu, X.: CO_2 retrievals from the Atmospheric Infrared Sounder: Methodology and validation, J. Geophys. Res., 113, D11301, https://doi.org/ 10.1029/2007JD009402, 2008.

Marenco, A., Thouret, V., Nédélec, P., Smit, H., Helten, M., Kley, D., Karcher, F., Simon, P., Law, K., Pyle, J., Poschmann, G., Von Wrede, R., Hume, C., and Cook, T.: Measurement of ozone and

water vapour by Airbus in-service aircraft: The MOZAIC airborne program, An overview, J. Geophys. Res., 103(D19), 25,631–25,642, https://doi.org/10.1029/98JD00977, 1998.

Matsueda, H. and Inoue, H. Y.: Measurements of atmospheric CO_2 and CH_4 using a commercial airliner from 1993 to 1994, Atmos. Environ., 30, 1647–1655, https://doi.org/10.1016/1352-2310(95)00374-6, 1996.

Nakatsuka, Y. and Maksyutov, S.: Optimization of the seasonal cycles of simulated CO_2 flux by fitting simulated atmospheric CO_2 to observed vertical profiles, Biogeosciences, 6(12), 2733–2741, 2009.

Nakazawa, T., Miyashita, K., Aoki, S., and Tanaka, M.: Temporal and spatial variations of upper tropospheric and lower stratospheric carbon dioxide, Tellus Ser. B Chem. Phys. Meteorol., 43(2), 106–117, https://doi.org/10.1034/j.1600-0889.1991.t01-1-00005.x, 1991.

Patra, P. K., Houweling, S., Krol, M., Bousquet, P., Belikov, D., Bergmann, D., Bian, H., Cameron-Smith, P., Chipperfield, M. P., Corbin, K., Fortems-Cheiney, A., Fraser, A., Gloor, E., Hess, P., Ito, A., Kawa, S. R., Law, R. M., Loh, Z., Maksyutov, S., Meng, L., Palmer, P. I., Prinn, R. G., Rigby, M., Saito, R., and Wilson, C.: TransCom model simulations of CH_4 and related species: linking transport, surface flux and chemical loss with CH_4 variability in the troposphere and lower stratosphere, Atmos. Chem. Phys., 11, 12813–12837, https://doi.org/10.5194/acp-11-12813-2011, 2011.

Pearman, G. I., and Beardsmore, D. J.: Atmospheric carbon dioxide measurements in the Australian region: 10 years of aircraft data, Tellus Ser. B Chem. Phys. Meteorol., 36(1), 1–24, https://doi.org/
10.1111/j.1600-0889.1984.tb00047.x, 1984.

Petzold A., Thouret, V., Gerbig, C., Zahn, A., Brenninkmeijer, C. A.M., Gallagher, M., Hermann, M., Pontaud, M., Ziereis, H., Boulanger, D., Marshall, J., Nédélec, P., Smit, H. G.J., Friess, U., Flaud, J.-M., Wahner, A., Cammas, J.-P., and Volz-Thomas, A.: Global-scale atmosphere monitoring by in-service aircraft - current achievements and future prospects of the European Research Infrastructure IAGOS, Tellus B, 67, 28452, https://doi.org/10.3402/tellusb.v67.28452, 2015.

Riese, M., Ploeger, F., Rap, A., Vogel, B., Konopka, P., Dameris, M., and Forster, P.: Impact of uncertainties in atmospheric mixing on simulated UTLS composition and related radiative effects, J. Geophys. Res., 117, D16305, https://doi.org/10.1029/2012JD017751, 2012.

Rödenbeck, C., Houweling, S., Gloor, M., and Heimann, M.: CO_2 flux history 1982– 2001 inferred from atmospheric data using a global inversion of atmospheric transport, Atmos. Chem. Phys., 3, 1919–1964, https://doi.org/10.5194/acp-3-1919-2003, 2003.

Saunois, M., Stavert, A. R., Poulter, B., Bousquet, P., Canadell, J. G., Jackson, R. B., Raymond, P. A., Dlugokencky, E. J., Houweling, S., Patra, P. K., Ciais, P., Arora, V. K., Bastviken, D., Bergamaschi,

P., Blake, D. R., Brailsford, G., Bruhwiler, L., Carlson, K. M., Carrol, M., Castaldi, S., Chandra, N., Crevoisier, C., Crill, P. M., Covey, K., Curry, C. L., Etiope, G., Frankenberg, C., Gedney, N., Hegglin, M. I., Höglund-Isaksson, L., Hugelius, G., Ishizawa, M., Ito, A., Janssens-Maenhout, G., Jensen, K. M., Joos, F., Kleinen, T., Krummel, P. B., Langenfelds, R. L., Laruelle, G. G., Liu, L., Machida, T., Maksyutov, S., McDonald, K. C., McNorton, J., Miller, P. A., Melton, J. R., Morino, I., Müller, J., Murgia-Flores, F., Naik, V., Niwa, Y., Noce, S., O'Doherty, S., Parker, R. J., Peng, C., Peng, S., Peters, G. P., Prigent, C., Prinn, R., Ramonet, M., Regnier, P., Riley, W. J., Rosentreter, J. A., Segers, A., Simpson, I. J., Shi, H., Smith, S. J., Steele, L. P., Thornton, B. F., Tian, H., Tohjima, Y., Tubiello, F. N., Tsuruta, A., Viovy, N., Voulgarakis, A., Weber, T. S., van Weele, M., van der Werf, G. R., Weiss, R. F., Worthy, D., Wunch, D., Yin, Y., Yoshida, Y., Zhang, W., Zhang, Z., Zhao, Y., Zheng, B., Zhu, Q., Zhu, Q., and Zhuang, Q.: The Global Methane Budget 2000–2017, Earth Syst. Sci. Data Discuss., https://doi.org/10.5194/essd-2019-128, in review, 2019.

Solomon, S., Rosenlof, K. H., Portmann, R. W., Daniel, J. S., Davis, S. M., Sanford, T. J., and Plattner, G.-K.: Contributions of stratospheric water vapour to decadal changes in the rate of global warming, Science, 327, 1219-1223, https://doi.org/10.1126/science.1182488, 2010.

Stephens, B. B., Gurney, K. R., Tans, P. P., Sweeney, C., Peters, W., Bruhwiler, L., Ciais, P., Ramonet, M., Bousquet, P., Nakazawa, T., Aoki, S., Machida, T., Inoue, G., Vinnichenko, N., Lloyd, J., Jordan, A., Heimann, M., Shibistova, O., Langenfelds, R. L., Steele, L. P., Francey, R. J., and Denning, A. S.: Weak northern and strong tropical land carbon uptake from vertical profiles of atmospheric CO_2, Science, 316(5832), 1732–1735, https://doi.org/10.1126/science.1137004, 2007.

Sweeney, C., Karion, A., Wolter, S., Newberger, T., Guenther, D., Higgs, J.A., Andrews, A.E., Lang, P.M., Neff, D., Dlugokencky, E., Miller, J. B., Montzka, S. A., Miller, B. R., Masarie, K. A., Biraud, S. C., Novelli, P. C., Crotwell, M., Crotwell, A. M., Thoning, K., and Tans, P. P.: Seasonal climatology of CO_2 across north america from aircraft measurements in the NOAA/ESRL global greenhouse gas reference network, J. Geophys. Res. Atmos., 120, 5155–5190, https://doi.org/10.1002/2014JD022591, 2015.

United Nations Environment Programme (UNEP): Emissions Gap Report 2019, UNEP, Nairobi, https://www.unenvironment.org/resources/emissions-gap-report-2019, 2019.

Volz-Thomas, A., Cammas, J.-P., Brenninkmeijer, C. A. M., Machida, T., Cooper, O., Sweeney, C., Waibel, A.: Civil Aviation Monitors Air Quality and Climate, Journal of the Air & Waste Management Association, October 2009, 16-19. 2009.

Wofsy, S. C.: HIAPER Pole-to-Pole Observations (HIPPO): fine-grained, global-scale measurements of climatically important atmospheric gases and aerosols, Phil. Trans. R. Soc. A, 369, 2073–2086, https://doi.org/10.1098/rsta.2010.0313, 2011.

WMO: GAW Report No. 242: 19th WMO/IAEA Meeting on Carbon Dioxide, Other Greenhouse Gases, and Related Measurement Techniques (GGMT-2017), Dübendorf, Switzerland, 27-31 August 2017, 2018.

World Meteorological Organization (WMO): WMO Greenhouse Gas Bulletin (GHG Bulletin) - No. 15: The State of Greenhouse Gases in the Atmosphere Based on Global Observations through 2018, Geneva, https://library.wmo.int/doc_num.php?explnum_id=10100, 2019.

Wunch, D., Toon, G. C., Wennberg, P. O., Wofsy, S. C., Stephens, B. B., Fischer, M. L., Uchino, O., Abshire, J. B., Bernath, P., Biraud, S. C., Blavier, J.-F. L., Boone, C., Bowman, K. P., Browell, E. V., Campos, T., Connor, B. J., Daube, B. C., Deutscher, N. M., Diao, M., Elkins, J.W., Gerbig, C., Gottlieb, E., Griffith, D. W. T., Hurst, D. F., Jimenez, R., Keppel-Aleks, G., Kort, E. A., Macatangay, R., Machida, T., Matsueda, H., Moore, F., Morino, I., Park, S., Robinson, J., Roehl, C.M., Sawa, Y., Sherlock, V., Sweeney, C., Tanaka, T., and Zondlo, M.A.: Calibration of the Total Carbon Column Observing Network using aircraft profile data, Atmos. Meas. Tech., 3, 1351–1362, https://doi.org/10.5194/amt-3-1351-2010, 2010.

Xiong, X., Barnet, C., Maddy, E., Sweeney, C., Liu, X., Zhou, L., and Goldberg, M.: Characterization and validation of methane products from the Atmospheric Infrared Sounder (AIRS), J. Geophys. Res., 113, G00A01, https://doi.org/10.1029/2007JG000500, 2008.

Yang, Z., Washenfelder, R. A., Keppel-Aleks, G., Krakauer, N. Y., Randerson, J. T., Tans, P. P., Sweeney, C., and Wennberg, P. O.: New constraints on Northern Hemisphere growing season net flux, Geophys. Res. Lett., 34, L12807, https://doi.org/10.1029/2007GL029742, 2007.

2 The IAGOS-core GHG package: a measurement system for continuous airborne observations of CO_2, CH_4, H_2O and CO

2.1 Introduction

CO_2 and CH_4 are the most important anthropogenic greenhouse gases (GHGs) and they play an important role in global climate change. Increased atmospheric concentrations of CO_2 and CH_4 caused a radiative forcing for 2011 relative to 1750 of 1.82 and 0.48 W/m^2, respectively (IPCC, 2013), which accounts for ~65 and ~17 %, respectively, of the total radiative forcing by long-lived GHGs [World Meteorological Organization (WMO), 2014]. Atmospheric CO has dominant sources from anthropogenic emissions, and thus it is a useful tracer for emissions of CO_2 and CH_4 from biomass and fossil fuel burning (Andreae and Merlet,2001; Levin and Karstens, 2007). Knowledge of the temporal and spatial atmospheric distribution of CO_2, CH_4 and CO is crucial information for the understanding of GHG budgets and their trends under a changing climate. Observations of these trace gases by ground-based stations (towers, ships, Fourier Transform Spectrometers, air sampling sites and so on) or satellites either do not cover at all or are not able to sufficiently resolve vertical structures throughout the troposphere and lower stratosphere. Airborne measurements done with in situ instruments, air sampling in flasks or other sampling systems such as AirCore (Karion et al., 2010) aboard research aircraft or balloons are quite limited in their temporal and spatial coverage. Regarding these aspects, passenger aircraft provide a unique platform for directly measuring atmospheric composition in the free troposphere and lower stratosphere with regular temporal coverage.

Some of the major programs, showing the great potential of using commercial aircraft, are the MOZAIC project (Measurement of Ozone and Water Vapour by Airbus In-Service Aircraft; Marenco et al., 1998), the CARIBIC project (Civil Aircraft for the Regular Investigation of the Atmosphere Based on an Instrument Container; Brenninkmeijer, 2007), and especially important for GHGs the CONTRAIL project (Comprehensive Observation Network for Trace gases by an Airliner; Matsueda and Inoue, 1996; Machida, 2008). These three programs follow different approaches: MOZAIC used five Airbus A340-300 that were permanently equipped with instruments to provide measurements of ozone and water vapour (operational since 1994), and since 2001 also CO (Nédélec et al., 2003) and NO_y (Volz-Thomas et al., 2005). Altogether, more than 25 000 long-range flights were performed until the last MOZAIC-equipped aircraft went out of service in 2014. Within the CARIBIC project, an airfreight container, equipped with in situ instruments and sampling devices for more than 60 different trace gases and aerosol properties, is deployed on board an Airbus A340-600 once per month for four long-range flights since 1997 (Brenninkmeijer, 2007). CONTRAIL started in 1993 with the installation of automated air sampling systems aboard passenger aircraft operated by Japan Airlines to obtain a long-term record of CO_2 and other trace gases. In 2005, the measurement equipment was extended by a continuous CO_2 analyser, based on non-dispersive infrared technique. IAGOS (In-service Aircraft for a Global Observing System; www.iagos.org), launched in 2005, continues the approach of MOZAIC (as 'IAGOS-core') and CARIBIC (as 'IAGOS-Caribic') but with modernized instrumentation and enhanced measurement

capabilities (Volz-Thomas et al., 2009; Petzold et al., 2015). New measurement systems for NO_x, GHGs, aerosols and cloud particles were developed and evaluated, and more international operating airlines were acquired to increase the number of equipped aircraft. Spatially, the program currently covers major parts of the world, with regular temporal coverage.

The IAGOS-core GHG package, measuring CO_2, CH_4, CO and water vapour using cavity ring-down spectroscopy (CRDS), was designed and tested in the framework of IAGOS - European Research Infrastructure (ERI), and the first package was successfully integrated in 2017. The aim is to have five systems deployed operationally aboard aircraft of different airlines within the next years, providing regular, long-term GHG observations covering major parts of the globe. With more than 600 flights per year and instrument, and on average 6 h per flight, the expected total flight-hours per year and instrument add up to more than 3600 h. The measurements will help to improve the predictive capabilities of global and regional climate models, which require a better understanding and quantification of processes and feedbacks controlling the atmospheric abundance of GHGs. Furthermore, observations of the vertical distribution of GHGs across the globe represent the most direct way to validate and anchor remote sensing based observations (e.g. GOSAT, OCO-2, TROPOMI) to the calibration scales used for in situ measurements (Araki et al., 2010), thus paving the way for a homogenized data basis to be used in inverse modelling of GHGs targeted at regional fluxes. Note that remote sensing instruments do not observe atmospheric abundances directly but derive them from measured radiances through retrieval algorithms. The atmospheric signature of the long-lived GHGs, CO_2 and CH_4, is closely related to the specifics of atmospheric transport, hence IAGOS GHG measurements provide essential data for validation and improvement of atmospheric tracer transport models (e.g. in simulating vertical transport), and help to assess stratosphere–troposphere exchange (STE) and lower stratosphere transport. A prominent example for such use of data collected by commercial airliners is given by Newell et al. (1999). Moreover, since all IAGOS data are sent by Global System for Mobile Communications to the central IAGOS-database directly after landing, and in future also near-real time via satellite in-flight, measurements are utilized by the Copernicus Atmospheric Monitoring Service (CAMS) and weather-prediction centers.

All data of the IAGOS-core GHG package, from near-real time to final, will be provided free and with unrestricted access for scientific (non-commercial) use at the IAGOS database (www.iagos.org) and, regarding near-real time data, within the World Meteorological Organization Information System (WIS). Final data will be also submitted to the World Data Centre for Greenhouse Gases.

CO_2 and CH_4 flight analysers based on CRDS have been used for several short-term airborne studies in the past years (Chen et al., 2010; Messerschmidt et al., 2011; Turnbull et al., 2011; Geibel et al., 2012; Peischl et al., 2012; Tadić et al., 2014). A system designed for long-term airborne operation, similar to what is intended here, is described by Karion et al. (2013). They have performed bi-weekly flights over Alaska, conducted with a Hercules C-130 aircraft from March to November each year, with a total of 38 successful flights during the first three seasons (2009–2011). The IAGOS GHG system however differs in its design due to different requirements within the IAGOS project: rather than bi-weekly there are daily flights throughout the year; the cruising altitude is

around 10–12.5 km (corresponding to about 260–180 hPa) compared to 8 km (around 360 hPa) for the Hercules C-130 aircraft; finally the instrument has to operate fully unattended over 6 months of deployment.

This chapter presents the IAGOS-core GHG measurement system, based on wavelength-scanned cavity ring-down technique, for the autonomous measurement of the GHGs CO_2 and CH_4, CO and water vapour. It is designed for the deployment aboard commercial aircraft to provide regular, long-term GHG observations with near-global coverage. The calibration strategy, partially developed within the IGAS project (IAGOS for the GMES Atmospheric Service, a European Commission's Seventh Framework Programme project) will be introduced, and results from test flights and laboratory tests which validate the performance and airworthiness of the instrument are presented. The measurement principle and setup of the system, as well as instrument operation are introduced in Section 2.2, followed by laboratory experiments and their results, which are used to assess instrument performance under flight conditions, in Section 2.3. The calibration chain, ensuring traceability of the measurements to the WMO primary scales, is described in Section 2.4. A detailed uncertainty analysis for the measurement data is presented in Section 2.5, while Section 2.6 contains results from a test flight of the measurement system. Section 2.7 concludes the chapter.

2.2 The Measurement System

2.2.1 Measurement principle

The instrument is based on a commercial analyser developed by Picarro Inc. (model G2401-m, Santa Clara, CA) and simultaneously measures CO_2, CH_4, CO and water vapour at high precision. The measurement principle is wavelength scanned CRDS technique, using spectral lines in the infrared (Crosson, 2008; Chen et al., 2010).

A sample cell (‘cavity’, 35 ml), equipped with three high-reflectivity mirrors (>99, 995 %), is constantly flushed with the sample gas during operation. For a measurement, laser light of a specific wavelength is injected into the sample cell through a partially reflecting mirror and gets reflected between the three mirrors (path length 15–20 km). The light intensity, which is monitored through a second partially reflecting mirror using a photodetector located outside the sample cell, builds up over time and as it reaches a threshold the laser is turned off. The following exponential decay of the light intensity (‘ring-down’) is modulated by absorption of the sample gas. Making use of the decay time (‘ring-down time’), the absorption coefficient can be calculated independent of fluctuations in the laser light intensity. By tuning the wavelength of the laser, a specific spectral line of a species can be scanned. Mathematical analysis of this absorption line provides a quantity, which at constant pressure and temperature is proportional to the mole fraction of the species.

The analyser uses selected spectral lines in the infrared for the measurements: at 1603 nm for $^{12}C^{16}O_2$, at 1651 nm for $^{12}CH_4$ and $H_2\ ^{16}O$ and at 1567 nm for $^{12}C^{16}O$. Three telecom-grade distributed feedback lasers provide light of the appropriate wavelengths.

To minimise impact on gas density and spectroscopy, pressure and temperature in the sample cell are kept constant.

2.2.2 Setup of the measurement system

The instrument is designed for but not limited to deployment aboard Airbus A340 and A330 aircraft as part of the IAGOS project. The IAGOS installation provides a mounting rack, installed in the avionics bay below the cockpit, with electrical [28 V power supply; Weight-on-Wheels (WoW) signal from the aircraft] and pneumatic (air inlet and exhaust; fan for ventilation) provisions for installation and operation, as well as the central data acquisition system which collects the aircraft position and other aircraft parameters that are relevant for georeferencing of the measurements. An aircraft-qualified aluminium box (350 mm × 300 mm × 530 mm), which is attached to a baseplate by six shock absorbers to provide a vibration-damped mounting of the instrument frame, serves as an enclosure for the components of the instrument. The modules of the commercial CRDS-analyser were evaluated regarding their airworthiness on board passenger aircraft, and parts were replaced where necessary. Particularly, the wiring and tubing required replacement by non-flammable components to meet the requirements regarding fire-prevention regulations. The modified parts, together with a specially designed calibration system, were integrated into the frame. Several circuit breakers, fuses and electromagnetic interference (EMI) filters were added to protect the electronic system of the instrument as well as the electronics of the aircraft. The selection of material in contact with either the sample or the calibration gases was not always optimal for the measured species, but it is subject to external constraints (e.g. only specific pressure regulators were qualified for use within IAGOS). Thus, specific care needed to be taken to work around any negative impacts on the quality of the measurements.

Table 2.1 shows an overview of the main parts of the instrument and their functions. A schematic gas flow diagram is given in Figure 2.1.

In order to provide uncontaminated ambient air to the instrument, it is equipped with an inlet line [3.18 mm (1/8”) OD Fluorinated Ethylene Propylene (FEP) tube, 60 cm], which is connected to a Rosemount Total Air Temperature (TAT) housing (model 102B; Stickney et al., 1994) mounted on the inlet plate at the fuselage of the aircraft. The Rosemount probe offers several advantages: it acts as a virtual impactor since the inlet line is pointed orthogonal to the airflow through the housing, and thus prevents from sampling larger aerosols (larger than about 2 µm), ice particles and water droplets; due to the strong speed reduction of the air it provides positive ram-pressure; and as standard housing for temperature and humidity sensors on board civil aircraft it already possesses the required certifications (Fahey et al., 2001; Volz-Thomas et al., 2005). The additional positive ram-pressure of around 60 hPa at the ceiling level of 12.5 km, together with a low sample gas flow of 100 ml/min (100 sccm) (standard conditions for all given flows and volumes here and in the following: T=20°C, p=101 kPa) and the relatively short inlet line ensures operation of the instrument throughout the aircraft altitude operating range up to 12.5 km without an upstream sampling pump. Selection of the inlet line material (FEP) was made considering its suitability for the measurement of different species, as the IAGOS-core GHG system can be fully interchanged with the IAGOS-core NO/NOx and NO/NOy system and the characteristics of the material are

particularly appropriate for these measurements. Given the short residence time of sample gas, the small inner surface area, the small mole fraction differences between ambient and cabin air and the low permeability of FEP, any impact from diffusion of CO2, CH4 and CO is minimal. The sample flow is exhausted through an exhaust line [6.35 mm (1/4") OD FEP tube, 60 cm] connected to the exhaust duct included in the inlet plate.

The connection between Calibration Stop Valve and the tee-connector (see Figure 2.1), which connects ambient air, calibration gas and the sample cell, is kept small [2.5 cm long 3.18 mm (1/8") OD tube, 2 mm ID] to minimise the dead volume when measuring ambient/cabin air. Diffusion flow from the dead volume into the sample gas is <0.1 % of the sample flow 30 s after switching from calibration to ambient/cabin sampling and can thus be neglected.

Table 2.1: Description of sub-assemblies and auxiliary parts

Part or assembly	function / description
Frame	Aluminium box hosting all parts and providing the mechanical, electrical, and pneumatic interface to the installation structure and to the calibration gas cylinders
Functional parts:	
Cavity Enclosure	Contains the sample cell (cavity). The enclosure is temperature controlled and set to T=45°C.
Wavelength Monitor Enclosure	Contains the wavelength monitor. The enclosure is temperature controlled. Setpoint is 45 °C.
Vacuum Pump	Provides the airflow through the instrument.
Laser System	The four-channel analyser uses three telecom-grade distributed feedback lasers, mounted on similar diode laser electronic boards. Laser light is carried by fibre optics. A Semiconductor Optical Amplifier (SOA) amplifies the laser light before the measurement.
Calibration System	Controls three valves to calibrate the instrument with standard gas provided by the two high pressure cylinders.
Thermo Switches	Interrupt the electrical power provision to the whole instrument at temperatures above 70°C.
Auxiliary parts:	
Data Acquisition System and Power management	Circuit breaker; DC/DC converters for generation of 12V, -12V, 3.3V, 5V and 24V; Computer board to manage the data storage and handling the data transfer to the PI data interface; Power Board and Logic Board to control the subunits; SSD; AD-converter

To protect the sample cell from contamination, filters (Wafergard II F Micro In-Line Gas Filters, Entegris Inc.) are implemented. They also ensure thermal equilibration of the sample gas, as they are kept at the same temperature as the sample cell.

Pressure in the sample cell is controlled to 186.65 hPa (=140 Torr, variations of less than 0.04 hPa) with a proportional valve ('inlet valve') upstream of the cell, and the temperature is kept at 45°C (variations of less than 20 mK). Gas flow through the sample cell is controlled at 100 ml/min by a fixed flow restrictor (capillary) downstream of the sample cell and upstream of the pump. This capillary acts as critical orifice, as the pressure drops by more than a factor two between sample

cell and pump. This makes the flow rate independent of ambient or cabin pressure. A pressure relief valve [set point 0.07 bar (1 PSIG)] protects the sample cell from accidental excess pressure. Each species is measured once every 2.3 s. The physical exchange time of the sample cell is 3.6 s (volume=35 ml, sample flow=100 ml/min, pressure=186.65 hPa, sample temperature=45°C), ensuring that the ambient air is continuously sampled given the shorter measurement interval of 2.3 s.

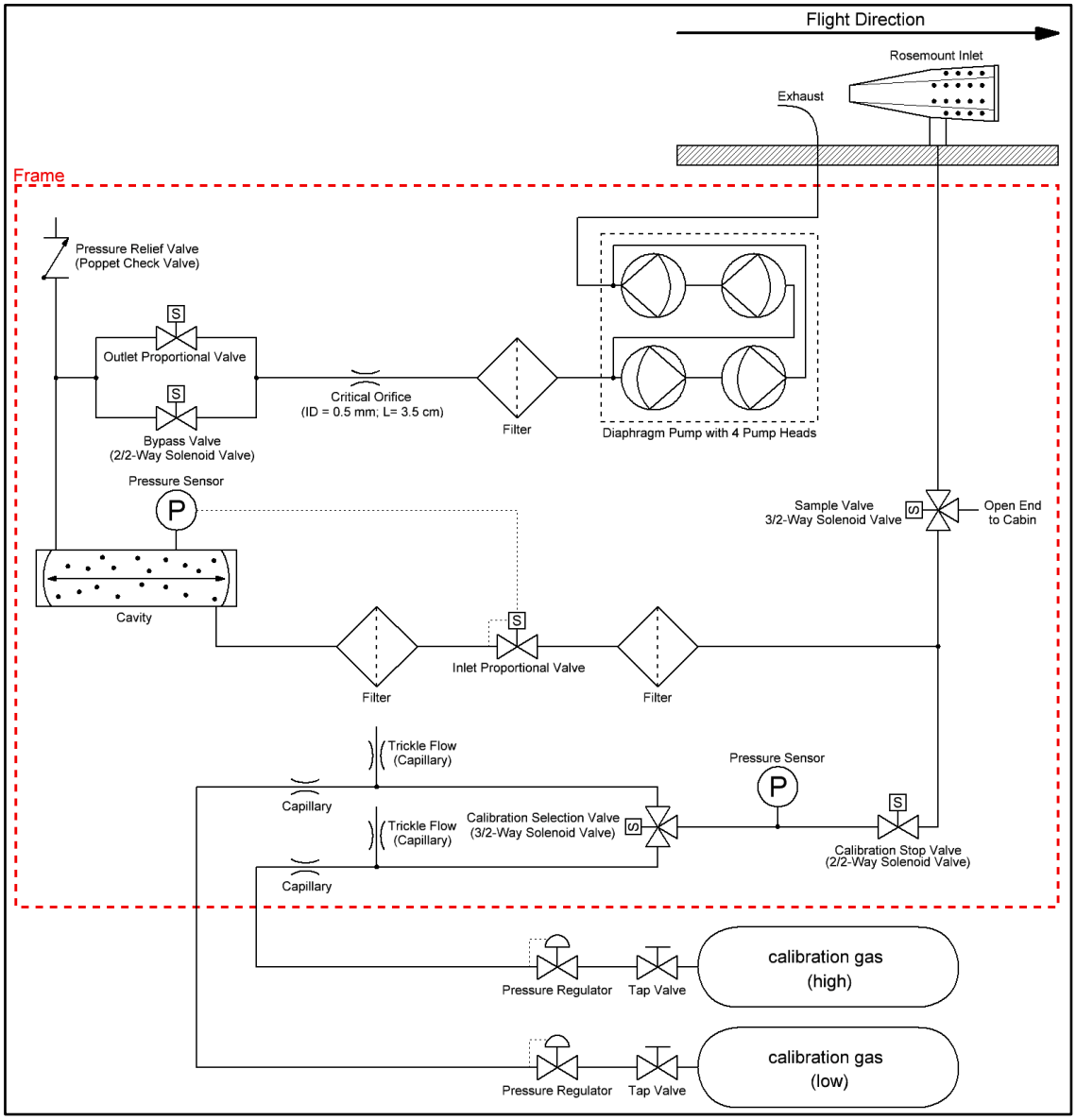

Figure 2.1: Schematic flow diagram of the IAGOS GHG measurement system.

The instrument has provisions to be connected to two fibre-wrapped aluminium cylinders (AVOX 897-94077 Cylinder and Valve Assembly, 17.1 l, max. filling pressure: 124 bar) filled with calibration gas. The connection to the outlets of the cylinder pressure regulators (AVOX 27660-19 Oxygen Regulator Assembly, sealing ring material: KEL-F81, membrane: silicon rubber) is made via coiled 1.59 mm (1/16") OD stainless steel tubes equipped with quick connectors [Stäubli Tec-Systems GmbH, model RBE03, sealing: fluoric rubber (FPM)]. The quick connectors are sealed

when not connected. During laboratory tests, it has been observed that the cylinder valves and pressure regulators can alter the composition of the calibration gas when the valves are open. For example, the pressure regulators were closed for different time spans and the gas composition was measured after they were opened again. It was found that already after 90 min of closing the CO_2 and CH_4 mole fractions at the beginning of the flushing period showed maximum deviations of more than 3 ppm, 4 ppb, respectively, from the final values, which were reached not until 30 min, 15 min respectively, of flushing. Such effects are known to be caused by permeation of CO_2 and CH_4 from the high- to the low-pressure side through polymer seal rings and by surface interaction effects (Sturm et al., 2004). Using theoretical calculations, the back-diffusion from the regulators into the cylinders was estimated to be <0.1 ml/min. Thus in order to eliminate back-diffusion and minimise the impact of the permeation and surface interaction effects in the regulator (in the following referred to as 'regulator effects'), a trickle flow of 2.8 ml/min is applied to constantly flush the regulators.

2.2.3 Instrument operation

The measurement system operates fully automatically and without interruptions as long as the aircraft has power. The functions of the instrument are controlled by a single-board PC using Picarro Inc. measurement software.

Two operation modes are implemented to fulfil the different measurement requirements while the aircraft is in air (about 12 h/day, depending on the exact flight schedule) or on ground (about 8 h/day):

1. Ground Mode: The instrument measures air from inside the frame (cabin air, i.e. outside air filtered by the air conditioning system) to protect the analyser from highly polluted air. Sample valve is off (see Table 2.2 and Figure 2.1). High frequency of calibrations enabled.
2. Flight Mode: Ambient air is measured, and the calibration frequency is lower than on the ground.

To switch between ground and flight modes, the WoW signal from the aircraft is used. In the laboratory, the instrument can be operated in ground mode, flight mode and manual mode, where all valves and I/O functions can be switched individually.

The instrument is calibrated at regular intervals by measuring calibration gas provided by two fibre-wrapped aluminium cylinders. Each cylinder contains dried ambient air, but with different CO_2, CH_4 and CO concentrations (high-span and low-span). With the help of three valves (sample valve, calibration stop valve, calibration selection valve; GEMS Sensors Inc., G- & GH-Series) the gas flow through the measuring cell can be switched between calibration gas and air from the inlet respectively in the cabin, as can be seen in Figure 2.1 and Table 2.2.

Table 2.2: Valve selection for different instrument modes

Instrument Mode	Sample Valve (off = cabin air)	Calibration stop valve	Calibration selection valve
Ground mode	Off	Off	Off
Calibration tank I (at ground)	Off	On	Off
Calibration tank II (at ground)	Off	On	On
Flight mode	On	Off	Off
Calibration tank I (during flight)	On	On	Off
Calibration tank II (during flight)	On	On	On

The calibration gas flow is maintained by capillaries acting as flow restrictors with an upstream pressure regulated to 570–670 kPa (5.7–6.7 bar, depending on the cylinder pressure and cabin pressure) with pressure regulators. This pressure is monitored with a pressure sensor in the calibration gas line (GCT-225 model, Synotech GmbH). Calibration gas flow is kept above 110 ml/min, ranging up to 165 ml/min with nearly empty cylinders and at lowest cabin pressure (800 hPa), and thus higher than the normal sample flow (100 ml/min). During calibration, the excess flow of at least 10 ml/min leaves the system backwards through the inlet to ensure that no air from outside is entering the system.

Although small variations in sample gas flow have no impact on the measurements, it is important to monitor the flow as it affects the exchange rate of the sample gas. When the instrument switches between ambient air, cabin air, or calibration gas measurement, time passes until the change in signal occurs. The flow is inversely proportional to this lag time and can be calculated if the inner volume of the flushed tubing is known. To allow a regular determination of the sample flow, the 'open end to cabin' in Figure 2.1 is realised as a 1.3 cm (0.5") ID tube with a length of about 22 cm. Thus, the lag time when switching from calibration gas to cabin air during ground operation is extended, which together with the cabin pressure measurement allows monitoring the flow with ~5 % accuracy.

For reporting dry air mole fractions, the system requires no drying of the sample air, as the simultaneously measured water vapour mole fraction is used to correct for dilution and spectroscopic (pressure-broadening) effects. The parameters of this wet-to-dry correction are based on laboratory experiments made with each IAGOS-core GHG instrument during each maintenance cycle, i.e. every 6 months, as this method has been shown to result in the lowest uncertainty in the water vapour correction (Chen et al., 2013; Rella et al., 2013).

Further tests will be made regarding the implementation of an updated software parameter, affecting the transition time between wet and dry measurements, to avoid artificial gradients between wet and dry air, e.g. boundary layer and free troposphere, or troposphere and stratosphere (Karion et al., 2013).

2.3 Laboratory tests

To prepare the IAGOS-core GHG instrument for deployment on board commercial aircraft and ensure a reliable performance of the analyser, tests in the laboratory were conducted to assess airworthiness and measurement characteristics, detect functional limits and develop needed corrections.

2.3.1 Instrument response stability

To assess the long-term stability of the measurement system and design an initial calibration strategy (particularly calibration frequency), dried ambient air from a high-pressure tank was measured continuously for 24 h. The first 3 h were removed to ensure dry and stable conditions. Analysis of the data by Allan variance technique (Allan, 1966, 1987), using the R-package 'allanvar', determined the standard deviations of the raw 0.4 Hz data as 0.039 ppm for CO_2, 0.40 ppb for CH_4 and 15 ppb for CO. As can be seen in the resulting Allan deviation plots (see Figure 2.2, blue data points) the CO and water vapour signals are, at a timescale of ~10 000 s, dominated by white noise (green line), while for CO_2 and CH_4 also other effects, e.g. drift, are an issue. Since random errors are uncorrelated, precision of the CO measurements can be reduced by applying temporal integration. Passenger aircraft travel approximately 1 km horizontal and 30 m vertical in 4 s. Therefore, an integration time of 3 min, reducing the precision to 1.7 ppb, would be sufficient for global and regional atmospheric models with typical horizontal resolutions of around 50–100 km. To eliminate drift impact on the CO_2 and CH_4 measurements, calibrations are needed. The Allan variances shown here are obtained under laboratory conditions and it needs to be assessed during the first flight period if they can be achieved under flight conditions, too. Therefore, a conservative initial frequency of three-hourly calibrations (every 10 800 s) during flight is chosen, which allows for at least two calibrations per flight. On ground, an even higher frequency with two-hourly calibrations is chosen, to utilise the time where no measurements are made for detailed drift analysis.

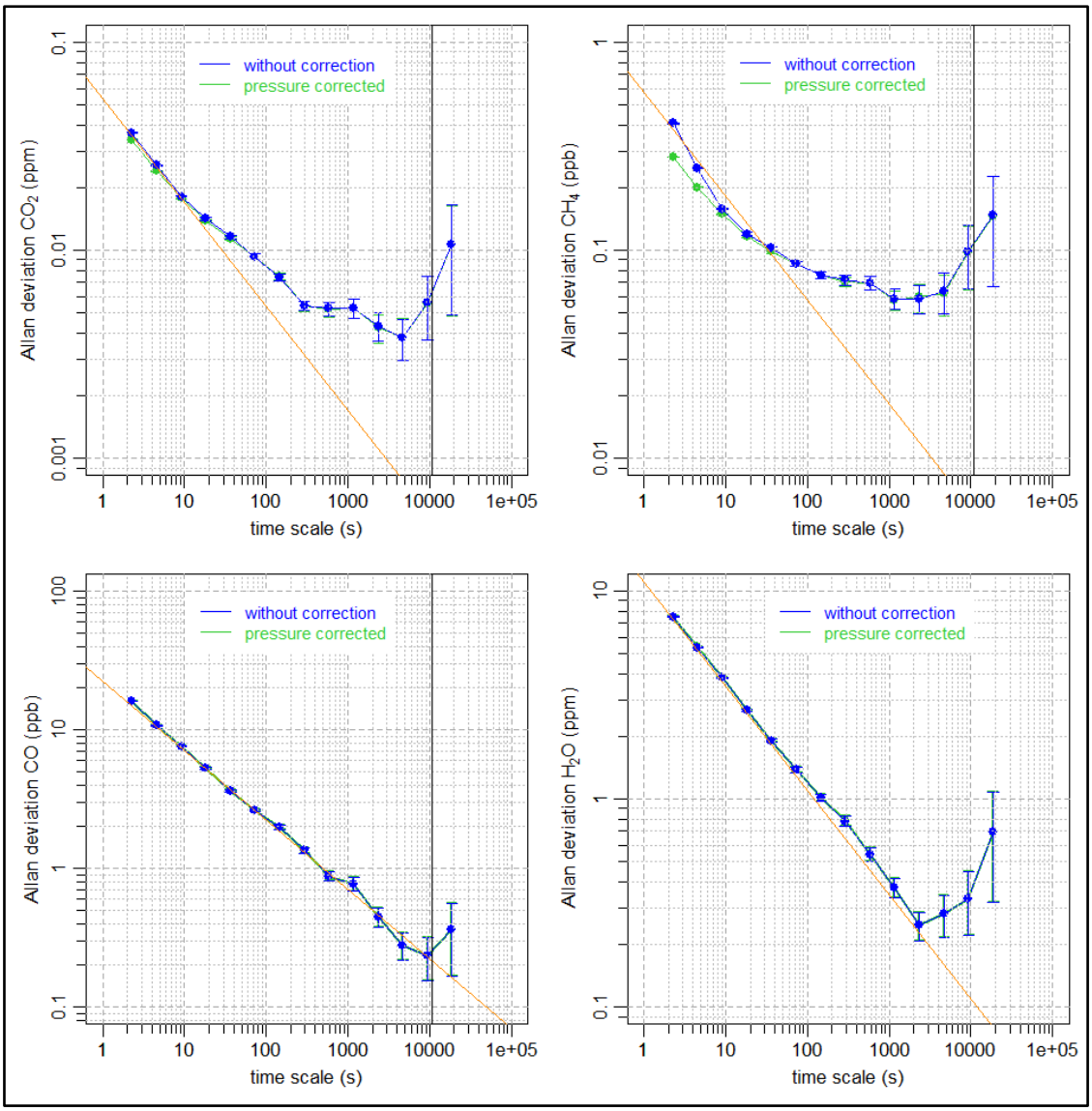

Figure 2.2: Allan deviation plots of a 21-h measurement of dried, ambient air from a high-pressure tank for CO_2, CH_4, CO and H_2O. The raw measurement data are shown in blue, data corrected for sample cell pressure deviations in green. The orange line (slope −0.5) shows the region of Gaussian or white noise. The black vertical lines at 10800 s (3 h) indicate the planned calibration frequency.

2.3.2 Calibration tests

The fully automated calibration system was tested in the laboratory by executing a typical measurement cycle during deployment of the instrument on board aircraft with alternating measurements of ambient air (during flight), respectively cabin air (on ground) and calibration gas. Trickle flow was adjusted to 2.8 ml/min. The 'Weight on wheels' signal from the aircraft was simulated with a mock-up to switch between ground and flight modes and hence between different calibration sequences (3 hourly in air, 2 hourly on ground). A calibration consisted of a high-span and a low-span measurement of 10 min each, whereby the measurement order was swapped every other calibration.

Figure 2.3 shows a single, low-span calibration measurement during the simulation. After starting the calibration, a distinct delay for CO_2 (black points) and CH_4 (dark green points) and H_2O (blue line) can be observed until the measurement is stable. For water vapour, this is caused by the switch from wet ambient/cabin air to dry calibration gas, and by desorption of H_2O from the walls of the inlet line downstream of the sample valve. For CO_2 and, to a lesser extent for CH_4, the main reasons for this 'transition effect' are diffusion and surface interaction effects in the pressure regulator of the calibration gas cylinder, mainly preferential permeation of CO_2 through sealing rings (membrane: silicon rubber; Sturm et al., 2004). The transition time from wet to dry gas related to the slow update of the CO_2 and CH_4 baselines in the Picarro measurement software (Karion et al., 2013) is not important here, since this effect is small and of shorter duration compared to the regulator effects. For CO, the measurement variability is too high to see any transition effects.

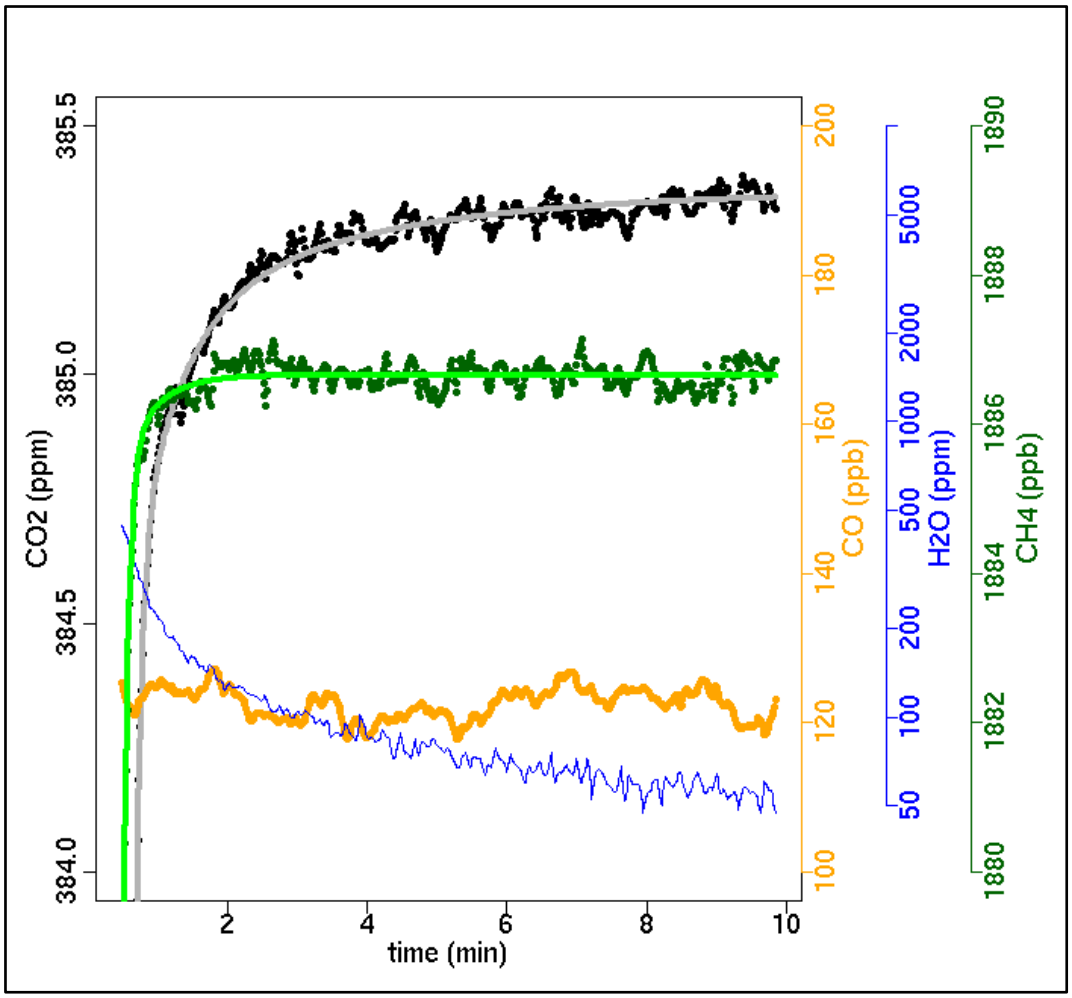

Figure 2.3: Low-span calibration measurement (CO_2 – black, CH_4 – light green, CO – yellow, H_2O – blue) during simulation of a typical measurement cycle with a trickle flow of 2.8 ml/min. 'Time' is the time after the calibration was started in minutes. For CO_2 and CH_4 exponential fitting curves to the calibration time series are shown in grey and light green, respectively.

Since the amount of calibration gas is limited and needs to last for a full 6-month deployment period, the duration of each calibration needs to be limited. However, especially the measured CO_2 signal might not yet have reached the final value at the end of the calibration cycle. To reduce the impact from non-equilibrium calibration gas measurements, a fit procedure is applied to each calibration measurement to estimate the equilibrium values for dry air mole fraction for each calibration gas (grey line for CO_2, light green line for CH_4). For this, a combination of exponential functions is used:

$$X = X_{equilibrium} + \sum_i a_i * e^{-(t-t_0)/\tau_i} \qquad \text{(Equation 2.1)}$$

Here, X is the mole fraction, t the time and t_0 the starting time of the calibration plus 30 s. The first 30 s of a calibration are removed to allow for some initial flushing. The number of exponential functions used varies between one and three depending on the species. The parameters $X_{equilibrium}$, a_i and τ_i for the different species are determined by fitting an averaged time series of all 10-min calibration cycles (six low-span calibrations + six high-span calibrations) performed in the laboratory. This procedure is possible since tests with different calibration frequencies (from hourly to daily) and different mole fractions of the previous measurements (350–420 ppm for CO_2, 1600–2000 ppb for CH_4, 20–300 ppb for CO) indicated, that the characteristics of the calibration time series are reproducible and nearly independent of the different calibration frequencies, and the difference in mole fraction to the previous measurement (after accounting for the 30 s flushing time). After the average temporal characteristic of the transition effect is captured with Equation 2.1, the following equation is used to fit each individual calibration:

$$X_j = c_j + X_{equilibrium} + b_j * \sum_i a_i * e^{-(t-t_0)/\tau_i} \qquad \text{(Equation 2.2)}$$

Here, a correction c_j to the equilibrium mole fraction $X_{equilibrium}$ and a factor b_j to scale the sum of the exponential functions are adjusted.

To assess to which degree this procedure allows for reducing the length of a calibration, Equation 2.2 was fitted to each individual time series of the above mentioned 10-mine calibrations, whereby the length of the time interval used for fitting was varied between 4 and 560 s. Figure 2.4 shows the mean and the standard deviation of the 12 fitted correction factors c_j for CO_2 and CH_4 depending on the time span used for the fit, i.e. the calibration length minus 30 s flushing. While the mean is not changing any more after around 30 s (variations of >0.005 ppm for CO_2 and 0.01 ppb for CH_4), the standard deviations still decrease. After 150 s (calibration length of 3 min) the standard deviation for CO_2 (CH_4) is 0.07 ppm (0.19 ppb), after 270 s (5 min calibration length) it is 0.05 ppm (0.17 ppb). Compared to a 10-min long calibration, this means an increase in the standard deviation, and thus an increase in the uncertainty of the correction factor c_j, of 0.03 ppm for CO_2 (0.04 ppb for CH_4) for a calibration length of 3 min, and of 0.01 ppm (0.03 ppb) for a calibration length of 5 min. This procedure will be regularly reassessed during maintenance.
For CO, the experiments showed that no fit procedure is needed, and the calibration gas measurement is obtained by averaging the measurement data, after discarding the first 30 s.

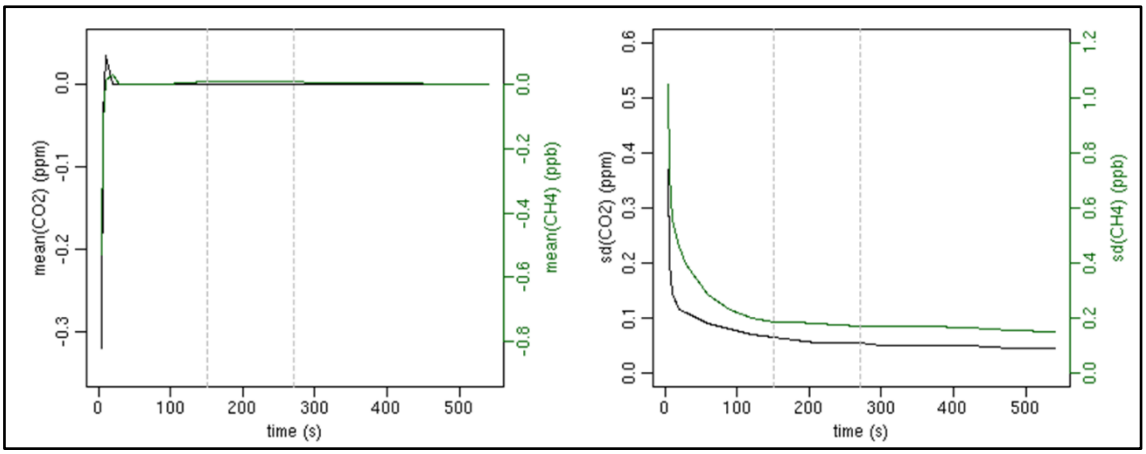

Figure 2.4: Mean and standard deviation (SD) of the eight fitted corrections c_j for CO_2 and CH_4 as a function of the time interval used for fitting the calibration measurement. 'Time' is the time after 30 s flushing. The grey vertical lines indicate 3- and 5-min calibration lengths (150 and 270 s, respectively).

2.3.3 Pressure test

During flight, the instrument faces a wide range of atmospheric pressures at the air inlet and outlet. Air pressure decrease during ascent varies from 100 hPa/min at lower altitudes (0–3 km, corresponding to 1000–700 hPa) to 10 hPa/min at higher altitudes (9–12 km, corresponding to 300–200 hPa). Similarly, pressure increase during descent lies between 100 and 20 hPa/min for lower and higher altitudes, respectively. At ceiling level (approximately 12 km), the inlet pressure drops to about 250 hPa. This is higher than the real air pressure at that height since the Rosemount inlet provides additional ram-pressure of around 60 hPa. For the backward-facing air-outlet negative ram-pressure has to be taken into account, which leads to outlet pressures down to about 130 hPa at ceiling level. To assure that the sampling pump downstream of the sample cell can cope with the low pressure conditions and keep the sample flow stable at 100 ml/min and that the pressure adjustment in the sample cell is fast enough to compensate for the strong pressure gradients, parameters of the pressure control loop were adjusted and an appropriate test was performed in the laboratory. Pressure at the outlet was lowered with the help of an additional pump downstream of the instruments pump, with a needle valve in between to adjust the pressure. To achieve the required inlet pressure variations, gas was provided to the instrument with an excess flow, which was lowered in pressure by a further pump, using a buffer volume and a needle valve for pressure control.

Figure 2.5 shows a complete pressure cycle including an ascending and descending flight profile with typical pressure gradients. Sample flow (in green) is nearly stable at 104 ml/min throughout the whole test with only small deviations during ascent (−2 ml/min) and descent (+2 ml/min) which are caused by the required pressure equilibration in the inlet line. This confirms the good performance of the sampling pump also at low air pressures. Pressure in the sample cell (in blue) is stable at its setpoint of 186.65 hPa (dark blue line) when the inlet pressure is stable regardless of whether the actual pressure is high or low. During normal changes of the inlet pressure, like they occur during flight, the sample cell pressure shows small deviations up to 0.03 hPa. Only for large changes in inlet pressure at pressure levels lower than 300 hPa (changes by 40 hPa/min, see

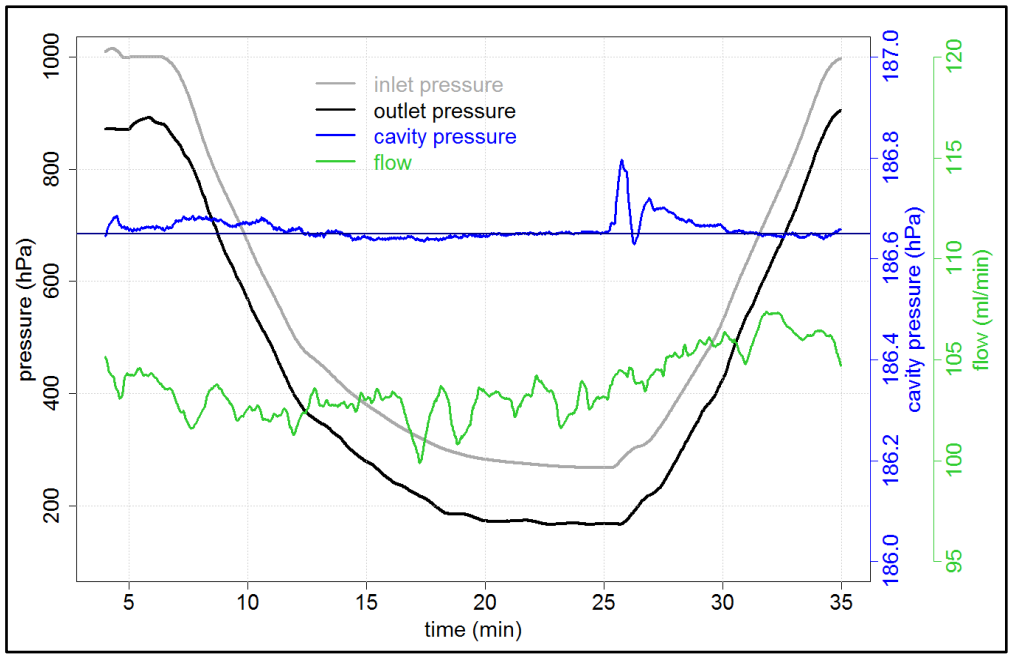

Figure 2.5: Typical pressure changes during flight profile measurements. Shown are the 30 s means of the pressure at the air inlet (in grey) and the air outlet (black), pressure in the sample cell (blue) and sample flow (green). The vertical dark blue line indicates the setpoint of the sample cell pressure at 186.65 hPa (corresponding to 140 Torr).

minute 26), the sample cell pressure deviation peaks at 0.15 hPa, indicating that the sample cell pressure adjustment is too slow to adapt.

Since the measurements of the instrument are calibrated at a sample cell pressure of 186.65 hPa, deviations in sample cell pressure result in erroneous GHG measurements due to changes in dilution and pressure-broadening effects with changing cell pressure. While dilution leads to higher signals with higher sample cell pressure, for pressure broadening it is the other way round. Figure 2.6 shows the deviation in the observed CO_2 signal due to pressure deviations in the sample cell, measured at a CO_2 mole fraction level of 390 ppm. The use of a linear fit (blue line) allows for a correction of the measurements. The correction factor (slope of the linear fit) is 0.35 ppm/hPa for CO_2, 6.18 ppb/hPa for CH_4 (at a CH_4 mole fraction level of 1920 ppb) and −2.1 ppb/hPa for CO (at a CO mole fraction level of 150 ppb). The negative correction factor for CO is likely due to a relatively stronger effect from pressure broadening than dilution for CO. Residuals of the raw CO_2 data can be seen in grey, the black points are mean values for sample cell pressure intervals of 0.1 hPa. It is obvious that the noise of the raw data is much larger than the actual correction. To assess quantitatively how much extra noise the sample cell pressure correction adds to measurement data, the data of the response stability test (Section 2.3.1) were pressure corrected using the raw 0.4 Hz sample cell pressure data, and the Allan variance was recomputed. The Allan Deviation plots in Figure 2.2 show the results for the uncorrected and the corrected data. The standard deviation of the corrected 0.4 Hz measurement data is decreased by 0.002 ppm for CO_2 and 0.1 ppb for CH_4 compared to the uncorrected values, while for CO and water vapour no changes were observed. This means that applying the sample cell pressure correction to the measurement data has no negative impact on the data quality.

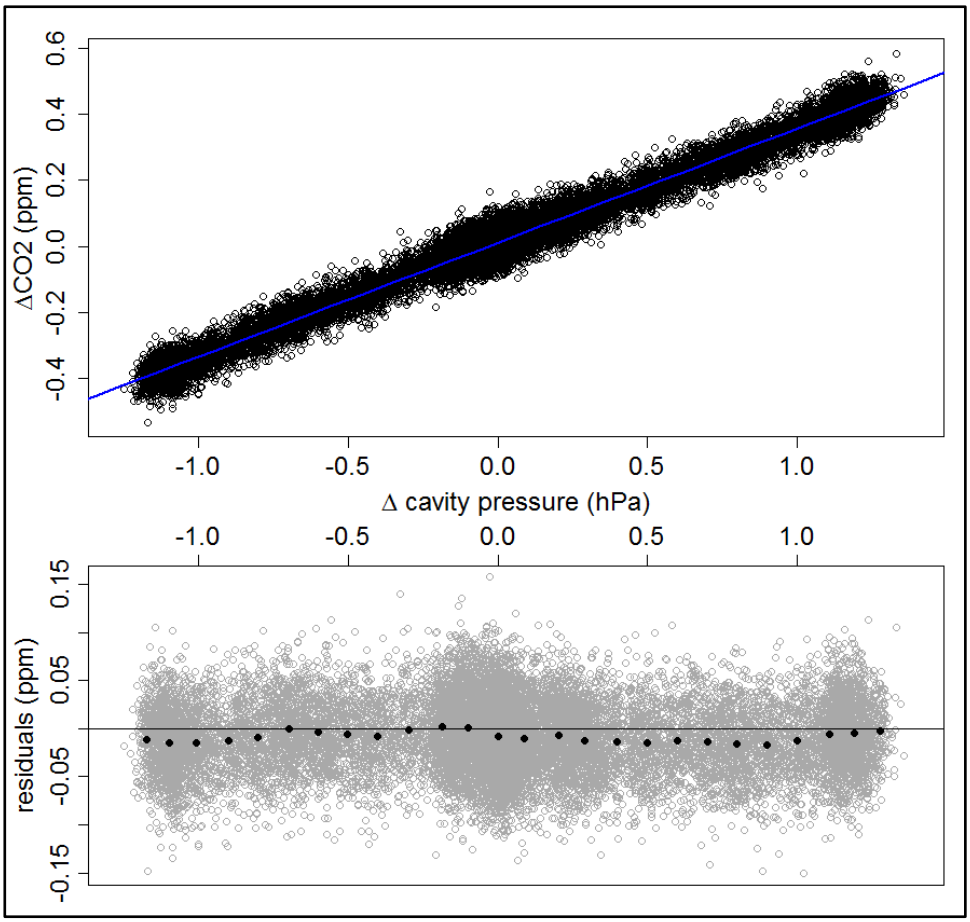

Figure 2.6: Error of the CO_2 measurement due to deviations in sample cell pressure referenced to the setpoint of 186.65 hPa (140 Torr), measured at a CO_2 mole fraction level of 390 ppm. The blue line is a linear fit of the data. The correction factor (slope of the linear fit) is 0.35 ppm/hPa for CO_2, 6.18 ppb/hPa for CH_4 (at a CH_4 mole fraction level of 1920 ppb) and −2.1 ppb/hPa for CO (at a CO mole fraction level of 150 ppb). Residuals are shown in grey, black points are the mean values for intervals of 0.1 hPa sample cell pressure.

2.3.4 Airworthiness tests

To assess the risks regarding mechanical and electrical performance (physical damage by loose or broken parts, EMI with the electronic system of the aircraft, exposure to abnormal power supply), the instrument was tested according to a specified qualification programme. Vibration and shock tests have been applied for all three orthogonal axes of the analyser. After the tests, no mechanical damages of the system have been detected. Tests concerning power input and voltage spikes, as well as EMI tests for conducted and radiated EMI proved that no inferences could adversely affect other aircraft systems.

After completing these qualification tests, the instrument was installed and tested in the first IAGOS equipped aircraft (Lufthansa D-AIGT) in May 2013. This 'Ground Test' included a general design inspection of the instrument as well as functional tests, and the absence of EMI with other aircraft systems was checked. The analyser passed all tests.

2.4 Calibration strategy

A single deployment period of the instrument in the frame of the IAGOS project lasts for approximately 6 months. The exact number of days depends on the maintenance schedule of the aircraft set by the airline. To ensure traceability of the IAGOS-core GHG measurements to the WMO primary scales, the calibration strategy includes measurements of standards traceable to the primary scale before and after the deployment period ('pre- and post-deployment calibration'), as well as regular measurements of calibration gas during the deployment ('In-flight calibrations'). When determining frequency and length of the in-flight calibrations, it has to be considered that the amount of calibration gas during one deployment period is limited by the size of the two gas cylinders (each with a capacity of 1600 standard litres of gas, which can be used for the calibrations) carried along.

2.4.1 CO_2, CH_4, CO

Traceability of the CO_2, CH_4 and CO measurements to the WMO primary scales [currently WMO X2007 scale for CO_2, WMO X2004 scale for CH_4, WMO X2014 scale for CO (WMO GAW report 206, 2012)] is ensured in a multi-step procedure:

During the 6-month deployment of the instrument aboard aircraft regular calibration takes place by measuring pressurised standard air from two calibration gas cylinders (mole fractions for CO_2, CH_4 and CO of approximately 375 ppm, 1700 ppb, and 70 ppb for the low and 400 ppm, 1900 ppb and 150 ppb for the high cylinder; 'in-flight calibrations'). Since the analyser detects only the most abundant isotopologue of each trace gas, standards were prepared with similar isotopic composition to that found in ambient background air. While the aircraft is on the ground, more frequent and longer calibrations will be made than during flight to ensure an optimal usage of measurement time in air. The first calibration on ground will always start 30 min after power is switched on to allow enough time for the warming phase of the instrument. After short power interruptions of some minutes, e.g. when the aircraft switches from self-power to gate-power and vice versa, the warm-up lasts for around 5 min. If the aircraft is parked longer without power supply, the warming phase takes longer. In air, the first calibration is scheduled after 1 h. That way no calibration takes place during ascent such that a full profile measurement is achieved. Nevertheless, after half-a-year deployment with usually two long-range flights per day and because of the different flight durations enough calibrations will be performed at all altitudes during descent so that any potential pressure effects can be detected. After landing, a calibration will be started immediately to assure that at least one calibration cycle is finished before power is shut off, when switching from self- to gate-power.

Figure 2.7 shows the lifetime of a calibration gas cylinder filling depending on the duration and number of in-flight calibrations and the trickle flow rate, which is used to constantly flush the regulator and thus minimise the impact of regulator effects. While a long calibration time and a large trickle flow reduce the uncertainty of the calibration gas measurement, a more appropriate drift correction can be achieved by a higher calibration frequency. As a compromise, in order to reach 6-month lifetime of the cylinder filling, a trickle flow of 3 ml/min and a 3 hourly calibration

frequency during flight, 2 hourly on ground, with 3 and 5 min duration of the calibrations in air and on ground, respectively, appears to be a suitable approach. It will be reviewed as soon as the first real flight data are available. Especially an envisioned 3-month test phase, which will allow for more frequent and longer calibrations, will be used to verify the calibration strategy.

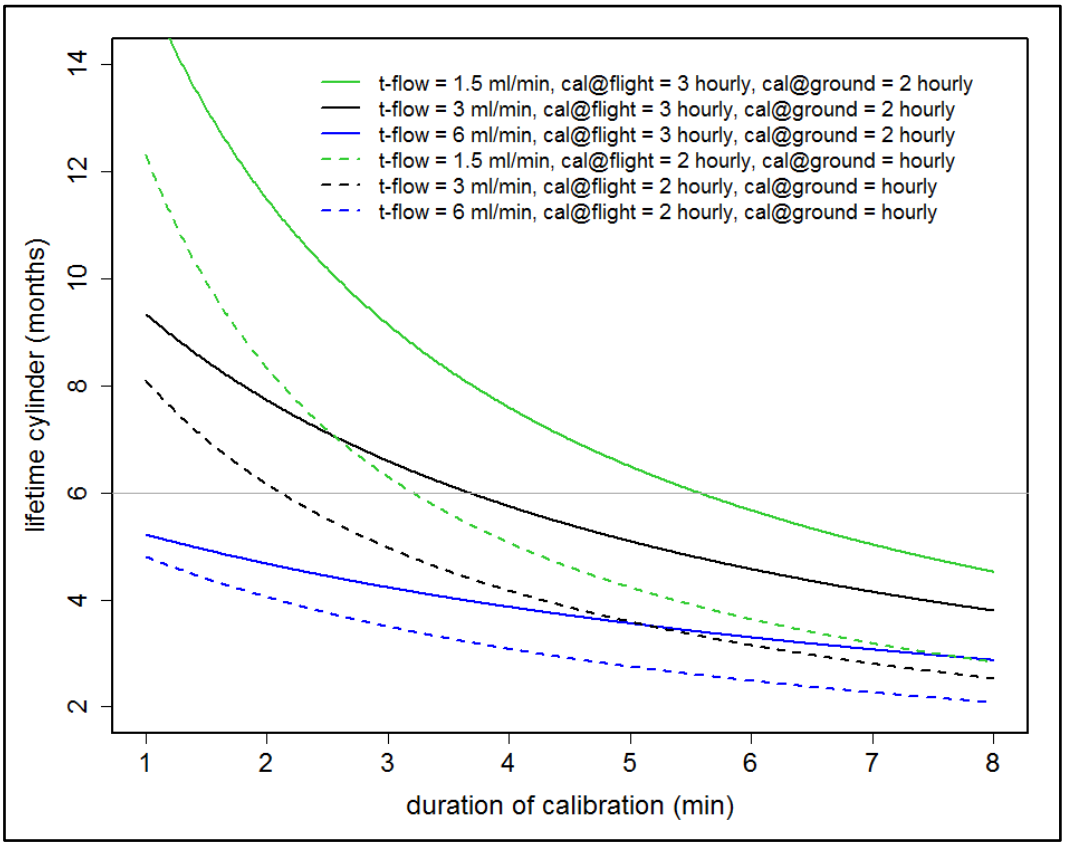

Figure 2.7: Lifetime of a calibration gas cylinder filling for various calibration scenarios. t-flow stands for trickle flow, cal@flight(ground) is the calibration frequency during flight (on ground). The grey horizontal line indicates a lifetime of 6 months.

After the deployment period, the calibration gas cylinder assembly (cylinders, pressure regulators, tubing) and the instrument get re-calibrated at the Max Planck Institute for Biogeochemistry (MPI-BGC) with the help of three working standards ('post-deployment calibration'). These working tanks are filled with pressurised, dried ambient air at the GasLab of the MPI-BGC and are measured against calibrated reference gas mixtures (tertiary standards) provided by the WMO Central Calibration Laboratory (CCL) that maintains the primary scale. The in-house tertiary standards are regularly (every 3–5 years) recalibrated by the CCL. CCL for all three species (CO_2, CH_4, CO) is NOAA/ESRL. The flow diagram in Figure 2.8 illustrates the calibration chain of the CO_2, CH_4 and CO measurements.

After the post-deployment, calibration and maintenance the calibration gas cylinders are refilled, and the calibration gas cylinder assembly and the instrument are calibrated again with the help of three working standards traceable to the respective primary scales ('pre-deployment calibration'). Later, instrument and cylinders are shipped for a new deployment period.

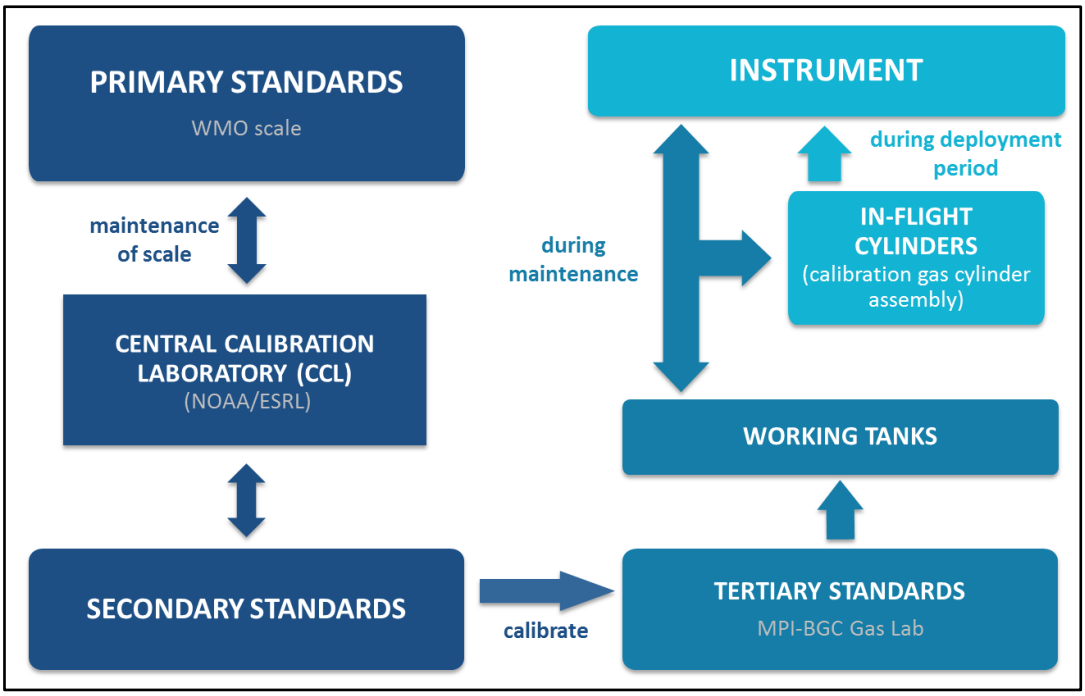

Figure 2.8: Calibration chain of the IAGOS-core instrument ensuring the traceability of the measurements to the World Meteorological Organization primary scales.

A settling time of 2 weeks between filling and measuring the calibration gas cylinders ensures that a representative measurement of the gas can be made, as experience with the first set of calibration gas cylinders indicated. Hence, the cylinders might be replaced by a different set for the next flight period depending on the time schedule.

During both, pre- and post-deployment calibrations, the same pressure regulators for the in-flight calibration gas cylinders are used as during flight operation. This minimises impact from potentially different effects on CO_2 from different regulators (i.e. with a different serial number). To reduce impact from wall effects in the calibration gas cylinders (release of CO_2 bound to the cylinder walls), the final pressure (at the end of the post-deployment calibration) is kept above 3 MPa (30 bar; Daube et al., 2002).

The role of the in-flight calibrations in the data processing will be assessed as soon as first data are available. Possible options: fully rely on each individual in-flight calibration; fully rely on the linear drift of the instrument between the pre- and post-deployment calibrations in the laboratory; or a mixture of both options, e.g. only a temporal average of the in-flight calibrations is used for the correction, as described by Karion et al. (2013).

The data management system allows for easy reprocessing and propagation of scale changes from the secondary standards to the final measurements.

2.4.2 Water vapour

Currently, the water vapour measurements are not calibrated regularly against a reference standard that is traceable to the primary scale. For the initial water calibration of the instrument, the calibration constants of a similar instrument (G1301-m, Picarro Inc.) calibrated at MPI-BGC Jena against a dew point mirror [Dewmet, Cooled Mirror Dewpointmeter, Michell Instruments

Ltd., UK, referenced to National Institute of Standards and Technology (NIST)] in the range from 0.7 to 3.0 % were transferred to all subsequently manufactured CRDS instruments by Picarro Inc. (Winderlich et al., 2010).

2.5 Uncertainty analysis

The current uncertainty analysis of the IAGOS-core GHG instrument measurements is based on laboratory tests and test flights on a research aircraft. For the first installation of the instrument aboard passenger aircraft, a 3-month test phase is envisioned. This will allow for detailed checks of all instrument functions, more frequent and longer calibrations than during normal 6-month deployment periods, and a review of the overall uncertainties. An up-to-date detailed uncertainty analysis will be provided and regularly updated in the document 'Standard Operation Procedure for the IAGOS-Core GHGs Instrument (P2d)' at the IAGOS database (www.iagos.org). Final data, stored at the database, include individual uncertainty components (e.g. from calibrations, wet-to-dry correction, isotopic effects) for every observation. These time-dependent uncertainty estimates will for CO_2, CH_4 and CO include effects from varying water vapour content, varying mole fractions (relative to the calibration range set by the low-span and high-span gases), and possibly effects rising from different air pressure. In the following, we discuss conservatively estimated uncertainties, but for mole fractions within the calibration range.

2.5.1 CO_2, CH_4, CO

Table 2.3 shows the different contributions to the overall uncertainties of the CO_2, CH_4 and CO measurements. The individual components concern the referencing of the in-flight calibration gases to WMO primary standards, but uncertainty in the conversion of observed wet mole fractions to dry air mole fractions is also included. Instrument response drift is compensated by regular calibrations. As the steps in calibration transfer are independent from each other, and independent of the uncertainty introduced by the wet-to-dry correction, propagation of uncertainties is made assuming that all contributions are independent (Gaussian error propagation assuming independent variables). Only the bias for isotopic effects is added linearly. MPI-BGC GasLab implementation of the WMO primary scale for CO_2 covers uncertainty of the NOAA secondary standards (0.014 ppm; Zhao and Tans, 2006) and tertiary standards (0.014 ppm). The MPI-BGC GasLab has seven tertiary standards available and thus, the uncertainty of the BGC-GasLab implementation of the WMO CO_2 primary scale can be calculated using the following equation:

$$\sqrt{(0.014\ ppm)^2 + (0.014\ ppm/\sqrt{7}\ )^2} = 0.015\ ppm \quad \text{(Equation 2.3)}$$

For CH_4, an uncertainty of the WMO tertiary standards of 0.7 ppb is assumed (Dlugokencky et al., 2013). This tertiary standard set includes standards at non-ambient mole fractions, which might be slightly biased, such that 0.7 ppb is taken as uncertainty of the MPI-BGC GasLab implementation of the WMO CH_4 primary scale. For CO, uncertainty of tertiary standards is adopted from the GAW Report No. 206 (WMO, 2012).

Table 2.3: Estimates of the different uncertainty components for the IAGOS-core CO_2, CH_4 and CO measurements and the resulting overall uncertainties (1-sigma). Also listed are the GAW compatibility goals for comparison.

Uncertainty contributions	CO_2	CH_4	CO
MPI-BGC GasLab implementation of the WMO primary scale	0.015 ppm	0.7 ppb	0.5 ppb or 0.25 % (whichever is greater)
Calibration transfer to the laboratory working tanks	0.02 ppm	0.15 ppb	0.7 ppb or 0.4 % (whichever is greater)
Calibration transfer from the working tanks via in-flight cylinders to the instrument	0.07 ppm	0.28ppb	2.8 ppb
Drift correction of the in-flight cylinders and regulator effects	0.05 ppm	-	-
Isotopic composition	0.019 ppm	-	-
Wet-to-dry correction	0.05 ppm	1 ppb	2 ppb
Measurement repeatability	0.039 ppm (2.3 s time resolution)	0.40 ppb (2.3 s)	1.7 ppb (3 min time resolution)
Achieved overall uncertainty (1-sigma)	**0.13 ppm**	**1.3 ppb**	**4 ppb**
WMO/GAW compatibility goal	**0.1 ppm/0.05 ppm (northern/southern hemisphere**	**2 ppb**	**2 ppb**

CO_2 and CH_4 calibration of the laboratory working tanks is made at the MPI-BGC GasLab using a CRDS analyser (G1301, Picarro Inc.), CO calibration using a vacuum ultraviolet resonance fluorescence (VURF) analyser (Aerolaser AL 5002). Each of these instruments is calibrated by working standards that are assigned relative to the above-mentioned suite of WMO tertiary standards. The uncertainty of the calibration transfer at MPI-BGC GasLab comprises the uncertainty of the GasLab working standard assignment (including its stability over time) and the reproducibility of the analytical method to assign the IAGOS working tanks.

The CRDS instrument is calibrated daily using three GasLab working standards spanning the atmospheric range of CO_2 and CH_4. The reproducibility of assignments of these standards for multiple calibration episodes relative to the WMO tertiary standard suite (ca. 10 episodes per working standard) is 0.01 ppm for CO_2 and 0.1 ppb for CH_4, respectively. Within this series of re-calibrations, drifts of CO_2 mole fractions of 0.01-0.015 ppm/yr have been detected in several working standards. A linear drift function is applied in these cases. In contrast, all working standards have been stable in their CH_4 mole fraction. Thus, the uncertainty of the CH_4 scale transfer to the GasLab working standards is corresponding to the standard error of 0.03 ppb (0.1 ppb/$\sqrt{n}$), whereas the uncertainty of the CO_2 scale transfer is approximated as 0.01 ppm.

The accuracy of the GasLab assignments of IAGOS working tanks is assessed based on the time series of daily target standard measurements. The standard deviation of these daily mean values is 0.015-0.02 ppm for CO_2, and 0.1-0.2 ppb for CH_4 for a 20-min measurement period. These long-term quality control records do not only represent the analysers precision but also additional

disturbances apparent in the laboratory operation (e.g. temporary small leakages). Combining the uncertainty of the GasLab working standard assignment and the general reproducibility of the analytical method yields a total MPI-BGC GasLab scale transfer uncertainty of 0.02 ppm for CO_2 and 0.15 ppb for CH_4.

For the VURF CO-analyser, a one-point calibration using a single working standard and a zero gas analysed each for 6 min is made every 30 min. The relative reproducibility of working standard assignments relative to the WMO tertiary standard suite (six episodes per working standard) is 0.2 % (0.4 and 0.8 ppb for two working standards at 246 and 426 ppb, respectively). The first working standard showed a steady increase of CO mole fractions at a drift rate of 0.6 ppb/yr that was accounted for using a linear interpolation. Similarly, one of the standards in the GasLab CO WMO tertiary standard set showed a CO growth of 1 ppb/yr and therefore has not been used for calibration. This points to a potential bias of the tertiary set due to a similar drift of the entire set as it has been reported by the WMO-CCL for CO in some primary standards at a rate of 0.3 ppb/yr (see www.esrl.noaa.gov/gmd/ccl/co_scale.html). Recent re-calibrations at the WMO-CCL of two tertiary standards, however, did not indicate any CO growth over a period of 9 years. Absolute values of the residuals of the seven tertiaries with CCL assignments obtained in different years since 2005 are less than 0.5 ppb with no systematic trend in the time series of residuals of any single standard. Based on this evidence, it is assumed to be unlikely that the MPI-BGC GasLab tertiary standard suite comprises any bias due to instabilities in the standard CO mole fractions. This is consistent with the absence of any significant drift in the time series of target standards. However, despite the absence of a clear indicator for drift of the GasLab tertiaries an upper limit of 0.5 ppb for the stability of the set is taken as conservative estimate for the uncertainty of the tertiary assignments considering the known problems with CO growth and the associated challenge of detecting small drifts. Accounting for this uncertainty, a relative calibration transfer uncertainty of the GasLab working standards of 0.3 % is derived for the working standard containing 246 ppb CO. Target standards are analysed daily in the same way as the IAGOS working tanks (15-min measurement period divided by a calibration). The record of these target standard measurements documents a long-term relative reproducibility of the VURF CO analysis of 0.25 %. By combining the uncertainty of the MPI-BGC GasLab working standard assignment and the reproducibility of the analytical method, the MPI-BGC GasLab scale transfer uncertainty for CO is estimated as 0.4 % relative or 0.7 ppb absolute (whichever is greater).

The last step of the calibration chain is the calibration of the IAGOS-core GHG instrument with the help of the working tanks and the in-flight calibration gas cylinders. Here, the repeatability of the instrument for the measurements of the working tank calibration gases and the in-flight calibration gases is deduced from laboratory experiments as 0.015 ppm for CO_2, 0.15 ppb for CH_4 and as 2 ppb for CO. For the in-flight calibrations the uncertainty of the free parameter c_j in Equation 2.2 has to be added to the measurement uncertainties for CO_2 and CH_4. Table 2.3 assumes the worst case, where instrument drift needs to be compensated for by 3-hourly calibrations. In the best case, the instrument does not drift significantly, and all calibrations (pre-, post- and all in-flight calibrations) can be statistically combined, which reduces the uncertainty significantly. For now, without flight experience, the worst-case scenario is considered for the

calculations to give an upper limit of the uncertainty. The uncertainty of the parameter c_j for 3-min calibrations is 0.07 ppm for CO_2 and 0.19 ppb for CH_4 (see Section 2.3.2). By combining the repeatability of the working tank measurements and the in-flight calibration gas measurements with the uncertainty of the parameter c_j, the overall uncertainty of this calibration transfer step is determined as 0.07 ppm for CO_2, 0.28 ppb for CH_4 and 2.8 ppb for CO. For the best-case scenario, the uncertainty would be 0.015 ppm for CO_2, 0.15 ppb for CH_4 and 2 ppb for CO.

Uncertainty due to drift correction of the in-flight calibration gas cylinders and due to regulator effects [e.g. parameters in Equations 2.1 and 2.2 determined beforehand change over time and in particular with decreasing tank pressure] is for now only estimated and will later be based on experience from operational QA/QC cycles. As known from experience, in-flight calibration gas cylinder drift and regulator effects are very small for CH_4, for CO they are small in relation to the uncertainty introduced by calibration transfer and instrument repeatability, respectively. Therefore, uncertainty due to these effects is assumed to be negligible for CH_4 and CO.

The CO_2 isotopic composition in the calibration gases is kept close to that of ambient air (-12 ‰ > $\delta^{13}C_{VPDB}$ > -8 ‰, 0 ‰ > $\delta^{18}O_{VPDB}$ > 7 ‰). Due to differences in the isotopic signature of CO_2 between the tertiary standards calibrated by the CCL and the laboratory working tanks (filled with the calibration gases), small measurement biases of maximal 0.019 ppm at 400 ppm level occur. Any further measurement bias from differences in the isotopic composition of the working standards and the in-flight standards can be excluded as their assignment is done with the same analytical technique. Measurement errors caused by deviations of the calibration gases in the isotopic composition of CH_4 were found to be negligible as the fraction of these deviations to total methane is small; in addition, the measured biases due to ^{13}C and deuterium compensate each other. For CO the isotopic composition is not known, but estimations based on similar values as for CO_2 are insignificant compared to the measurement repeatability.

The wet-to-dry correction is based on laboratory experiments made with each instrument during each maintenance cycle. Thus, the smallest uncertainties can be achieved as described in Rella et al. (2013) for CO_2 and CH4 and Chen et al. (2013) for CO. With the experience of repeated wet-to-dry experiments in the laboratory over a long period, the uncertainty estimates will be optimised.

Measurement repeatability of the instrument is given at 2.3 s time resolution for CO_2 and CH_4; for CO an integration time of 3 min is applied (see Section 2.3.1).

Propagation of all these uncertainty contributions (Gaussian error propagation assuming independent variables, bias due to isotopic composition added linearly) results in an overall uncertainty (1-sigma) of the IAGOS-core GHG measurement system of 0.13 ppm for CO_2, 1.3 ppb for CH_4 and 4 ppb for CO. A less conservative assumption of instrument drift in the third step of the calibration chain (calibration transfer from the working tanks via in-flight cylinders to the instrument) results in overall uncertainties of 0.10 ppm for CO_2, 1.3 ppb for CH_4 and 3.4 ppb for CO. The uncertainty estimates are in good agreement with the overall uncertainty (0.15 ppm for CO_2, 1.4 ppb for CH_4, 5 ppb for CO) of the similar CRDS measurements made by Karion et al. (2013). Note that the WMO GAW compatibility goals shown in Table 2.3 should actually represent most upper limits, as individual measurement programmes should strive for significantly smaller

uncertainties. However, the fact that those are likely not met for CO_2 and CO indicates that this is hard to achieve with aircraft measurement programmes.

2.5.2 Water vapour

For water vapour, the overall uncertainty includes an instrument response drift of <100 ppm or <0.5 % (whichever is greater) over 6 months and traceability to the NIST (Gaithersburg, MD) scale. Uncertainty of the calibration transfer from NIST scale to the instrument is 0.2°C dewpoint at 20°C dewpoint, linearly increasing to 0.4°C dewpoint at −60°C dewpoint, corresponding to the specifications of the Cooled Mirror Dewpointmeter from Michell Instruments used for calibration. A conservative estimate of the measurement repeatability is 4 ppm for mole fractions <100 ppm, and 4 % (relative) for mole fractions >100 ppm (see Section 2.6). The resulting overall uncertainty (1-sigma) of the water vapour measurements for the different measurement ranges can be seen in Table 2.4.

Table 2.4: Overall uncertainty (1-sigma values) of the water vapour measurements

Measurement range	Achieved Overall Uncertainty
<100 ppm	<15 ppm
100 300 ppm	<25 %
300 1000 ppm	<11 %
1000 10000 ppm	<6 %
>10000 ppm	<4 %

2.6 Flight test – DENCHAR flight campaign

In May–June 2011, the gas analyser (G2401-m, Picarro Inc.) was tested, as it was purchased before being repacked, in a flight campaign based in Hohn (Germany). This inter-comparison campaign was conducted within the framework of the DENCHAR (Development and Evaluation of Novel Compact Hygrometers for Airborne Research) project, funded by the European Facility for Airborne Research (EUFAR), to compare well-established reference instruments with newly developed systems measuring water vapour. During the inter-comparison campaign, four flights with a Learjet 35A took place in an area between North-Germany and South-Norway and North-Poland and the North Sea respectively. Altitudes up to 13 km were reached, hence also the lower stratosphere was covered.

Since the CRDS analyser and the inlet system components, a 1 m-long 3.18 mm (1/8”) FEP-tube connected to a Rosemount TAT housing (model 102BX) installed on a window plate of the Learjet, are identical to those in the repacked IAGOS-core GHG package this test setup ensures full comparability with the deployment of the analyser within IAGOS.

Figure 2.9 shows a profile for each species measured during the campaign at noon on 1 June 2011. The steep gradient at approximately 800 m indicates the mixing height covering the planetary boundary layer. At approximately 10 km, the aircraft crossed the tropopause which can be clearly

seen by the strong decrease in the mole fractions of all four species with altitude, characteristic for the lower stratosphere.

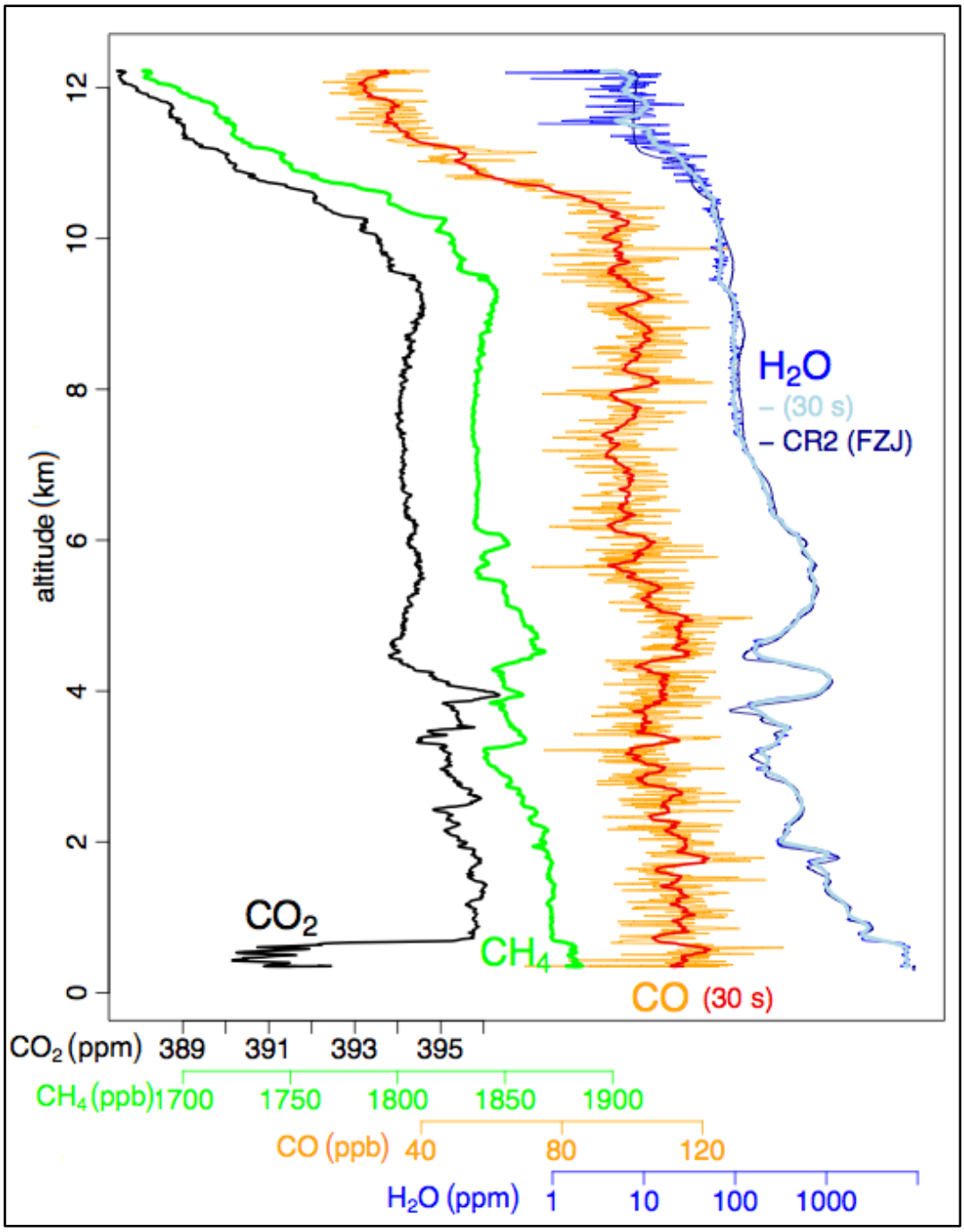

Figure 2.9: Measured profiles (0.4 Hz data) by the CRDS analyser during noon on 1 June 2011 over Hohn (Germany) for CO_2 (black), CH_4 (green), CO (orange, 30 s average in red) and H_2O (blue, 30 s average in light blue). The measurements from the frost point hygrometer CR2 can be seen in dark blue.

Upper limits for the measurement repeatability of the instrument during the test flights were determined during time periods with stable atmospheric conditions. The results are shown in Table 2.5. Note that the time resolution during the flight test campaign (2.5 s) was different to the laboratory tests (2.3 s) due to small modifications to the instrument after the flight test.

Table 2.5: Upper limits of the measurement repeatability during the DENCHAR flight campaign

Species	Time resolution	measurement repeatability
CO_2	2.5 s	0.06 ppm
CH_4	2.5 s	1 ppb
CO	2.5 s	10 ppb
H_2O	2.5 s	4 ppm @ H2O <100 ppm 4 % (rel.) @ H2O >100 ppm

Furthermore, the campaign allowed for the initial validation of the long-term IAGOS-core H_2O measurements by CRDS against reference instruments with a long performance record: the Fast In situ Stratospheric Hygrometer (FISH; Zöger et al., 1999) and the CR2 frost point hygrometer, both operated by the research centre Juelich. The comparison shows that the analyser is reliable and has a good long-term stability (note that the H_2O calibration scale was transferred via comparison against an analyser at the Picarro Company immediately after manufacturing). Regarding response time, it is comparable to the FISH instrument (not shown in Figure 2.9) and faster than the CR2 which oscillates strongly after changes in concentration and needs relatively long time to stabilise as can be seen in Figure 2.9.

Flight data of periods for which atmospheric homogeneity was assumed suggest a conservative repeatability of the water vapour measurements of 4 ppm for mole fractions <100 ppm, and 4 % (relative) for mole fractions >100 ppm. These results were confirmed by a comparison against the WASUL-Hygro instrument, a dual-channel photoacoustic humidity measuring system, operated by the University of Szeged (Tátrai et al., 2015). Accuracy at mole fractions below 50 ppm was difficult to assess, as the reference instruments suffered from lack of stability.

2.7 Conclusions

A measurement system for the GHGs CO_2 and CH_4, as well as CO, and water vapour, based on CRDS, was developed for deployment aboard passenger aircraft within the frame of the IAGOS infrastructure. To ensure traceability of the CO_2, CH_4 and CO measurements to the WMO primary scales a two-standard calibration system was designed and tested allowing for calibrations in-flight and on ground during each 6-month deployment period, to complement the calibrations of the instrument before and after the deployment. Taking advantage of the simultaneously measured water vapour no sample drying is needed, since dilution and spectroscopic effects affecting the measurements can be corrected to achieve dry air mole fractions for CO_2, CH_4 and CO. Tests of the prototype IAGOS-core GHG instrument in the laboratory regarding response stability, sensitivity to pressure changes and airworthiness proved the fully sufficient performance of the analyser. A correction for deviations in the pressure of the sample cell was developed and was proven to have no negative impact on the data quality. Measurement repeatability of the instrument for 0.4 Hz data is 0.039 ppm for CO_2, 0.4 ppb for CH_4 and 15 ppb for CO in the laboratory. During a test flight, upper limits for the measurement repeatability were determined as 0.06 ppm for CO_2, 1 ppb for CH_4 and 10 ppb for CO. Applying temporal integration of 3 min

reduces the repeatability to >1.7 ppb for CO. Overall uncertainty of the measurements, accounting for the uncertainty of referencing the in-flight calibration gases to WMO primary standards, uncertainty in the applied wet-to-dry correction and the actual instrumental repeatability was determined as <0.13 ppm for CO_2, <1.3 ppb for CH_4 and <4 ppb for CO, based on laboratory tests. A less conservative assumption of instrument drift reduces the overall uncertainties to <0.10 ppm for CO_2, <1.3 ppb for CH_4 and <3.4 ppb for CO. The uncertainty estimation will be updated as needed, as real IAGOS flight data are available.

Test flights of the instrument on a Learjet during the DENCHAR flight campaign allowed for an initial validation of the water vapour measurements. The flight data suggest a conservative repeatability estimate for the water vapour measurements of 4 ppm for mole fractions between 50 and 100 ppm, and 4 % (relative) for mole fractions >100 ppm.

Assembly and integration of five additional systems is planned within the next years, increasing the fleet to five operationally deployed GHG systems plus a spare instrument. Thus, data from more than 600 flights per year and instrument, and specifically over 6000 vertical profiles per year, will be available for inverse modelling of GHG fluxes, validation of remote sensing observations and process studies (e.g. STE, or vertical transport by moist convection). Spatial coverage of the data depends on the flight routes of the aircraft equipped; however, major parts of the globe will be covered as soon as several instruments are operational.

2.8 References

Allan, D. W.: Statistics of Atomic Frequency Standards, Proceedings of IEEE, 54(2), 221-230, 1966.

Allan, D. W.: Time and Frequency (Time-Domain) Characterization, Estimation, and Prediction of Precision Clocks and Oscillators, IEEE Transactions on Ultrasonics Ferroelectrics and Frequency Control, 34(6), 647–654, 1987.

Andreae, M. O. and Merlet, P.: Emission of trace gases and aerosols from biomass burning, Global Biogeochemical Cycles, 15, 955–966, 2001.

Araki, M., Morino, I., Machida, T., Sawa, Y., Matsueda, H., Ohyama, H., Yokota, T., and Uchino, O.: CO_2 column-averaged volume mixing ratio derived over Tsukuba from measurements by commercial airlines, Atmos. Chem. Phys., 10(16), 7659–7667, 2010.

Brenninkmeijer, C. A. M., Crutzen, P., Boumard, F., Dauer, T., Dix, B., Ebinghaus, R., Filippi, D., Fischer, H., Franke, H., Frieß, U., Heintzenberg, J., Helleis, F., Hermann, M., Kock, H. H., Koeppel, C., Lelieveld, J., Leuenberger, M., Martinsson, B. G., Miemczyk, S., Moret, H. P., Nguyen, H. N., Nyfeler, P., Oram, D., O'Sullivan, D., Penkett, S., Platt, U., Pupek, M., Ramonet, M., Randa, B., Reichelt, M., Rhee, T. S., Rohwer, J., Rosenfeld, K., Scharffe, D., Schlager, H., Schumann, U., Šlemr, F., Sprung, D., Stock, P., Thaler, R., Valentino, F., van Velthoven, P., Waibel, A., Wandel, A., Waschitschek, K., Wiedensohler, A., Xueref-Remy, I., Zahn, A., Zech, U., and Ziereis, H.: Civil Aircraft for the regular investigation of the atmosphere based on an instrumented container: The new CARIBIC system, Atmos. Chem. Phys., 7, 4953-4976, 2007.

Chen, H., Winderlich, J., Gerbig, C., Hoefer, A., Rella, C. W., Crosson, E. R., Van Pelt, A. D., Steinbach, J., Kolle, O., Beck, V., Daube, B. C., Gottlieb, E. W., Chow, V. Y., Santoni, G. W., and Wofsy, S. C.: High-accuracy continuous airborne measurements of greenhouse gases (CO_2 and CH_4) using the cavity ring-down spectroscopy (CRDS) technique, Atmos. Meas. Tech., 3(2), 375-386, doi:10.5194/amt-3-375-2010, 2010.

Chen, H., Karion, A., Rella, C. W., Winderlich, J., Gerbig, C., Filges, A., Newberger, T., Sweeney, C., and Tans, P. P.: Accurate measurements of carbon monoxide in humid air using the cavity ring-down spectroscopy (CRDS) technique, Atmos. Meas. Tech., 6, 1031–1040, doi:10.5194/amt-6-1031-2013, 2013.

Crosson, E. R.: A cavity ring-down analyser for measuring atmospheric levels of methane, carbon dioxide, and water vapour, Appl. Phys. B, 92, 403–408, doi:10.1007/s00340-008-3135-y, 2008.

Daube Jr., B. C., Boering, K. A., Andrews, A. E. and Wofsy, S. C.: A high-precision fast-response airborne CO_2 analyser for in situ sampling from the surface to the middle stratosphere, J. Atmos. Oceanic Technol., 19(10), 1532–1543, 2002.

Dlugokencky, E., Crotwell A., Lang P., Thoning, K. and Hall B.: Extension of the WMO CH_4 standard scale beyond the background ambient range. presented at WMO, 17th WMO/IAEA Meeting on

Carbon Dioxide, Other Greenhouse Gases, and Related Measurement Techniques (GGMT-2013), Beijing, China, 10-14 June 2013, http://ggmt-2013.cma.gov.cn/dct/page/70029, 2013.

Fahey, D. W., Gao, R.S., Carslaw, K. S., Kettleborough, J., Popp, P. J., Northway, M. J., Holecek, J. C., Ciciora, S. C., McLaughlin, R. J., Thompson, T. L., Winkler, R. H., Baumgardner, D. G., Gandrud, B., Wennberg, P. O., Dhaniyala, S., Mckinney, K., Peter, Th., Salawitch, R. J., Bui, T. P., Elkins, J.W., Webster, C. R., Atlas, E. L., Jost, H., Wilson, J. C., Herman, R. L., Kleinböhl, A., and von König, M.: The Detection of Large HNO_3-Containing Particles in the Winter Arctic Stratosphere, Science, 291, 1026–1031, 2001.

Geibel, M. C., Messerschmidt, J., Gerbig, C., Blumenstock, T., Chen, H., Hase, F., Kolle, O., Lavric, J. V., Notholt, J., Palm, M., Rettinger, M., Schmidt, M., Sussmann, R., Warneke, T. and Feist, D. G.: Calibration of column-averaged CH_4 over European TCCON FTS sites with airborne in-situ measurements, Atmos. Chem. Phys., 12, 8763–8775, 2012.

IPCC: Climate Change 2013: The Physical Science Basis. Contribution of Working Group I to the Fifth Assessment Report of the Intergovernmental Panel on Climate Change [ed. Stocker, T.F., D. Qin, G.-K. Plattner, M. Tignor, S.K. Allen, J. Boschung, A. Nauels, Y. Xia, V. Bex and P.M. Midgley], Cambridge University Press, Cambridge, United Kingdom and New York, NY, USA, 1535 pp., 2013.

Karion, A., Sweeney, C., Tans, P. and Newberger, T.: AirCore: An Innovative Atmospheric Sampling System, J. Atmos. Oceanic Technol., 27(11), 1839–1853, 2010.

Karion, A., Sweeney, C., Wolter, S., Newberger, T., Chen, Andrews, A., Kofler, J., Neff, D., Tans, P.: Long-term greenhouse gas measurements from aircraft, Atmos. Meas. Tech., 6, 511-526, doi:10.5194/amt-6-511-2013, 2013.

Levin, I. and Karstens, U.: Inferring high-resolution fossil fuel CO_2 records at continental sites from combined $^{14}CO_2$ and CO observations, Tellus B, 59, 245–250, 2007.

Machida, T., Matsueda, H., Sawa, Y., Nakagawa, Y., Hirotani, K., Kondo, N., Goto, K., Nakazawa, T., Ishikawa, K.:T. Ogawa: Worldwide Measurements of Atmospheric CO_2 and Other Trace Gas Species Using Commercial Airlines, J. Atmos. Oceanic Technol., 25(10), 1744–1754, doi:10.1175/2008JTECHA1082.1, 2008.

Marenco, A., Thouret, V., Nédélec, P., Smit, H., Helten, M., Kley, D., Karcher, F., Simon, P., Law, K., Pyle, J., Poschmann, G., Von Wrede, R., Hume, C., and Cook, T.: Measurement of ozone and water vapour by Airbus in-service aircraft: The MOZAIC airborne program, an overview, J. Geophys. Res., 103(D19), 25631–25642, 1998.

Matsueda, H. and Inoue, H.Y.: Measurements of atmospheric CO_2 and CH_4 using a commercial airliner from 1993 to 1994, Atmos. Environ., 30, 1647–1655, 1996.

Messerschmidt, J., Geibel, M. C., Blumenstock, T., Chen, H., Deutscher, N.M., Engel, A., Feist, D. G., Gerbig, C., Gisi, M., Hase, F., Katrynski, K., Kolle, O., Lavric, J. V., Notholt, J., Palm, M.,

Ramonet, M., Rettinger, M., Schmidt, M., Sussmann, R., Toon, G. C., Truong, F., Warneke, T., Wennberg, P. O., Wunch, D. and Xueref-Remy, I.: Calibration of TCCON column-averaged CO2: the first aircraft campaign over European TCCON sites, Atmos. Chem. Phys., 11, 10765–10777, doi:10.5194/acp-11-10765-2011, 2011.

Nédélec, P., Cammas, J.-P., Thouret, V., Athier, G., Cousin, J. M., Legrand, C., Abonnel, C., Lecoeur, F., Cayez, G., Marizy, C.: An improved infrared carbon monoxide analyser for routine measurements aboard commercial Airbus aircraft: technical validation and first scientific results of the MOZAIC III programme, Atmos. Chem. Phys., 3, 1551-1564, 2003.

Newell, R. E., V. Thouret, J. Y. N. Cho, P. Stoller, A. Marenco, and Smit, H. G.: Ubiquity of quasi-horizontal layers in the troposphere, Nature, 398, 316-319, 1999.

Peischl, J., Ryerson, T. B., Holloway, J. S., Trainer, M., Andrews, A. E., Atlas, E. L., Blake, D. R., Daube, B. C., Dlugokencky, E. J., Fischer, M. L., Goldstein, A. H., Guha, A., Karl, T., Kofler, J., Kosciuch, E., Misztal, P. K., Perring, A. E., Pollack, I. B., Santoni, G. W., Schwarz, J. P. Spackman, J. R., Wofsy, S. C., Parrish, D. D.: Airborne observations of methane emissions from rice cultivation in the Sacramento Valley of California, J. Geophys. Res.,117, D00V25, doi:10.1029/2012JD017994, 2012.

Petzold, A., Thouret, V., Gerbig, C., Zahn, A., Brenninkmeijer, C.A.M., Gallagher, M., Hermann, M., Pontaud, M., Ziereis, H., Boulanger, D., Marshall, J., Nédélec, P., Smit, H. G.J., Friess, U., Flaud, J.-M., Wahner, A., Cammas, J.-P., and Volz-Thomas, A.: Global-scale atmosphere monitoring by in-service aircraft - current achievements and future prospects of the European Research Infrastructure IAGOS, Tellus B, 67, 28452, doi:10.3402/tellusb.v67.28452, 2015.

Rella, C. W., Chen, H., Andrews, A. E., Filges, A., Gerbig, C., Hatakka, J., Karion, A., Miles, N. L., Richardson, S. J., Steinbacher, M., Sweeney, C., Wastine, B., and Zellweger, C.: High accuracy measurements of dry mole fractions of carbon dioxide and methane in humid air, Atmos Meas. Tech., 6(3), 837–860, doi:10.5194/amt-6-837-2013, 2013.

Stickney, T. M., Shedlov, M. W. and Thompson, D. I.: Goodrich total temperature sensors, Aerospace Division, Rosemount, Inc., Tech. Rep. 5755, Revision C, 30 pp, 1994.

Sturm, P., Leuenberger, M., Sirignano, C., Neubert, R. E. M., Meijer, H. A. J., Langenfelds, R., Brand, W. A., Tohjima, Y.: Permeation of atmospheric gases through polymer O-rings used in flasks for air sampling, J. Geophys. Res., 109, D04309, doi:10.1029/2003JD004073, 2004.

Tadić, J.M., Loewenstein, M., Frankenberg, C., Butz, A., Roby, M., Iraci, L. T., Yates, E. L., Gore, W., Kuze, A.: A Comparison of In Situ Aircraft Measurements of Carbon Dioxide and Methane to GOSAT Data Measured Over Railroad Valley Playa, Nevada, USA, IEEE Transactions on Geoscience and Remote Sensing, 52(12), 7764-7774, doi:10.1109/TGRS.2014.2318201, 2014.

Tátrai, D., Bozóki, Z., Smit, H., Rolf, C., Spelten N., Krämer, M., Filges, A., Gerbig, C., Gulyás, G., and Szabó, G.: Dual-channel photoacoustic hygrometer for airborne measurements: background, calibration, laboratory and in-flight intercomparison tests, Atmos. Meas. Tech., 8, 33-42, doi:10.5194/amt-8-33-2015, 2015.

Turnbull, J.C., Karion, A., Fischer, M.L., Faloon, I., Guilderson, T., Lehman, S. J., Miller, B. R., Miller, J. B., Montzka, S., Sherwood, T., Saripalli, S., Sweeney, C. and Tans, P. P.: Assessment of fossil fuel carbon dioxide and other anthropogenic trace gas emissions from airborne measurements over Sacramento, California in spring 2009, Atmos. Chem. Phys., 11, 705-721, 2011.

Volz-Thomas, A., Berg, M., Heil, T., Houben, N., Lerner, A., Petrick, W., Raak, D., Pätz, H.-W.: Measurements of total odd nitrogen (NO_y) aboard MOZAIC in-service aircraft: instrument design, operation and performance. Atmos. Chem. Phys., 5(3), 583–595, 2005.

Volz-Thomas, A., Cammas, J.-P., Brenninkmeijer, C. A., Machida, T., Cooper, O., Sweeney, C., Waibel, A.: Civil Aviation Monitors Air Quality and Climate, EM Magazine, Air & Waste Management Association, October 2009, 16-19, 2009.

Winderlich, J., Chen, H., Gerbig, C., Seifert, T., Kolle, O., Lavrič, J. V., Kaiser, C., Höfer, A., and Heimann, M.: Continuous low-maintenance CO_2/CH_4/H_2O measurements at the Zotino Tall Tower Observatory (ZOTTO) in Central Siberia, Atmos. Meas. Tech., 3(4), 1113–1128, doi:10.5194/amt-3-1113-2010, 2010.

WMO: GAW Report No. 206: 16th WMO/IAEA Meeting on Carbon Dioxide, Other Greenhouse Gases, and Related Measurement Techniques (GGMT-2011), Wellington, New Zealand, 25-28 October 2011, 67 pp, 2012.

WMO (Atmospheric Environment and Research Division): WMO-GAW Annual Greenhouse Gas Bulletin No. 10, World Meteorological Organization, Geneva, Switzerland, 2014.

Zhao, C. L., and Tans, P. P.: Estimating uncertainty of the WMO mole fraction scale for carbon dioxide in air, J. Geophys. Res., 111, D08S09, 2006.

Zöger, M., Afchine, A., Eicke, N., Gerhards, M.-T., Klein, E., McKenna, D. S., Mörschel, U., Schmidt, U., Tan, V., Tuitjer, F., Woyke, T., and Schiller, C.: Fast in situ stratospheric hygrometers: A new family of balloon-borne and airborne Lyman-α photofragment fluorescence hygrometers, J. Geophys. Res., 104(D1), 1807-1816, doi:10.1029/1998JD100025, 1999.

3 Evaluation of the IAGOS-Core GHG package H_2O measurements during the DENCHAR airborne inter-comparison campaign

3.1 Introduction

Water vapour is a crucial factor for various atmospheric processes, weather, and climate. It is the most important greenhouse gas (Kiehl and Trenberth, 1997) and shows strong feedback to changes in the climate system (Dessler et al., 2008). Especially in the upper troposphere and lower stratosphere (UTLS) the amount of water vapour has a large impact on the radiative balance of the atmosphere (e.g., Smith et al., 2001; Forster and Shine, 2002; Solomon et al., 2010). However, due to only a few existing measurement data in the UTLS, and limitations in prognostic model simulations of this region (Solomon et al., 2010), uncertainties in chemistry, transport processes, and trace gas composition are relatively large. This significantly influences the estimation of, e.g., radiative effects (Riese et al., 2012; Kunz et al., 2013).

Water vapour observations covering the whole troposphere and at least lower parts of the stratosphere are achieved mainly by instruments based on balloons, aircraft or satellites, and from ground-based remote sensing techniques. The longest measurement time series was started in 1980 in Boulder (Colorado, US) with balloon-borne frost point hygrometers (Oltmans et al., 2000; Hurst et al., 2011). First long-term global satellite data were obtained in the mid-1980s as part of the Stratospheric Aerosol and Gas Experiment II (SAGE II) (Rind et al., 1993). Recent observations have been made by, e.g., the Michelson Interferometer for Passive Atmospheric Sounding (MIPAS) (Milz et al., 2005; von Clarmann et al., 2009) and the Scanning Imaging Absorption Spectrometer for Atmospheric Chartography (SCIAMACHY) (Rozanov et al., 2011; Weigel et al., 2016), both aboard ENVISAT (Environmental Satellite). The main drawbacks of satellite data and remote sensing observations from ground (e.g., Schneider et al., 2006) are their insufficient vertical resolution in the troposphere and lower stratosphere and disturbances of the measurements by clouds. As shown by Hoareau et al. (2013), vertical resolutions <500 m are needed for the simulation of cirrus clouds. To represent the very sharp gradient of 40 to 6 ppm water vapour within 0–2 km at the tropopause (Zahn et al., 2014), resolutions of even 400 m and higher have to be achieved (Poshyvailo et al., 2018). On the other hand reliable radiosonde water vapour data up to stratospheric heights, e.g., from the GCOS (Global Climate Observing System) Reference Upper-Air Network (GRUAN) (Dirksen et al., 2014), as well as data sets from research aircraft, are quite limited in time and space.

The use of commercial aircraft as cost-efficient platforms for dedicated instruments can at least partially bridge this gap, providing regular measurements in the UTLS along major flight routes. For example, five Airbus A340 passenger aircraft were equipped with capacitive humidity sensors from 1994 to 2014 as part of the MOZAIC (Measurement of Ozone and Water Vapour by Airbus In-Service Aircraft) project (Marenco et al., 1998). The acquired data set is crucial for the study of chemical and dynamic processes in the upper troposphere and lower stratosphere (e.g., Gierens et al., 1999).

However, accurate and reliable airborne measurements of atmospheric water vapour are still a challenge. The large range from mole fractions of several percent at the ground to only a few parts per million (ppm = µmol/mol) in the stratosphere and the highly variable structures of water vapour in the atmosphere are demanding for analysers regarding accuracy and time response.

Kley et al. (2000) give a detailed summary of the most important water vapour instruments used on board aircraft. Besides frost point hygrometers (e.g., Vömel et al., 2007, 2016; Hurst et al., 2011; Hall et al., 2016) these are mainly Lyman-α hygrometers, based on fluorescence techniques, for example the Harvard Water Vapour instrument (HWV) (Weinstock et al., 2009) and the Fast In situ Stratospheric Hygrometer (FISH) (Zöger et al., 1999; Meyer et al., 2015). More recently infrared absorption spectrometers like the Jet Propulsion Laboratory Laser Hygrometer (JLH) (May, 1998), the Integrated Cavity output Spectrometer (ICOS) (Sayres et al., 2009), or the Hygrometer for Atmospheric Investigations (HAI) (Buchholz et al., 2017), and the Atmospheric Ionization Mass Spectrometer (AIMS) (Kaufmann et al., 2016) have been deployed. The central problems of all these different types of analysers are the unexplained discrepancies between water vapour measurements in the range below 10 ppm (e.g., Kley et al., 2000; Vömel et al., 2007; Weinstock et al., 2009). While the instruments compare well during static experiments (Fahey et al., 2014), they disagree significantly during airborne inter-comparisons in the UTLS. For the recent Mid-latitude Airborne Cirrus Properties Experiment (MACPEX) in 2011 Rollins et al. (2014) estimated the differences to be on the order of 20 % at water vapour mixing ratios of 3–4 ppm, whereas the measurement uncertainties of the instruments account only for 5 %–10 %. Thus, possibilities, e.g., to identify long-term trends in stratospheric water vapour or to study ice microphysical processes, are limited (Rollins et al., 2014).

In this context the DENCHAR (Development and Evaluation of Novel Compact Hygrometers for Airborne Research) project was initiated by the European Facility for Airborne Research (EUFAR) to support the development and characterization of novel or improved compact airborne hygrometers for different airborne applications within EUFAR, including investigation of the sampling characteristics of different gas/ice inlets (e.g. Tátrai et al., 2015). As part of the DENCHAR inter-comparison flight campaign in Hohn (Germany) in May–June 2011, a commercial cavity ring-down spectroscopy (CRDS) gas analyser (G2401-m, Picarro Inc., US), measuring CO_2, CH_4, CO and water vapour, was tested and compared against well-established reference hygrometers and newly developed water vapour instruments. The former were the Learjet version of the Fast In situ Stratospheric Hygrometer (FISH) (Meyer et al., 2015) and a CR-2 Cryogenic Aircraft hygrometer (Buck Research Instruments L.L.C., Boulder, US, http://www.hygrometers.com), both operated by Research Centre Jülich.

The same CRDS analyser and corresponding inlet system components are scheduled for deployment on board passenger aircraft within the IAGOS (In-service Aircraft for a Global observing System) project (Filges et al., 2015). IAGOS was launched in 2005 as the successor program of MOZAIC, but with modernized instrumentation and enhanced measurement capabilities (Volz-Thomas et al., 2009; Petzold et al., 2015). The current fleet of IAGOS-equipped aircraft as well as the spatial coverage of all flights can be found at the IAGOS database (http://www.iagos.org). There are plans to equip five IAGOS aircraft with the CRDS system, named

the 'IAGOS-core Greenhouse Gas (GHG) package', in the next years. In contrast to the CO_2 measurements from the CRDS, which have been studied thoroughly and have shown good performances, the quantitative capabilities of the CRDS water vapour measurements have never been evaluated and reviewed in detail before. Precision in the laboratory is known from previous studies to be around 6 ppm for a 2.3 s integration time but is related to white noise (Filges et al., 2015). Thus, sample averaging over 30 min can result in a precision of down to 0.3 ppm, which in principle can result in numerous scientific applications of the data. Each IAGOS aircraft is also equipped with the MOZAIC humidity device (Helten et al., 1998; Smit et al., 2008, 2013), which provides the unique opportunity to compare both instrument types under the same conditions over a long-time period. IAGOS water vapour measurements include regular in situ data in the sensible UTLS region and vertical profiles of H_2O in the troposphere and lower stratosphere for major parts of the globe. They are essential for validation of remote sensing based observations from satellites and ground, are needed for improving the performance of climate models and weather forecasts and can be used for climate trend studies.

This chapter presents the water vapour measurements made with the CRDS system during the DENCHAR inter-comparison flight campaign in 2011. The flight data are validated against reference instruments with a long performance record to evaluate the water vapour measurements made by the CRDS instrument. Furthermore, the analyser was calibrated with the help of different hygrometers, and a novel independent calibration method was tested. The corresponding results are analysed and discussed regarding the feasibility of the different methods for the long-term operation of the analyser within the IAGOS project.
The measurement system is introduced in Section 3.2, followed by an overview of the water vapour calibration approaches in Section. 3.3. Results from the flight tests are presented in Section. 3.4. Section 3.5 concludes the chapter.

3.2 The measurement system

The measurements were conducted by a G2401-m wavelength scanned cavity ring-down spectroscopy analyser from Picarro Inc. (US) (CFKB2004), which simultaneously measures CO_2, CH_4, CO and water vapour (Crosson, 2008; Chen et al., 2010).
The CRDS technique determines the mole fraction of a gas using the decay time of light intensity ('ring-down time') due to absorption by the gas. Laser light of a specific set of wavelengths is injected into a mirrored sample cell (the 'cavity', 35 cm^3, effective optical path length 15–20 km), which is flushed with the sample gas. When the light intensity reaches a predetermined threshold, the laser is turned off, after which the optical energy in the cavity decays with a characteristic exponential time constant of the light intensity in the cavity (the ring-down). The total absorption of the cavity (including both the absorption of the gas and the loss of the mirrors) is calculated directly from the exponential time constant. By tuning the wavelength of the laser, a specific spectral line of a species is scanned, and analysis of the obtained spectrogram provides the peak

height, which at constant pressure and temperature is proportional to the mole fraction of the species.

The analyser uses selected spectral lines in the infrared for the measurements: at 1603 nm for $^{12}C^{16}O_2$, at 1651 nm for $^{12}CH_4$ and H162O, and at 1567 nm for $^{12}C^{16}O$.

To minimize the impact of pressure and temperature on gas density and spectroscopy, both are kept constant in the sample cell. Pressure in the sample cell is controlled to 186.65 ± 0.04 hPa (140 Torr) using a proportional valve ('inlet valve') upstream of the cell, and the temperature is kept at 45 ± 0.02 ◦C. Gas flow through the sample cell was controlled at 100 sccm with the help of a fixed needle valve, acting as a flow-restricting orifice, downstream of the sample cell and upstream of the pump. Thus, the flow rate was independent of ambient and, respectively, cabin pressure.

To protect the sample cell from contamination, two filters (Wafergard II F Micro In-Line Gas Filters, Entegris Inc.) are located in the sample line upstream of the sample cell. They also ensure thermal equilibration of the sample gas, as they are kept at the same temperature as the sample cell.

Each species was measured once every 2.5 s. The physical exchange time of the sample cell is 3.6 s (volume = 35 cm^3, sample flow = 100 sccm, pressure = 186.65 hPa, sample temperature = 45 ◦C), ensuring that the ambient air was continuously sampled given the shorter measurement interval of 2.5 s.

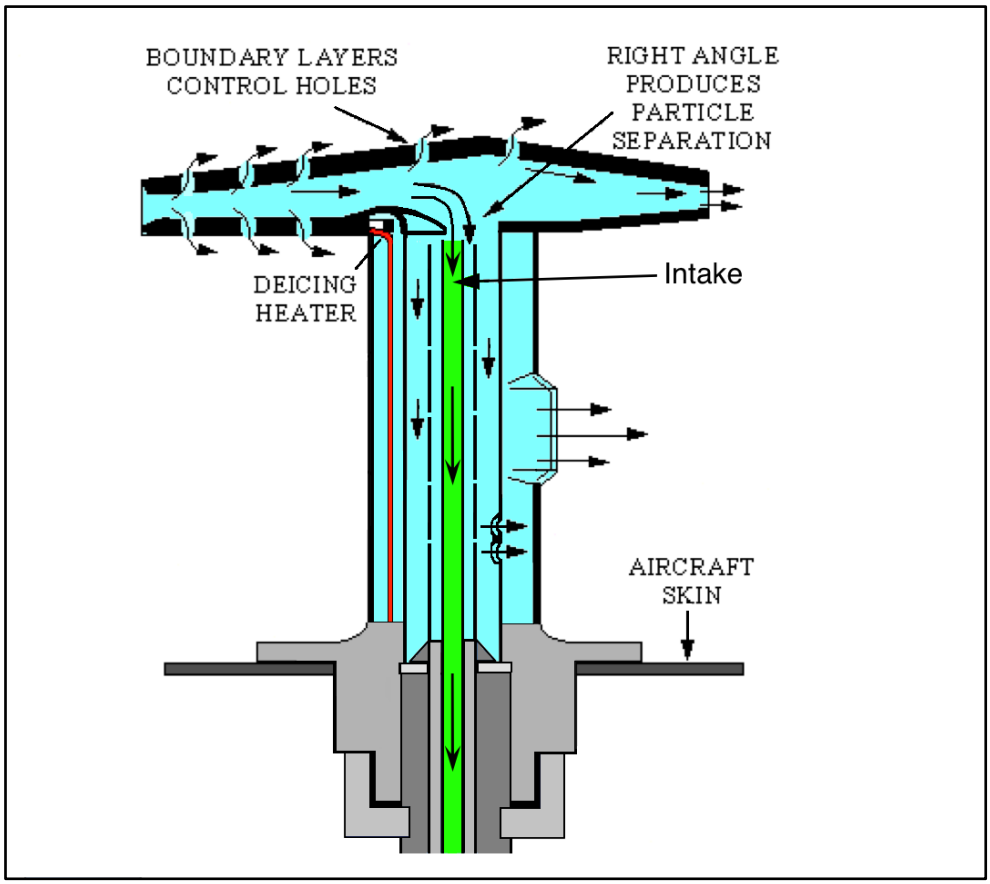

Figure 3.1: Cross section of the inlet line (green) mounted into a Rosemount Total Air Temperature housing (model 102B, adapted from Stickney et al. (1994)). The inlet line is pointed orthogonal to the airflow through the housing to prevent from sampling larger aerosols, ice particles, and water droplets.

The instrument was equipped with a 50 cm long inlet line (3.18 mm (1/8″) OD, 1.58 mm (1/16″) ID, fluorinated ethylene propylene (FEP) tube), which was connected to a Rosemount Total Air Temperature (TAT) housing (model 102B; Stickney et al., 1994) mounted on a window plate of the Learjet. The Rosemount probe acts as a virtual impactor since the inlet line is pointed orthogonal to the airflow through the housing (see Figure 3.1), and thus prevents sampling of larger aerosols (larger than about 2 µm), ice particles, and water droplets (Volz-Thomas et al., 2005; Fahey et al., 2001; Smit et al., 2013). Furthermore, it provides positive ram pressure due to the reduction of the air velocity. This additional positive ram pressure, together with the low sample gas flow of 100 sccm and the relatively short inlet line, ensured operation of the instrument with a controlled pressure in the sample cell of 186.65 hPa (140 Torr) throughout the aircraft altitude operating range up to 12.5 km without an upstream sampling pump. Diffusion effects of water vapour in the inlet line are minimal, given the short residence time of the sample gas, the small inner surface area, the small differences in humidity between the air-conditioned cabin and the ambient air, and the low permeability of FEP. The sample flow was exhausted into the cabin of the aircraft. The CRDS analyser and the inlet system components are identical to those chosen for integration aboard commercial airliners within the IAGOS (In-service Aircraft for a Global observing System) project. This setup ensures full comparability with the deployment of the IAGOS-core Greenhouse Gas package (Filges et al., 2015).

3.3 Calibration

In contrast to calibration of the CO_2, CH_4 and CO measurements, for which traceability to the World Meteorological Organization (WMO) primary scales is ensured by measurement of gas standards traceable to the primary scale, calibration of the water vapour measurements of the instrument is not as straightforward. There is no globally valid primary scale, but several national standards exist (WMO, 2012; see Part I, chap. 4). Calibration of an instrument is done by means of other hygrometers that are traceable to one of the national standards, often gravimetric hygrometers. In the following different calibration methods for the CRDS analyser are presented and compared.

3.3.1 Methods

Offset correction

Prior to calibration of the CRDS analyser against, e.g., a dew point mirror, an offset correction is required once to improve measurements at low water levels (<1000 ppm). This offset correction can be estimated by measuring dried ambient air from a high-pressure tank. At the MPI-BGC GasLab the tanks (volume: 50 L) were filled with air, which was dried using magnesium perchlorate ($Mg[ClO_4]_2$). The dew point of the air is around -75 °C, corresponding to 2.4 ppm water vapour. The offset stability of different CRDS instruments was checked regularly over a time period of up to 10 years and no significant drift was observed.

Dew point mirror

The factory calibration of the Picarro Inc. CRDS analyser consists of two parts: a self-broadening correction and a comparison with a dew point mirror.

Water vapour mole fraction is calculated using the peak height of the selected water absorption line. In this process self-broadening effects must be taken into account, which broaden the line shape and hence decrease the peak height as the water vapour level increases. To avoid an underestimation of the water vapour mole fraction, a quadratic correction is implemented in the Picarro analyser (Rella, 2010):

$$H_2O_{corrected} = H_2O_{reported} + 0.02525 * H_2O^2_{reported}. \qquad \text{(Equation 3.1)}$$

Here, H_2O is water vapour mole fraction in %. In 2009 a G1301-m CRDS instrument from Picarro, measuring CO_2, CH_4 and H_2O, was calibrated at MPI-BGC Jena against a dew point mirror (Dewmet TDH, Cooled Mirror Dewpointmeter, Michell Instruments Ltd., UK, referenced to the National Institute of Standards and Technology (NIST) primary scale) in the range from 7000 to 30 000 ppm water vapour mole fraction (Winderlich et al., 2010). The calibration constant obtained in this experiment was transferred to all greenhouse gas CRDS instruments manufactured by Picarro Inc. (Rella, 2010):

$$H_2O_{calibrated} = 0.772 * H_2O_{corrected} = 0.772 * \left(H_2O_{reported} + 0.02525 * H_2O^2_{reported}\right). \qquad \text{(Equation 3.2)}$$

This calibration transfer from one to all other instruments is possible since their water vapour measurements agree within a sufficient range and are stable over time as shown by Rella et al. (2013). Here, three different analysers (models G2401-m and Envirosense 3000) were compared at different times against one selected standard instrument (CFADS37, model G1301-m). One of the comparisons was repeated after more than 3 years. All results ($H_2O_{analyser}$ - $H_2O_{CFADS-37}$) lie within a range of ±125 ppm for water vapour mole fractions ranging from around 5000 to 30 000 ppm. Hence, a good transferability and long-term stability of the analysers' water vapour measurements can be assumed.

In order to examine the robustness of the 2009 calibration it was repeated in 2013 using a G2401-m analyser (CFKBDS2003) in comparison to the identical dew point mirror (Dewmet TDH, Michell Instruments Ltd.) that was used for the calibration in 2009. Both instruments measured simultaneously dried ambient air from a high-pressure tank, which was humidified by a dew point generator (Li-610 from Li-Cor) to specific water levels between 2 and 20 °C dew point. Higher and lower water vapour levels could not be reached due to the environmental conditions in the laboratory.

During the 2009 calibration the dew point mirror measurement was based on its original calibration, conducted by the manufacturer against test equipment traceable to the NIST primary standard at the end of 2000. In 2010 the dew point mirror was recalibrated by the manufacturer; however, no information was given on how the calibration factors changed. Another calibration by the manufacturer in 2014, shortly after the 2013 comparison of the CRDS instrument and the dew point mirror, showed no drift beyond the uncertainty range of the dew point mirror (given

by the manufacturer: 0.2 °C at +20 °C dew point, increasing linearly to 0.4 at −60 °C dew point (2 σ)) compared to the calibration in 2010.

Calibration bench for the FISH instrument

During the DENCHAR inter-comparison campaign in 2011 CRDS analyser CFKB2004 was compared against the laboratory calibration bench used regularly for calibration of the FISH reference instrument. This calibration bench consists of a humidifier, a mixing unit to mix dry and humid air, and a reference water vapour instrument, the MBW Dew Point instrument (model K-1806/DP30-SHSX-III, MBW Elektronik AG, Switzerland, http://www.mbw.ch) (Meyer et al., 2015). For the comparison the CRDS instrument was connected to the calibration bench via a 3 m long 1/8'' OD FEP line. Since the calibration bench provided a flow of about 3500 sccm an open split was installed in front of the FEP line to allow the CRDS analyser to sample at its low flow rate of 100 sccm. During the comparison four humidity steps covering the range of 2 to around 600 ppm were measured. This corresponds to the standard calibration range of the FISH calibration bench and is a good addition to the dew point mirror calibration range. Maximum uncertainty of the calibration bench is given as ± 4 % (1 σ) by Meyer et al. (2015).

Due to the low sample flow (100 sccm) through the analyser and the large difference in water vapour mole fraction between the measured air and the outside air during the comparison, permeation of water vapour through the FEP tube (3 m length in the calibration setup) has to be considered. To provide information from which a correction factor for the permeation effect could be determined, a dry tank air stream (~ 2 ppm water vapour mole fraction) at different flow rates (100 and 3500 sccm) was provided through the FEP tube. Assuming that for a flow of 3500 sccm the contribution of the permeation to the water vapour mole fraction in the flow is negligible, the correction factor was computed as the difference in the calibrated CRDS H_2O mole fraction between these two measurements.

Calibration by the CO_2 dilution effect

In addition to the standard calibrations by different hygrometers, a novel and completely independent calibration method was tested, which takes advantage of the high-precision CO_2 measurements by the CRDS analyser. Specifically, the dilution effect of water vapour on the CO_2 mole fraction is used: if water vapour is added to dry air, while total pressure and temperature of the gas remain unchanged, the mole fractions of the residual air components decrease. The mole fraction of CO_2 in dry air is

$$X_{CO_2}^{dry} = \frac{n_{CO_2}}{n_{air}+n_{CO_2}}, \qquad \text{(Equation 3.3)}$$

whereas the CO_2 mole fraction in wet air is given as

$$X_{CO_2}^{wet} = \frac{n_{CO_2}}{n_{air}+n_{CO_2}+n_{H_2O}} \qquad \text{(Equation 3.4)}$$

Together with the wet air mole fraction of water,

$$X_{H_2O}^{wet} = \frac{n_{H_2O}}{n_{air}+n_{CO_2}+n_{H_2O}}, \qquad \text{(Equation 3.5)}$$

Equations 3.3 and 3.4 yield

$$\frac{X_{CO_2}^{wet}}{X_{CO_2}^{dry}} = 1 - X_{H_2O}^{wet} \qquad \text{(Equation 3.6)}$$

Thus, the amount of water vapour in air is directly linked to the ratio of the CO_2 wet and dry air mole fractions of the air. However, the measured CO_2 mole fraction from the CRDS instruments in wet air is not only influenced by the dilution effect, but also by pressure-broadening effects of the water vapour. To separate both effects the measurement software of the analyser was modified to allow for a fine scan of the CO_2 and water vapour absorption line. While the peak height, which is normally used for the measurement, is influenced by both effects, the peak area only changes due to the dilution effect. The fine scan, combined with spectral models and fitting procedures optimized for this purpose, provides the peak areas with sufficient precision.

To test the concept, pressurized zero air with 3000 ppm CO_2 from a high-pressure tank was split into two paths, as can be seen in Figure 3.2. The air in one path was humidified in a bubbler. Afterwards the dry and wet gas streams were recombined and then measured by a CRDS analyser (CFADS2196, model G2301) in fine scan mode. With the help of mass flow controllers in both paths the water concentration of the combined stream could be varied without changing the CO_2 dry mole fraction by changing the flow of each path while the total flow was kept constant. The adjustable water vapour levels were limited by the remaining humidity in the pressurized air on the one hand and the environmental conditions in the laboratory on the other. The measurements alternated between the water line and the CO_2 line, requiring about 1.3 s to make one pair of measurements. Since the pressure and temperature in the sample cell were kept constant, the measured peak areas were proportional to the mole fractions:

$$X_i = C_i * A_i \qquad \text{(Equation 3.7)}$$

where *A* is the peak area and *C* the proportionality or 'calibration' factor. With Equation 3.6 this yield

$$A_{CO_2}^{wet} = A_{CO_2}^{dry}\left(1 - C_{H_2O} * A_{H_2O}\right) \qquad \text{(Equation 3.8)}$$

If the measured area of the CO_2 line is plotted as a function of the measured area of the water line, the calibration factor for water vapour C_{H2O} is just the ratio of the slope and the intercept. The scan of the water line also provided the conventional water vapour measurement using the peak height of the absorption line, which allowed for comparison of the two water vapour estimates.

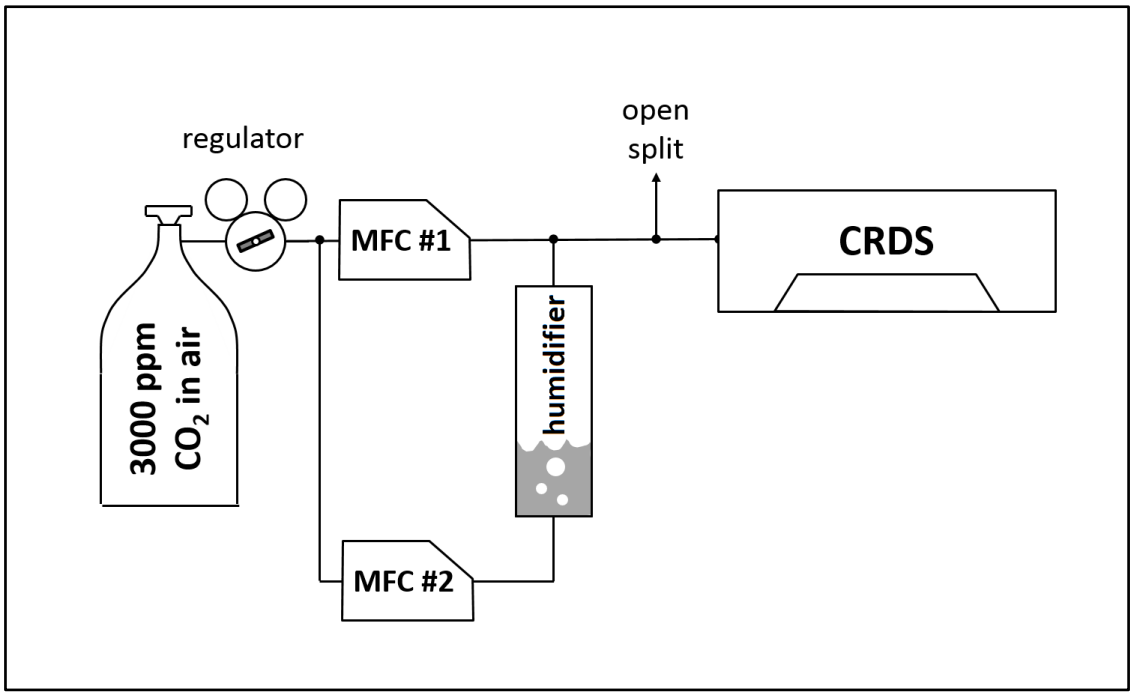

Figure 3.2: Experimental setup for the water vapour calibration by the CO2 dilution effect. MFC #1 and 2 are mass flow controllers.

3.3.2 Results and discussion

Dew point mirror

Plot a) in Figure 3.3 shows the self-broadening and offset corrected, but uncalibrated, water vapour mole fraction measured by the Picarro CRDS instrument (in the following referred to as '$H_2O_{uncalibrated}$') against the measurements from the dew point mirror (using its factory calibration from 2010, which was confirmed in 2014) during the comparison in 2013. The Dewmet measurements were converted from dew point to wet air mole fraction based on the Goff-Gratch equation (Goff, 1957). The corresponding fit can be seen as a blue line; the grey line indicates the calibration curve of the 2009 experiment (Equation 3.2). The uncertainty of the fitted slope is composed of the fitting error and the uncertainty of the dew point mirror. Uncertainty of the Dewmet is given by the manufacturer as 0.2 °C at +20 °C dew point, increasing linearly to 0.4 °C at -60 °C dew point (2 σ), which corresponds to a relative uncertainty of 1.3 %. In order to check the linearity of the CRDS instrument the CRDS and Dewmet data were also fitted using a quadratic fit. The slope of the quadratic fit was determined as 0.807 ± 0.011, which agrees well with the slope of the linear fit (0.802) taking account of the uncertainty range. The impact of the quadratic term (determined as 0.0024 ± 0.0021) on the result is small compared to the overall uncertainty range. Thus, the CRDS analyser can be considered linear.

Figure 3.3b shows the difference between the 2009 and 2013 calibrations. The error bars demonstrate the uncertainty range, which comprises the dew point mirror uncertainty during the 2009 and 2013 experiments. The relative difference of the two calibrations, shown on the right axis, increases from 1.7 % at 9800 ppm CRDS water vapour mole fraction (2.2 % with regard to the

measured mole fraction from the dew point mirror) up to 3.6 % at 30 600 ppm (4.4 %), indicating significant differences for water vapour mole fractions above about 10 000 ppm.

This difference between the 2009 and 2013 calibrations is much larger than the uncertainties of the instruments and the calibration transfer give reason to expect. The largest source of uncertainty is the dew point mirror with 1.3 % uncertainty. Precision of the CRDS analyser is given as <14 ppm by the manufacturer. Uncertainty of the calibration transfer between different Picarro analysers, which has to be considered since the two calibrations were done with different CRDS instruments, is <125 ppm (or 0.5 % relative at 25 000 ppm water vapour mole fraction) (Rella et al., 2013). Since the difference between the two calibrations is up to 3.6 % (4.4 %), the dew point mirror, the Picarro analyser, or both instruments must have been drifting.

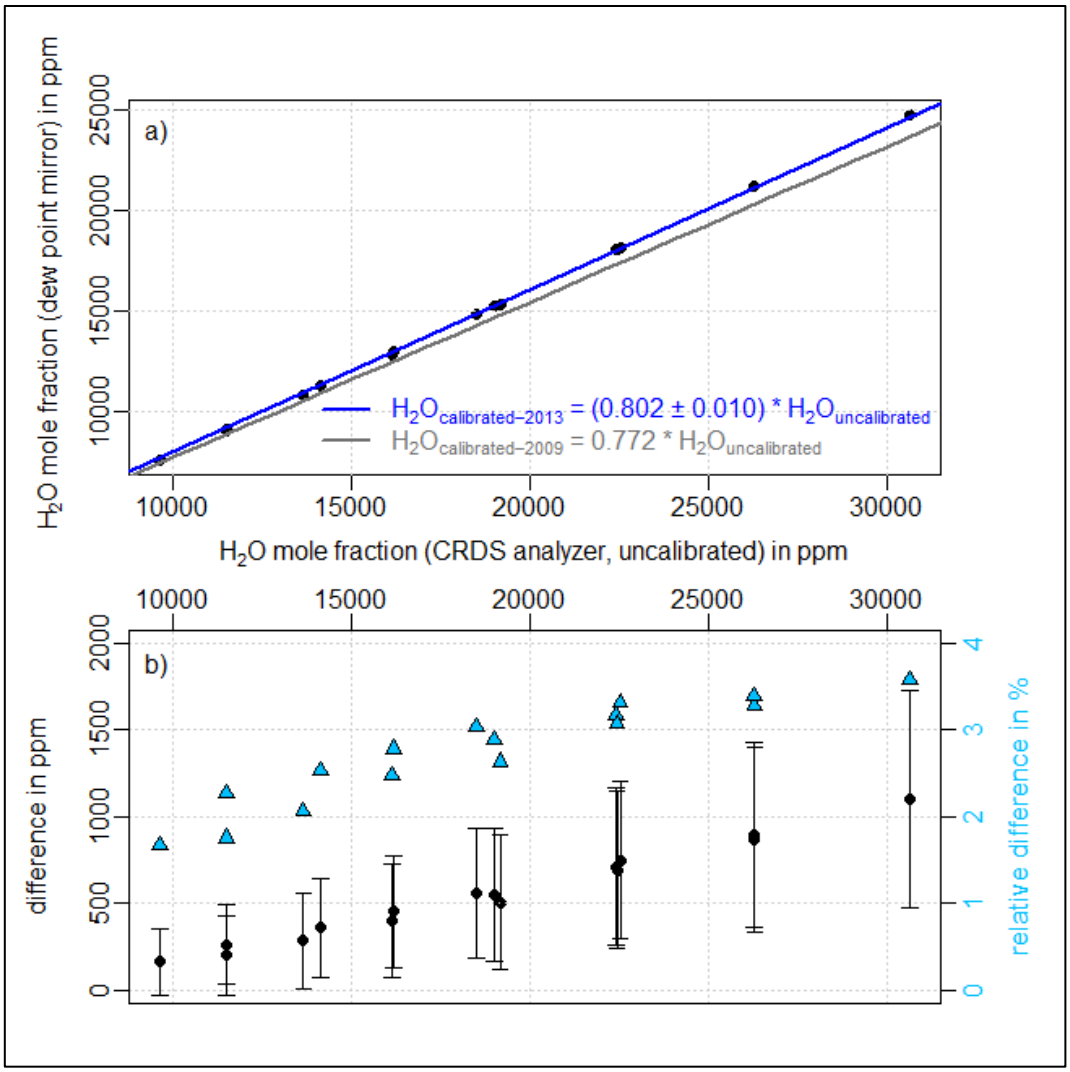

Figure 3.3: a) Uncalibrated water vapour measurements from the Picarro CRDS analyser (CFKBDS2003) against the measurements from the dew point mirror (Dewmet TDH) during the 2013 calibration. The corresponding fit is shown as blue line, the calibration curve of the 2009 comparison as a grey line. The uncertainty of the fitted slope is composed of the fitting error and the uncertainty of the dew point mirror. b) Water vapour difference between the 2009 and 2013 experiments. The error bars indicate the uncertainty range, which results from the combination of the dew point mirror uncertainties during the 2009 and the 2013 calibration. The relative differences are plotted on the right axis as light blue triangles.

In order to test the stability of the water vapour measurements of the CRDS analyser, the CFKBDS2003 instrument was compared to another Picarro CRDS analyser (CFADS37, model G3101-m) once in 2011 and again in 2014. During the experiments both instruments measured in parallel pressurized, dried ambient air from a high-pressure tank, which was humidified by a dew point generator (Li-610 from Li-Cor) to specific water levels between 2 and 20 ◦C dew point. Plot a) in Figure 3.4 shows the result of the 2014 comparison. The blue line is the quadratic fit of the 2011 comparison. The relative difference (right axis in plot b) between the two experiments is <0.3 % for water vapours <8000 ppm. Since it is unlikely that both instruments drifted in the same way, this strongly suggests that the CFKBDS2003 analyser did not drift significantly in the 3 years between the two comparisons against the dew point mirror.

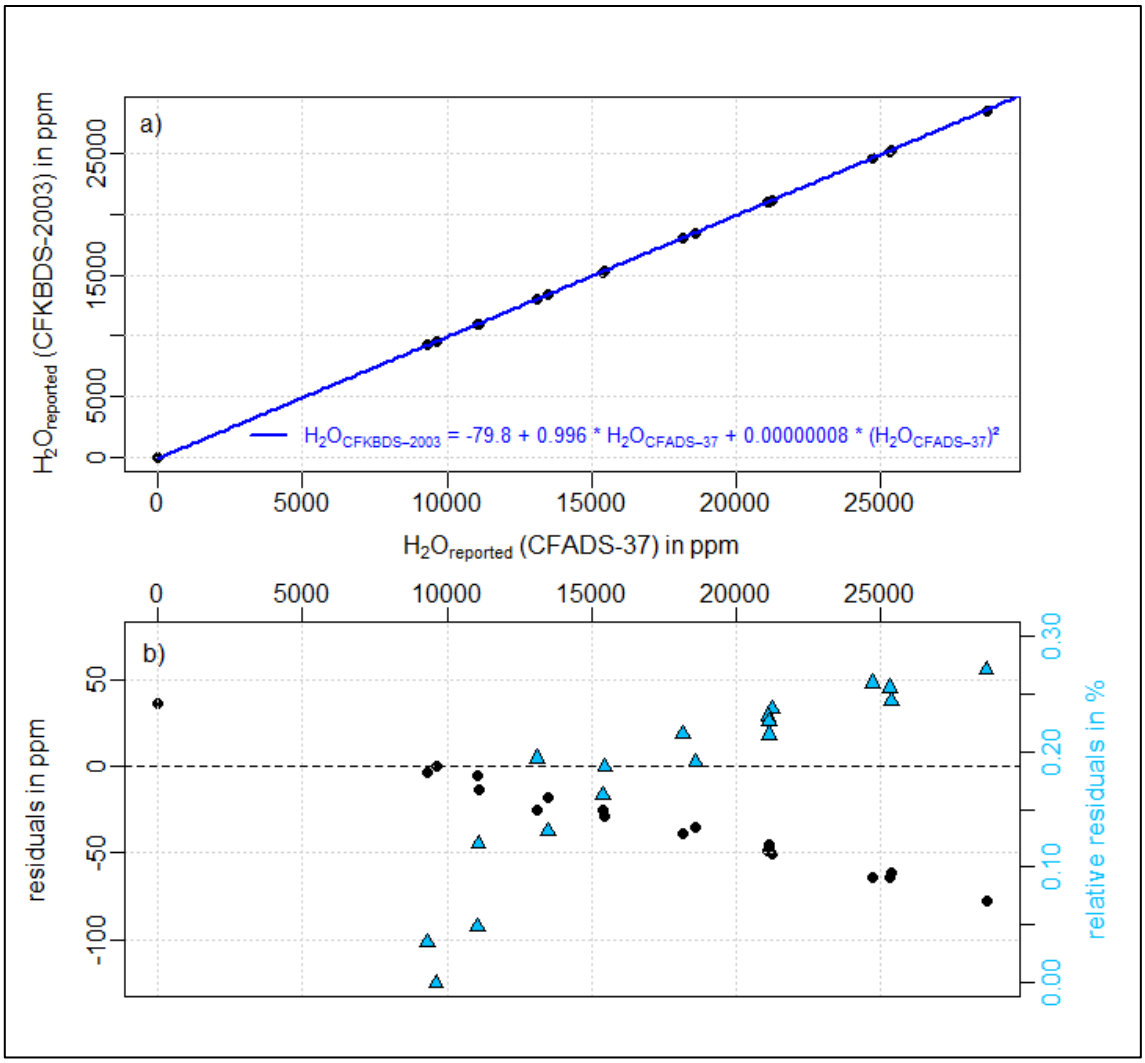

Figure 3.4: a) Uncalibrated water vapour mole fractions from the two Picarro CRDS analysers CFADS37 and CFKBDS2003 during a comparison experiment in 2014 (black points). The blue line indicates the quadratic fit of an earlier comparison between the same instruments in 2011. The differences between the two comparisons, thus the drift of the two analysers over the three years from 2011 to 2014, are shown in plot (b). The relative residuals are plotted on the right axis as light blue triangles. Since the analysers were not offset corrected before the experiment, the relative difference of 800 % of the data point at 4.5 ppm is less meaningful and is therefore not shown in order to improve the clarity of the plot.

This conclusion together with the calibration history of the dew point mirror (see Section 3.3.1) suggests that the large differences between the two calibrations of the CRDS instrument in 2009 and 2013 are caused by drift of the dew point mirror calibration. The dew point mirror had not been calibrated for nearly 9 years when it was used for the 2009 experiment but was calibrated well during the 2013 experiment. Thus, only the results of the 2013 experiment, corresponding to a calibration factor of 0.802 for the CRDS water vapour measurements, are considered reliable. Accuracy of the calibration is limited by the uncertainty range of the dew point mirror (1.3 %, 2 σ). For water vapour levels <7000 ppm the calibration is only extrapolated based on the measurements between 7000 and 25 000 ppm, which has to be accounted for in the uncertainty estimate.

Calibration bench for the FISH instrument

Plot a) in Figure 3.5 shows the result of the comparison between the CRDS analyser and the FISH calibration bench, during which four different water levels in the range 2-600 ppm were measured. The water vapour measurements from the CRDS analyser are offset corrected and calibrated according to the 2013 dew point mirror comparison, and additionally corrected for another 3.5 ppm resulting from permeation of water vapour from air surrounding the 3 m FEP inlet line. Subsequently, the CRDS measurements were converted from wet to dry air mole fractions according to

$$H_2O_{dry} = \frac{H_2O_{wet}}{1-H_2O_{wet}} \qquad \text{(Equation 3.9)}$$

A linear fit of the data shows that the dew point mirror calibration of the CRDS was within 3 % of the FISH calibration bench and showed an offset of 12.2 ppm. Uncertainties of the fit coefficients (slope: ±0.04, offset: ±0.5 ppm) were estimated assuming a worst-case scenario by including 4 % bias of the FISH calibration bench and 1.3 % uncertainty of the dew point mirror calibration. The residuals (difference between the FISH calibration bench and the fit) for water vapours >100 ppm, which can be seen in plot b, are small compared to the uncertainty range of the FISH calibration bench of 4 % indicated by the error bars. For the measurement point at 2 ppm water vapour the relative residuals are larger (6.2 %), due to the influence of the 12.2 ppm offset.

The CRDS analyser and the FISH calibration bench agree within 3 % in the water vapour range up to 600 ppm after correcting for an offset of 12 ppm. This confirms that extrapolation of the dew point mirror calibration to water vapour levels below 7000 ppm is appropriate, at least within the uncertainty of 4 % assumed for the calibration bench. Regarding the offset of 12.2 ppm it has to be considered that the measured air at the lowest water level, which has the largest effect on the estimation of the offset, was perhaps not completely in equilibrium with the inner surface of the connection line between the CRDS instrument and the calibration bench and the tubing inside the analyser. If the water vapour mole fraction in the gas stream decreases, water molecules adsorbed at the surface are released until a new equilibrium with the air is reached. Due to the large length of the connection line (3 m) the inner surface is relatively large and, thus, the equilibration process takes a relatively long time. For the higher measured water levels the equilibrium is reached faster.

Furthermore, except for the highest measured level, memory effects were cancelled out by measuring the water level twice: once from low to high, and once going from high to low mole fractions. The differences in the two measurement sequences are smaller than 1 ppm. Another possibility would be that the offset was caused by either an outgassing or a very small leak.

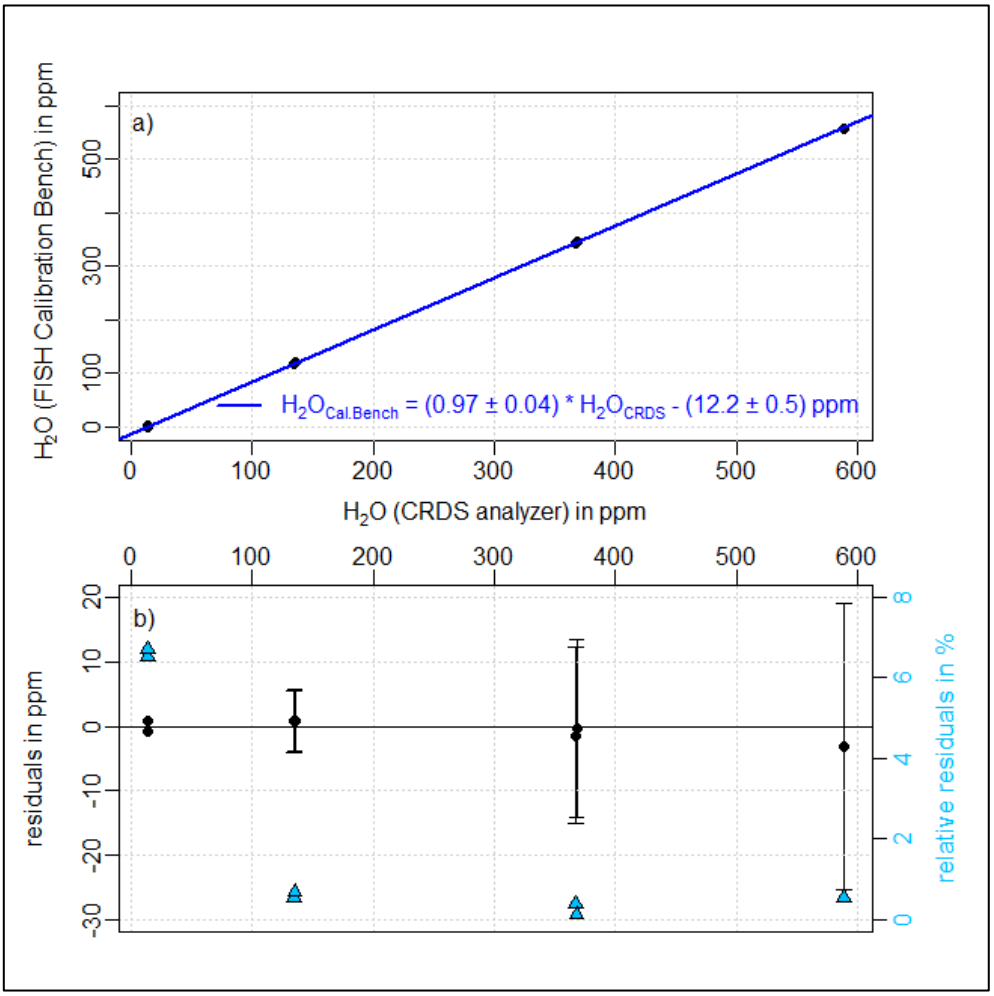

Figure 3.5: a) Dry air water vapour mole fractions measured by the CFKB2004 CRDS analyser and the FISH calibration bench during a comparison in 2011. The CRDS data are offset corrected and calibrated according to the 2013 comparison against a dew point mirror. The corresponding fit is shown in blue. Residuals (difference between water vapour mole fractions measured by FISH calibration bench and the linear fit) can be seen in the plot (b). Error bars indicate the uncertainty range of the calibration bench of 4 %. The relative residuals are plotted on the right axis as light blue triangles.

Calibration by CO_2 dilution effect

Figure 3.6a shows the comparison of the water vapour mole fraction determined with the help of the CO_2 dilution method and the conventional water vapour measurements, which are offset corrected and calibrated according to the 2013 dew point mirror comparison, during the fine scan experiment. A linear fit of the data indicates a bias of 2.9 % of the dilution-based water vapour compared to the dew point mirror calibration and an offset of 16.1 ppm. The uncertainty estimates (slope: ± 0.013, offset: ±1.6 ppm) are based on the uncertainty of the dew point mirror calibration (1.3 %, 2 σ). Residuals can be seen in plot b) of Figure 3.6.

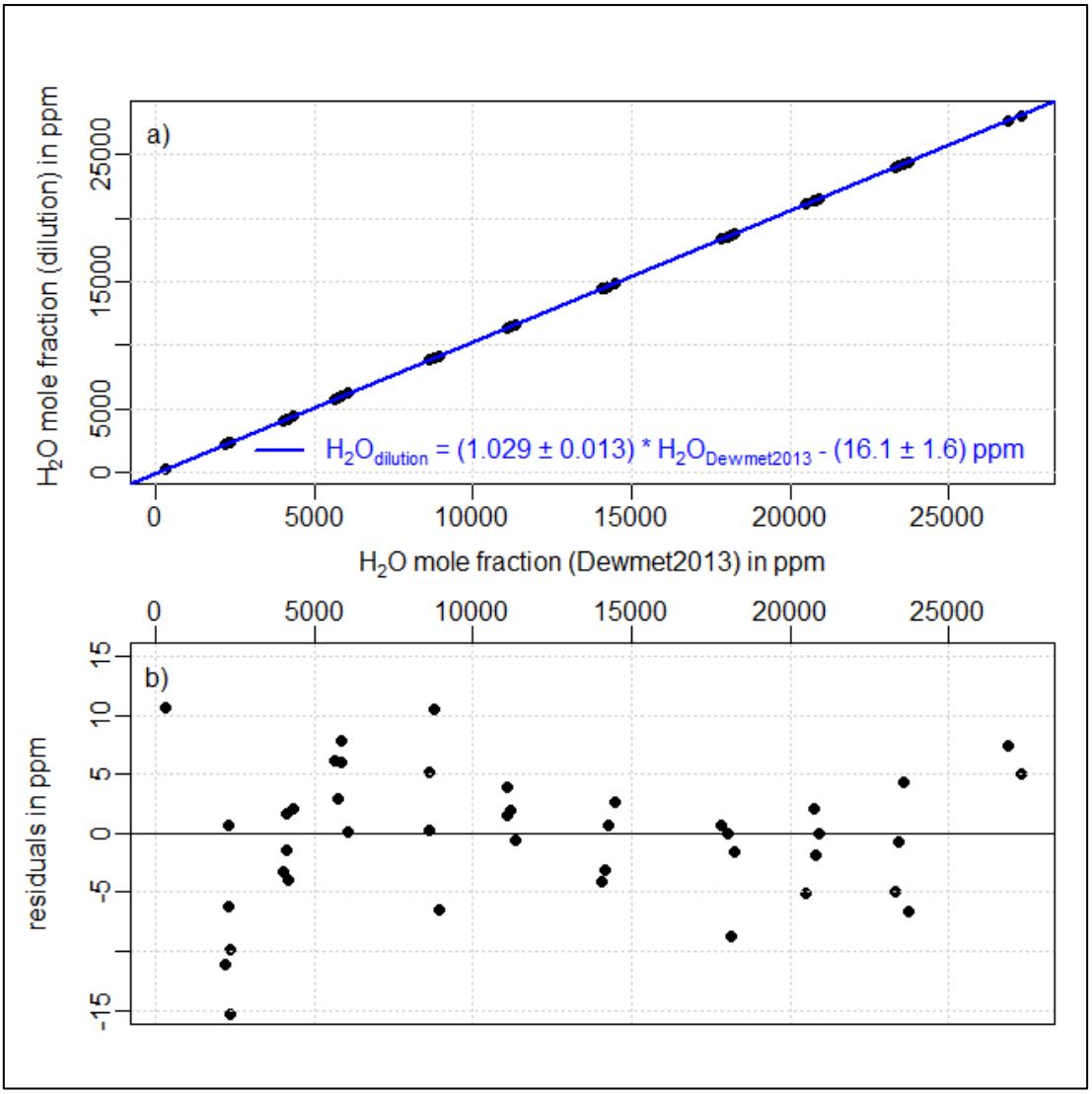

Figure 3.6: a) Water vapour mole fraction based on the CO_2 dilution method plotted against the water vapour mole fraction measurement from the CRDS analyser (offset corrected and calibrated according to the comparison against a dew point mirror in 2013) during the fine scan experiment. The corresponding fit is shown in blue. Residuals (difference between water vapour mole fraction based on dilution method and the linear fit) can be seen in plot (b).

The water vapour mole fraction calculated with the CO_2 dilution method and the conventional water vapour measurements calibrated according to the 2013 dew point mirror comparison agree within 2.9 % in the water vapour range from 300 to 27 000 ppm. The residuals (difference between water vapour mole fraction based on dilution method and the linear fit) are small, but show a slight systematic shape depending on the water vapour level. An offset was determined as 16.1 ppm; however, the lowest measurement was made at around 300 ppm and, thus, the offset is based on extrapolation. Higher scatter in the residuals at low water vapour (<2500 ppm) might indicate a different behaviour for this range. Hence, the estimated error of 1.6 ppm for the offset is likely a significant underestimate.

Estimating the uncertainty of the CO_2 dilution method is not straightforward. The repeatability of the peak area measurements accounts only for less than 0.1 % uncertainty (1 σ), whereas systematic errors can have a larger influence on the accuracy. One potential error is the direct spectroscopic interference of either water on CO_2 or vice versa, which we tried to avoid by careful selection of the used absorption lines and detailed spectral models. To check for remaining influences an additional test was conducted: since a direct spectroscopic interference would affect the measurements differently for different CO_2 concentrations, the fine scan experiment was repeated with 400 ppm CO_2 instead of the original 3000 ppm CO_2. Unfortunately, the pressurized air with 400 ppm CO_2 also contained 2 ppm of methane, whereas the 3000 ppm CO_2 air was pure CO_2 in zero air. Thus, a neighbouring methane absorption line had to be considered, which added another variable to the analysis. In future experiments this should be excluded by preparing a set of high-pressure tanks of exactly the same air composition but different CO_2 concentrations. The calibration constant C_{H2O} of the water measurements (see Equations.3.7 and 3.8) measured for 400 ppm CO_2 was 0.6 % larger than the calibration constant measured for 3000 ppm CO_2. Another systematic error can arise if the spectroscopic models and fitting procedures do not perfectly account for the changes in the absorption line shapes during varying water vapour mole fractions. For this experiment the absorption line shape model was carefully tested over the range of conditions in the analyser, and it was found that the corresponding error can be neglected compared to the other sources of uncertainty.

Recently, a potentially serious source of systematic error regarding the pressure control in the sample cell was discovered: observations suggest that the pressure sensor has a nonlinear dependence on water vapour and, thus, the pressure in the sample cell is stabilized to a humidity-dependent value instead of the fixed 186.65 hPa (= 140 Torr) (Reum et al., 2017). A possible reason could be adsorption of water molecules on the sensor. While this error in the CRDS water vapour measurements is corrected by the calibration of the instrument with another hygrometer, it has to be considered for the dilution calibration, since the used CO_2 measurements are affected as well. To assess the quantitative effect of such an incorrect pressure adjustment we assume the pressure in the measurement cell to be

$$p = p_0 + \Delta p \,, \qquad \text{(Equation 3.10)}$$

where p_0 is the actual set point at 186.65 hPa (140 Torr) and Δp is a pressure difference depending on the water vapour mole fraction. Experiments with an additional independent pressure measurement presented by Reum et al. (2017), as well as analysis of the behaviour of the proportional valve, which controls the pressure in the sample cell, show that Δp changes linearly with water vapour for mole fractions >2500 ppm (see Figure 2 in Reum et al., 2017). Therefore, the peak areas of the absorption lines follow

$$A(p) = A(p_0) * (1 + \frac{\Delta p}{p_0}) \,. \qquad \text{(Equation 3.11)}$$

Substituting $A_{CO2}(p_0)$ and $A_{H2O}(p_0)$ according to Equation 3.11 in Equation 3.8 yields

$$A_{CO_2}^{wet}(p) = A_{CO_2}^{dry}\left(1 - C_{H_2O}(p_0) * A_{H_2O}(p) + \frac{\Delta p}{p_0}\right) \qquad \text{(Equation 3.12)}$$

Thus, the bias in the sample cell pressure introduces an error to the calibration constant $C_{H2O}(p_0)$, which is proportional to the relative pressure change $\Delta p / p_0$. Reum et al. (2017) determine Δp as about 0.7 mbar (0.5 Torr) for a water vapour mole fraction of 30 000 ppm. Hence, the pressure bias causes an error of <0.4 % to the CO_2 dilution calibration method. Note however that the change in cell pressure with humidity is not linear for water vapour mole fractions <2500 ppm, which could be the reason for the slightly systematic shape in the residuals at this low water vapour levels (Figure 3.6b).

In summary it can be said that an uncertainty at percent or even sub-percent level is achievable for the dilution method in future experiments. Using a conservative estimate of 1 % uncertainty (1 σ) for assessing water vapour from the CO_2 dilution experiment presented here, added to the 1.3 % uncertainty of the dew point mirror calibration, comparison of the dilution-based estimate ($H_2O_{dilution}$ = (1.029 ± 0.023) · $H_2O_{dewmet2013}$) with the FISH calibration bench ($H_2O_{CalBench}$ = (0.97 ± 0.04) · $H_2O_{dewmet2013}$) (neglecting the offsets) shows an overlap within their combined uncertainty. Note that this also means that the H_2O calibration via dilution of CO_2 is statistically consistent with the classical calibration using dew point or frost point hygrometers. This is a promising result for this experiment, especially when considering that different CRDS instruments were used and the comparisons took place 2 years apart.

Follow-on experiments can achieve better and more reliable results for the water calibration by CO_2 dilution if low water vapour levels (<300 ppm) are also measured, the sample cell pressure is corrected for deviations due to different water vapour levels, optimized spectral models and fitting procedures are applied, and sample air with a CO_2 mole fraction in the atmospheric range is used. To determine a calibration factor for the water vapour estimates based on peak height measurements, which is the standard measurement method of the CRDS analysers at the moment, since it provides better short-term precision than the peak area measurements, the experiment can be simplified. As can be seen in equation 3.8 the water vapour mole fraction ($C_{H2O} \cdot A_{H2O}$) can be calculated if the dry and wet peak areas of the CO_2 absorption line are known. Thus, the measurement of the water vapour peak area can be skipped, which reduces the overall uncertainty. On the other hand, for low water vapour mole fractions (<10 ppm) a wrong pressure reading (as described above) has a higher impact since it affects the wet peak area, but not the dry peak area measurement. By looking at the deviation of the ratio between wet and dry peak areas to one the error gets enhanced even more.

Obviously, the dilution method can be applied to other species, too, and is not limited to CO_2 and water vapour. The same principle can be used for any species measurable by a CRDS analyser, provided that the corresponding dilution effect is large enough to be detectable with sufficient precision.

Calibration summary

Table 3.1 shows in summary the results of the different calibration experiments. The water vapour ranges used in the comparison were determined by the experimental setups of the experiments and the standard calibration ranges of the instruments. The uncertainties of the coefficients for the FISH calibration bench comparison result from the dew point mirror calibration uncertainty and the uncertainty of the calibration bench. For the CO_2 dilution effect, it is the dew point mirror calibration uncertainty plus a conservative estimate of the dilution method uncertainty. Note that both offset uncertainties are likely not reliable.

Based on these experiments the calibration constant of 0.802 ± 0.010 from the dew point mirror comparison in 2013 is recommended for the water vapour measurements from the CRDS instrument.

Table 3.1: Overview of the different calibration methods.

Method	Water vapour mole fraction range [ppm]	Result
dew point mirror (Dewmet) from 2013	7000-25000	$H_2O_{Dewmet2013} = (0.802 \pm 0.010) * H_2O_{uncalibrated}$
FISH calibration bench	2-600	$H_2O_{calBench} = (0.97 \pm 0.04) * H_2O_{Dewmet2013} - (12.2 \pm 0.5)$ ppm
CO_2 dilution effect	300-27000	$H_2O_{dilution} = (1.029 \pm 0.023) * H_2O_{Dewmet2013} - (16.1 \pm 1.6)$ ppm

3.4 Analysis of the flight data and comparison with the reference instruments

During the DENCHAR flight campaign between 23 May and 1 June 2011 four inter-comparison flights with a total flight time of about 14 h were conducted with a Learjet 35A. Starting from an airbase in Hohn, Germany, the flights covered a region ranging from northern Germany and Poland to southern Norway and the North and Baltic seas, and altitudes up to 12.5 km, so that the lower stratosphere was also reached. Two instruments served as reference instruments for the water vapour measurements. The first was CR-2, a frost point hygrometer with an accuracy of ± 0.1 °C (1 σ) dew point (manufacturer data, Buck Research Instruments L.L.C., US, http://www.hygrometers.com). The second reference instrument was FISH, which is based on the Lyman-α photofragment fluorescence technique and has an accuracy of 6 % to 8 % (1 σ) in the range from 4 to 1000 ppm and 0.3 ppm for lower mixing ratios down to 1 ppm (Meyer et al., 2015). The CR-2 was connected to a backward-facing inlet to avoid sampling of cloud and ice particles. In contrast, FISH measured total water instead of only water vapour during the campaign, since its forward-oriented inlet resulted in sampling of cloud droplets and ice crystals when present.

3.4.1 Measurement precision

To assess the measurement precision of the CRDS analyser, water vapour measurements during the periods with stable atmospheric conditions, such as pressure and temperature, were selected. Of course, there are still natural variations left in the data; therefore, only upper limits of the precision can be estimated. After correcting for offset and calibration (according to the 2013 dew point mirror comparison, in the following simply referred to as CRDS measured water vapour), the standard deviation of the difference between the 0.4 Hz data and the 60 s moving average is calculated as a measure of short-term fluctuations. In order to avoid additional noise from variations in sample cell pressure, periods with unstable sample cell pressure were neglected. Deviations of the sample cell pressure from its set point of 186.65 hPa can occur during sudden, fast changes in altitude for which the pressure adjustment is too slow to adapt. Figure 3.7 shows the resulting short-term fluctuations (i.e., the standard deviations of the difference between the 0.4 Hz data and the 60 s moving average) for different water vapour ranges. The significance of the results certainly depends strongly on the number of data, which were available to calculate the standard deviations in each water vapour interval. Thus, in order to find a reliable estimate for the measurements, results based on a larger number of data are highlighted. Although high scatter of the data between 30 and 100 ppm makes it difficult to find a reliable estimate, the flight data suggest an upper limit for the measurement precision (1 σ) of 4 ppm for H_2O <10 ppm, 20 % or 10 ppm (whichever is smaller) for 10 ppm < H_2O < 100 ppm, and 5 % or 30 ppm (whichever is smaller) for water vapour >100 ppm.

For comparison precision estimates of the CRDS water vapour measurements determined under laboratory conditions, at 2.5 s time resolution and for an integration time of 30 s, are shown in Table 3.2. They were derived from experiments during which the CRDS analyser measured pressurized, dried ambient air from a high-pressure tank, which was humidified by a dew point generator (Li-610 from Li-Cor) to specific water levels. For water vapour <100 ppm the results of the flight and laboratory data are in good agreement. For water vapour >1000 ppm the laboratory data indicate that a precision of 30 ppm for the flight data is a very conservative estimate, which is most likely due to natural variations in the atmosphere.

Compared to the reference instruments the precision of the CRDS analyser is worse at low water vapour levels (<100 ppm), but comparable at higher levels.

Table 3.2: Precision estimates (1-sigma) of the CRDS water vapour measurements derived from laboratory experiments.

water vapour mole fraction [ppm]	precision at 2.5 s time resolution [ppm]	precision at 30 s integration time [ppm]
3	<6	<2
30	<10	<5
5000	<9	<5
8000	<10	<2
12000	<10	<4
19000	<12	<6

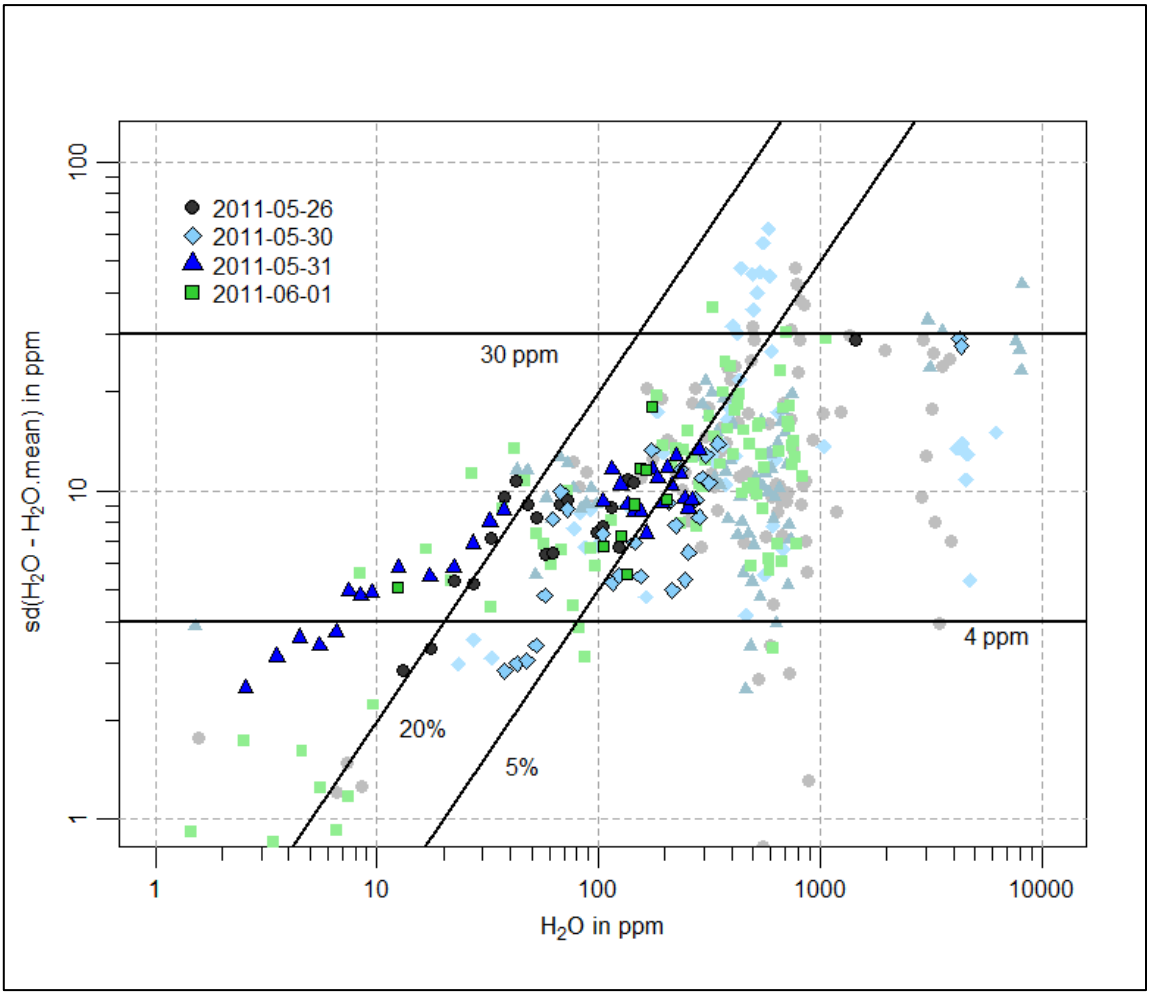

Figure 3.7: Standard deviation of the difference between the 0.4 Hz CRDS flight data and the 60 second averages, averaged for intervals of 1 ppm, 5 ppm, 10 ppm, and 100 ppm water vapour in the corresponding water vapour ranges of 0-10 ppm, 10-100 ppm, 100-1000 ppm, 1000-10000 ppm, respectively. Different colours and symbols indicate different flights. Results with higher priority are highlighted. The horizontal and diagonal black lines indicate standard deviations of 4 and 30 ppm, and 5 and 20 % respectively.

3.4.2 Response time

Figure 3.8 and Figure 3.9 show selected time periods of the third flight on 31 May and the fourth flight on 1 June, respectively. CRDS measured water vapour is shown along with the flight data from reference instruments CR-2 and FISH. Water vapour measurements from two additional analysers that participated in the inter-comparison campaign are also presented: flight data of WaSul-Hygro, a tunable diode laser-based dual-channel photoacoustic humidity measuring system (Tátrai et al., 2015) and flight data of the Selective Extractive Airborne Laser Diode Hygrometer (SEALDH-1), which is based on tunable diode laser absorption spectroscopy (Buchholz et al., 2012) (please note: not to be confused with the currently used new instrument SEALDH-II, which has a much better performance and smaller uncertainties). Furthermore, the saturated water vapour is added to point out that the measurements were taken outside of clouds.

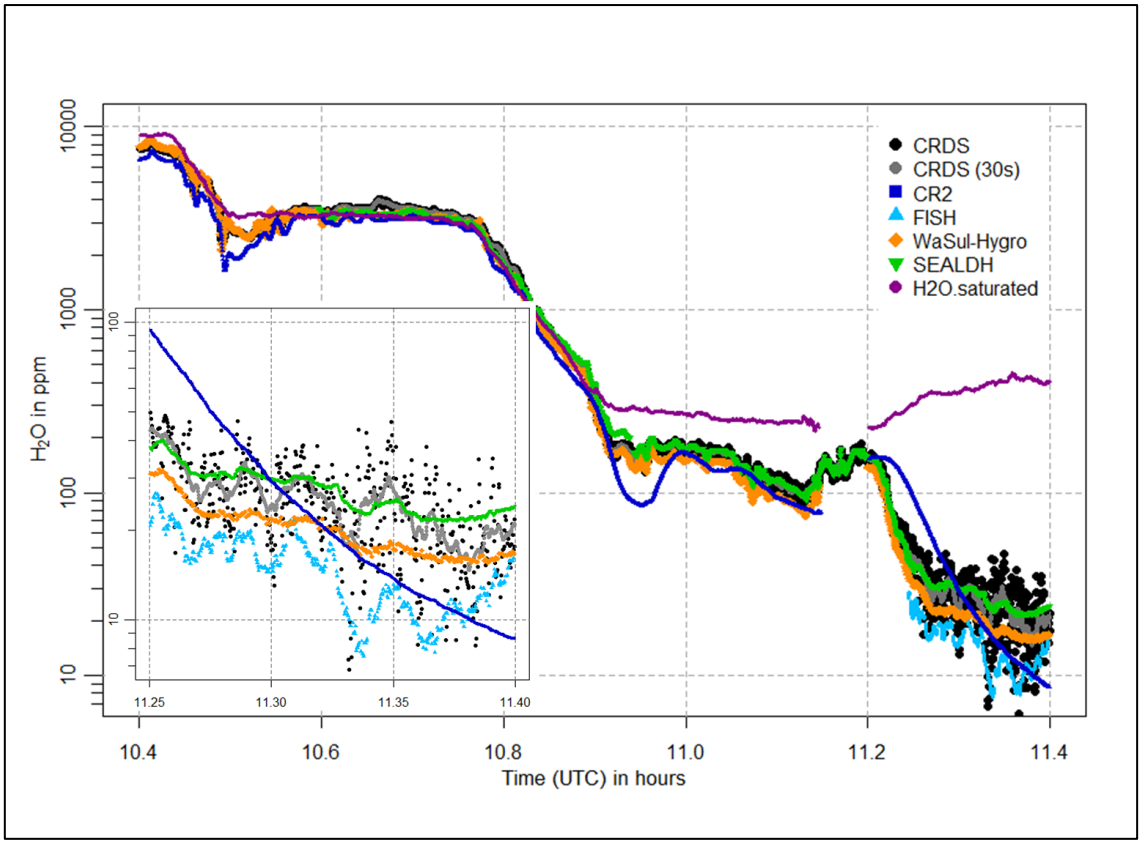

Figure 3.8: Water vapour mole fractions measured by the CRDS analyser (black points, 30 seconds mean as grey points), the CR-2 (dark blue squares) and FISH (light blue triangles) instruments, as well as the WaSul-Hygro (orange diamonds) and SEALDH-I (green triangles) analysers, for a time period during the flight on 31 May 2011. An enlarged section for the time period from 11:15 to 11:24 is shown in the lower left part of the plot.

The flight data of all analysers in Figure 3.8 and Figure 3.9 indicate that the response time of the CRDS is similar to that of the other instruments. This applies for the whole water vapour range and for both transition directions: from wet to dry conditions as well as from dry to wet. For water vapours <100 ppm the response time is comparable to the FISH instrument, as shown in the enlarged section of Figure 3.8. During the increase in water vapour from 200 to 1200 ppm in about 1 min, shown in the enlarged section in Figure 3.9, no significant delay can be detected. Thus, the low sample gas flow of 100 sccm and the 50 cm long inlet line cause no disadvantages. As expected, the slowest response is shown by the CR-2, whose measurement signal tends to overshoot and oscillate after fast changes in water vapour.

Results of a simple laboratory test, where a three-way valve was used to switch between wet (around 23 000 ppm) and dry (around 10 ppm) air, allowed us to estimate the 10 % to 90 % rise and 90 % to 10 % fall times as 6-7 s and the recovery time to 99 % of the final water vapour level as 25 s. For a step from 23 000 to 10 ppm water vapour mole fraction the measurement takes about 200 s to get down. The times are pretty much identical regardless of whether or not the 50 cm long inlet line is included.

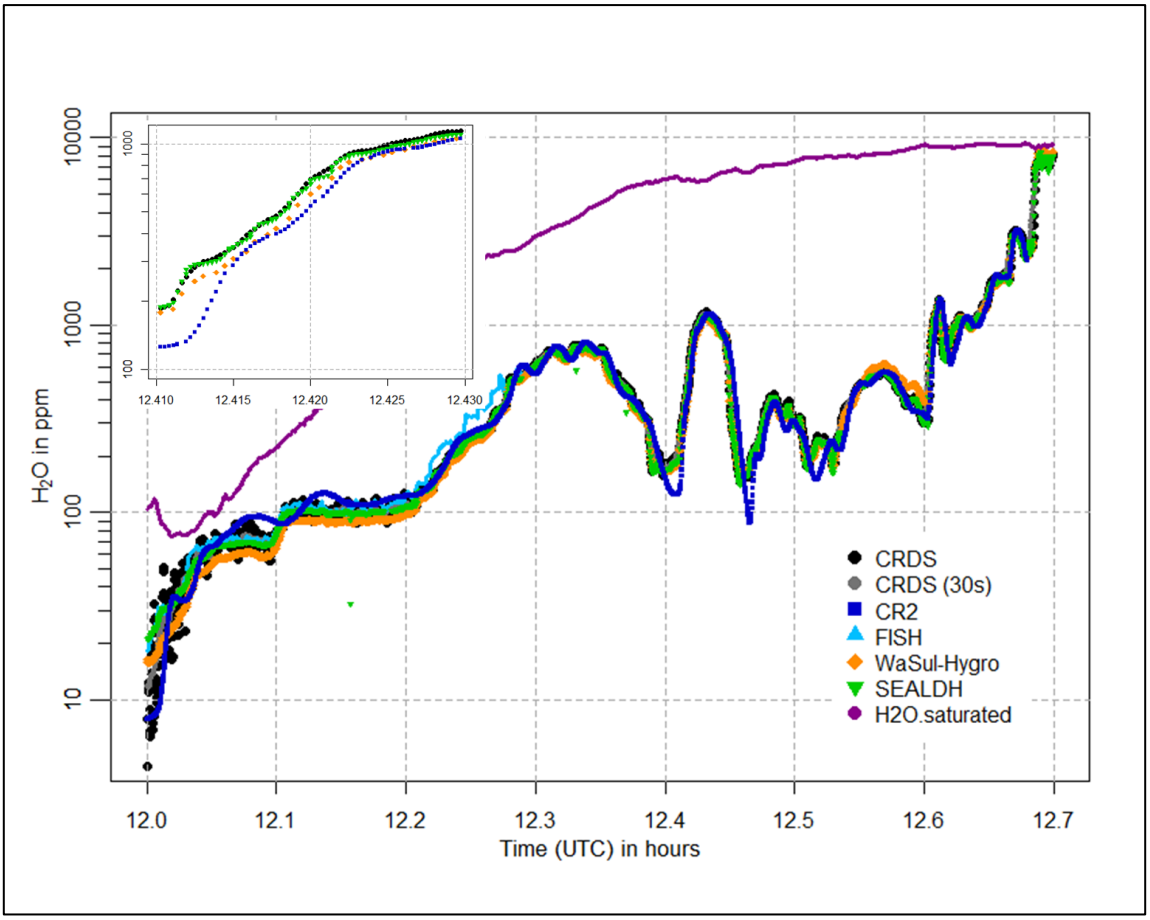

Figure 3.9: Same as Figure 3.8, but for a time period during the flight on 1 June 2011. An enlarged section for the time period from 12:24:36 to 12:25:48 is shown in the upper left part of the plot. Here the water vapour increases in one minute about an order of magnitude from 200 to 1200 ppm.

3.4.3 Comparison to reference instruments

Figure 3.10 shows the in-flight CRDS measured water vapour and the CR-2 and FISH reference instruments, as well as the corresponding atmospheric pressure levels, for all four flights. Due to an internal leak FISH could not deliver reliable data for the first two flights. CRDS data from the first flight after around 13:00 were compromised by icing of the inlet, since the de-icing of the Rosemount inlet was accidentally not switched on during that flight.

The water vapour differences between the three instruments for different water vapour intervals are plotted in Figure 3.11. CRDS data influenced by icing during the first flight are omitted. Likewise, measurement data of all instruments in the presence of clouds are excluded, since FISH measured total water. Based on observations during the flights, which are recorded in the flight logs, this concerns in particular all measurements made between 11:13 and 11:40 on flight 4 (1 June).

A reliable evaluation is hard to make as the FISH reference instrument operated successfully for only two of the four flights, and for flight 4 the measurements diverge significantly from the CR-2 data to a large extent. Moreover, the slow response of the CR-2 and the oscillations of the signal after sudden changes in water vapour are problematic for the comparison.

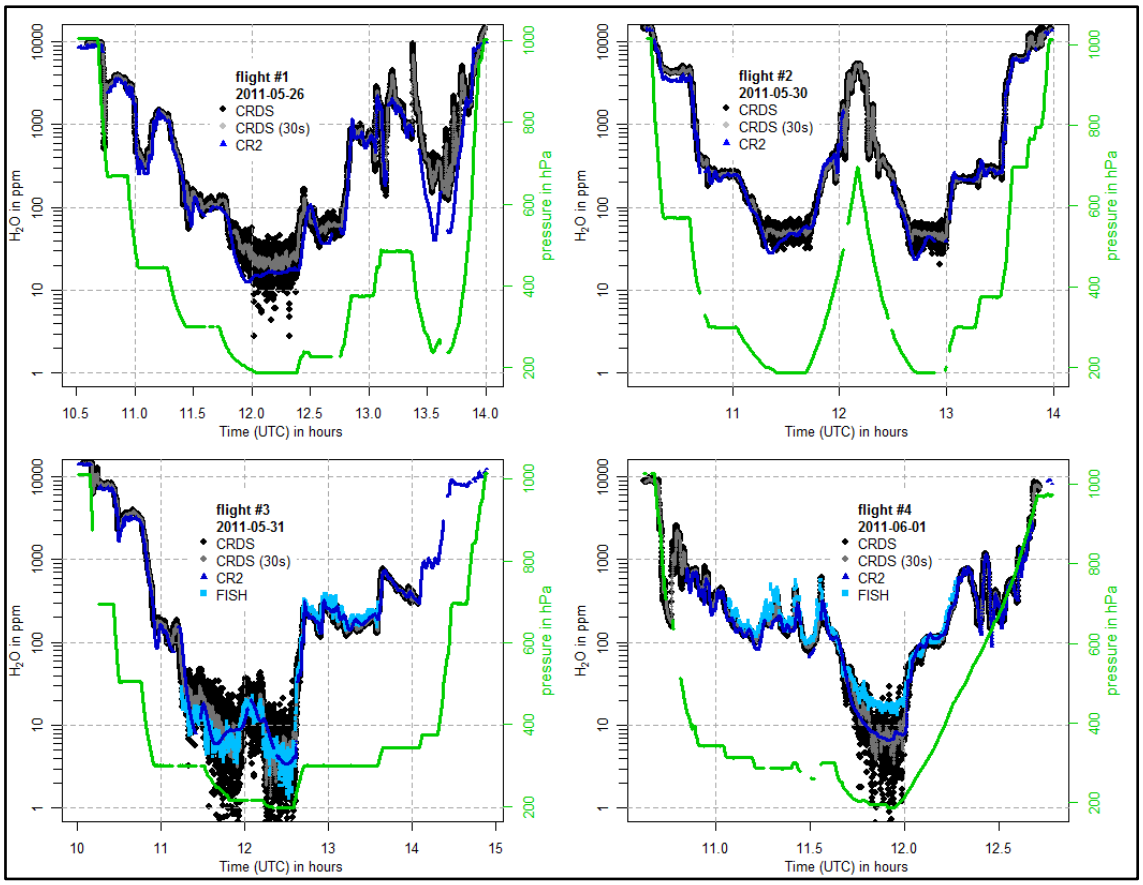

Figure 3.10: In-flight water vapour data from the CRDS analyser (in black, 30 seconds mean in grey) and the reference instruments CR-2 (in dark blue) and FISH (in light blue) for the four flights on 26 May, 30 May, 31 May, and 1 June 2011. The corresponding atmospheric pressure levels are shown in green. The CRDS data are offset corrected and calibrated according to the 2013 dew point mirror comparison.

Furthermore, flight data between 11:13 and 11:40 for flight 4 could not be used, due to the occurrence of clouds. However, it is interesting that the CRDS water vapour measurements deviate from the CR-2 during that period, as can be seen in Figure 3.10. Figure 3.12 shows a closer look at this cloud-affected flight section. The CRDS measured water vapour is plotted together with flight data of CR-2, FISH, Wasul-Hygro and SEALDH-I. The latter two show approximately the same behaviour as the CR-2. This is in line with expectation, since all three shared the same backward-faced inlet, which prevented from sampling cloud droplets. However, the CRDS shows a behaviour similar to that of FISH (measuring total water) with H_2O mole fractions within clouds larger than that corresponding to saturated water vapour. This indicates that the CRDS sampling was likely also affected by cloud particles, i.e., the separation in the Rosemount air inlet of ice particles and water droplets from the sample air is not fully efficient. In fact, relative humidity measurements from the MOZAIC humidity device, which uses the same type of Rosemount Inlet housing, occasionally show similar artefacts, when measuring within clouds, containing liquid water (air temperature > −40 °C) (Smit et al., 2013). Most likely some small ice particles and water droplets are able to follow the sharp right angle turn of the minor air flow into the inner part of the Rosemount housing, instead of flying straight through the main channel of the housing (see Figure 2.6 in Smit et al., 2013). Such small enough particles could be produced, e.g., by the

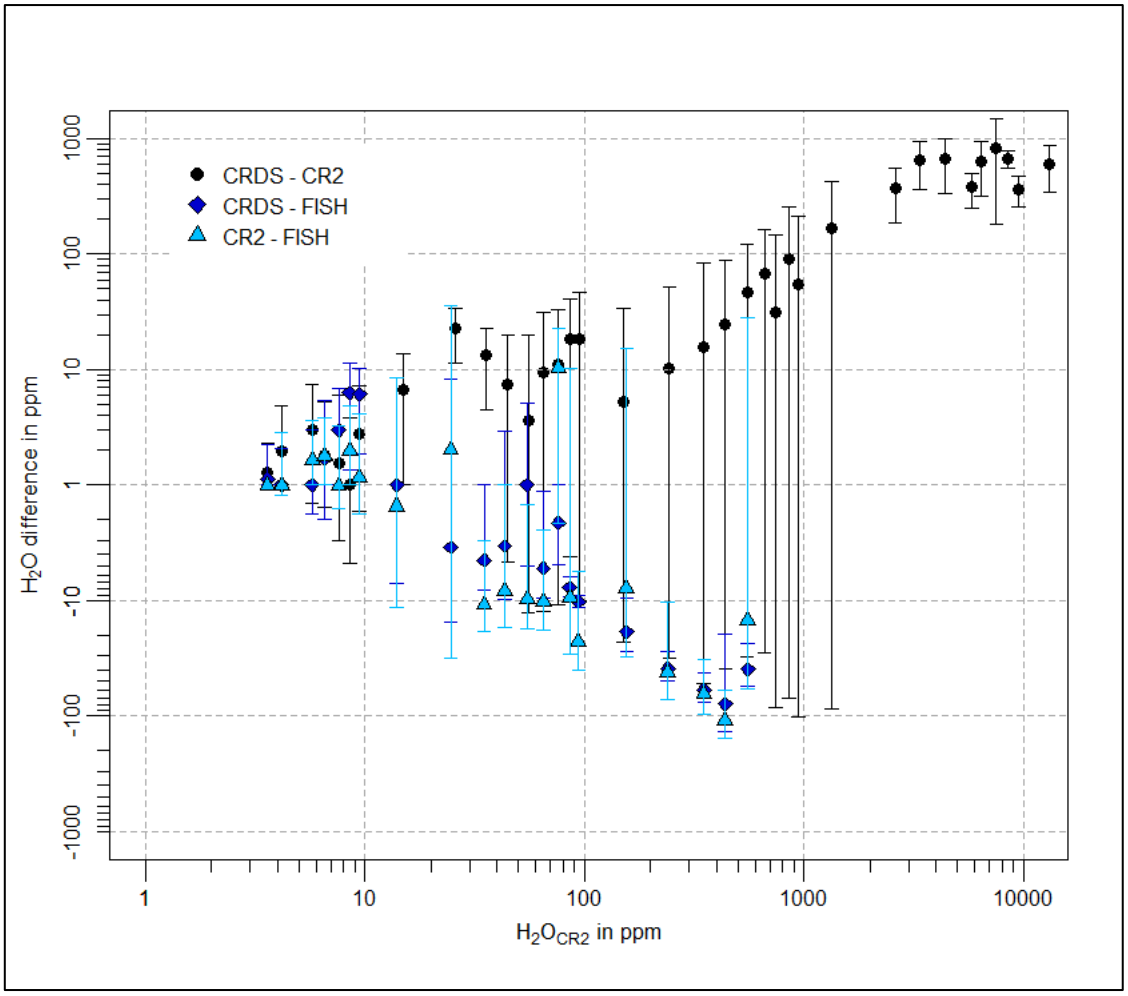

Figure 3.11: Differences of the 30 seconds mean CRDS and CR-2 in-flight data (black points), CRDS and FISH data (dark blue diamonds), and CR-2 and FISH data (light blue triangles) averaged over intervals of 1 ppm, 10 ppm, 100 ppm, 1000 ppm, and 10000 ppm water vapour in the corresponding water vapour ranges of 0-10 ppm, 10-100 ppm, 100-1000 ppm, 1000-10000 ppm, and >10000 ppm, respectively, against the CR-2 water vapour flight data. Error bars indicate the standard deviations of the average differences. The water vapour measurements of CR-2 are chosen as x-axis, because they cover all flights in contrast to the FISH data. For plotting reasons all differences <1 ppm were set to 1 ppm.

shattering of water droplets or ice crystals in the Rosemount housing. However, due to the very short time period the sample air stays inside the housing until it passes the sensor elements and leaves again through a small outlet, only the liquid water droplets can evaporate fast enough to be observed by the humidity device. In contrast, as can be seen in Figure 3.12, the CRDS measurements do show cloud artefacts also at air temperatures below -40 °C, i.e., in pure ice clouds. Most likely the reason for this is that water droplets and ice particles enter the inlet line of the CRDS and are evaporated within the inlet line or at the heated inlet filter of the CRDS. Meaningful statistics about how often droplets and ice particles are measured in clouds can be obtained as soon as more flight data from the CRDS analyser are available within the IAGOS project, since every IAGOS aircraft equipped with the GHG package is also equipped with the MOZAIC humidity device and a cloud probe.

The absolute differences in Figure 3.11 indicate a positive difference between the CRDS and CR-2 of <10 % or 10 ppm (whichever is greater) for water vapour ranges >10 ppm. FISH has a negative deviation to both instruments in that range. For water vapour >100 ppm the data imply a difference of 10 % to 20 %. For the interval of 10-100 ppm water vapour the difference to the CRDS is around 10 %, to CR-2 about 10 ppm. At very low water vapour (<10 ppm) the reference instruments show a good agreement during flight 3 but disagree strongly during flight 4. On average the CR-2 has a positive bias <2 ppm against FISH. For the CRDS the water vapour data suggest a positive bias <2-3 ppm to the CR-2, but the measurements are highly affected by the slow response of the CR-2. Comparison to FISH likewise indicates a positive difference <2-3 ppm. During comparison against the FISH calibration bench the CRDS analyser showed a positive bias of 12.2 ppm (see Section 3.3.2), which strengthens the presumption that the air has not been in equilibrium for the lowest water vapour level measured during the experiment.

Meyer et al. (2015) report an agreement of FISH with other in situ and remote sensing hygrometers under field conditions of about ± 5 % to 20% at <10 ppm and ± 0 % to 15 % at >10 ppm. Thus, results of the comparison between CRDS and FISH during the DENCHAR inter-comparison campaign are at the upper end of that range.

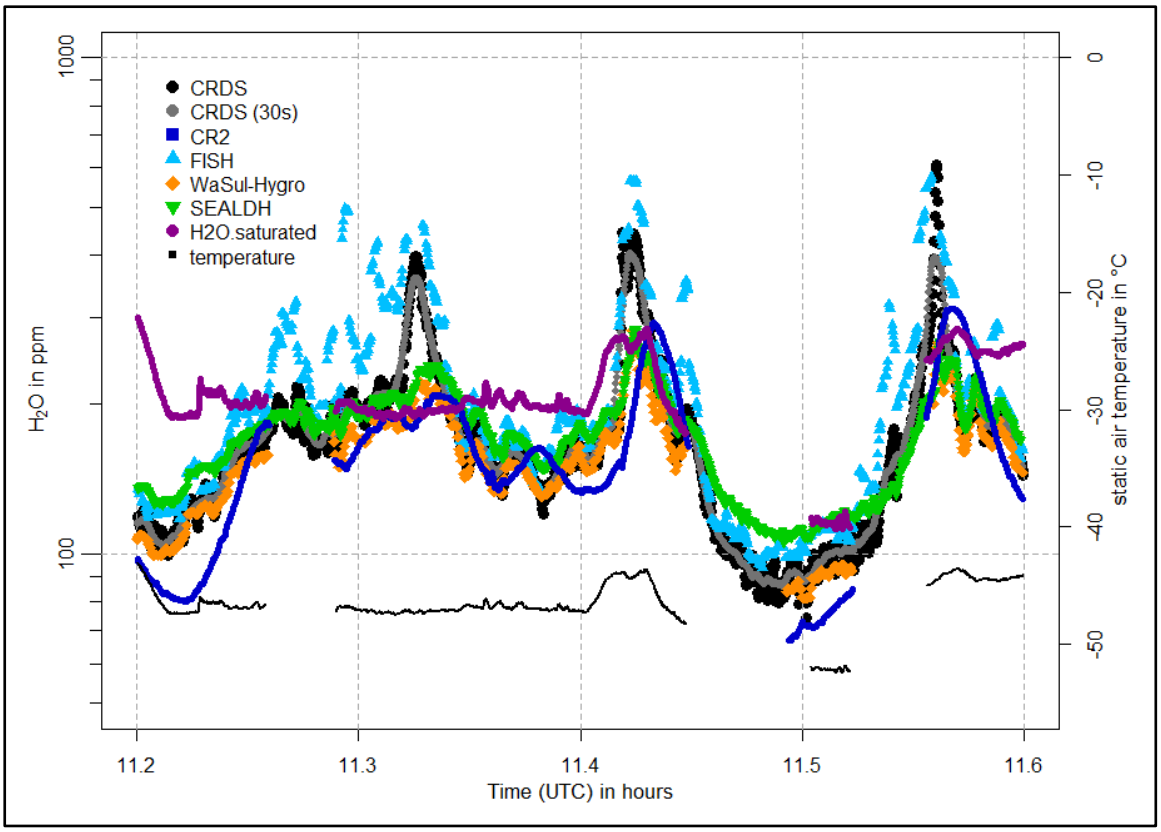

Figure 3.12: Water vapour mole fractions from the CRDS analyser (black points, 30 seconds mean as grey points), the CR-2 (dark blue squares) and FISH (light blue triangles) instruments, as well as the WaSul-Hygro (orange diamonds) and SEALDH-I (green triangles) analysers, during the flight on 1 June 2011, in the presence of clouds. Also shown are the water vapour mole fraction corresponding to saturation (violet points) and the static air temperature (black line).

3.5 Conclusions

During the DENCHAR inter-comparison flight campaign in Hohn (Germany) in May–June 2011 a commercial cavity ring-down spectroscopy (CRDS) based gas analyser (G2401-m, Picarro Inc., US) was installed on a Learjet to measure atmospheric water vapour, CO_2, CH_4 and CO. The components of the instrument and the inlet system are identical to those chosen for the IAGOS-core Greenhouse Gas package.

For the calibration of the water vapour measurements three different methods were tested. The standard calibration of the CRDS analyser is the comparison against a dew point mirror (Dewmet TDH, Cooled Mirror Dewpointmeter, Michell Instruments Ltd., UK) in the range from about 8000 to 30 000 ppm water vapour mole fraction. If the dew point mirror is calibrated regularly by the manufacturer, the accuracy of this calibration method is limited by the uncertainty range of the dew point mirror (1.3 %, 2 σ). A comparison against the FISH calibration bench, during the DENCHAR flight campaign, in the range from 2 to 600 ppm water vapour, confirmed that the extrapolation of the dew point mirror calibration down to low water vapour levels is possible, and that the standard calibration of the CRDS analyser is in agreement with the FISH calibration within the 4 % uncertainty range (1 σ) of the FISH calibration bench. Furthermore, a new and completely independent calibration method, which is based on measurement of the dilution effect of water vapour on the CO_2 mole fraction, was presented. This new method was found to agree with the dew point mirror calibration within 2.9 % in the water vapour range from 300 to 27 000 ppm. Assuming a conservative 1 % uncertainty (1 σ) for the CO_2 dilution method, comparison of the dilution-based estimate with the FISH calibration bench showed an overlap within their combined uncertainty. Thus, the water vapour calibration via dilution of CO_2 is statistically consistent with the classical calibration using dew point or frost point hygrometers. The dilution method can be used for the calibration of other species, too, provided they and the corresponding diluted species are measurable by a CRDS analyser and the dilution effect is large enough to be within the detection limits.

An upper limit of the precision (1 σ) of the water vapour measurements by the CRDS was determined from flight data of the DENCHAR inter-comparison campaign, as 4 ppm for H_2O <10 ppm, 20 % or 10 ppm (whichever is smaller) for 10 ppm < H_2O < 100 ppm, and 5 % or 30 ppm (whichever is smaller) for water vapour >100 ppm. A more reliable estimate will be possible as soon as more H_2O flight data are available. During the four DENCHAR flights the CRDS analyser showed a good time response (10 % to 90 % rise and 90 % to 10 % fall times: 6-7 s, recovery time to 99 % of the final water vapour level: 25 s) and long-term stability for the water vapour measurements. Comparison against the reference instruments was difficult, due to lack of data availability of FISH, the slow response of CR-2, the exclusion of data, which were affected by clouds, and the partly poor agreement between FISH and CR-2. However, for water vapour levels >10 ppm the flight data imply a negative difference between the CRDS and FISH from about 10 % to 20 % and a positive difference between the CRDS and CR-2 of <10 % or 10 ppm (whichever is greater). For water vapour <10 ppm the flight data suggest a positive bias of <2-3 ppm to both FISH and CR-2.

Accuracy (1 σ) of the CRDS instrument was estimated, based on the laboratory calibrations, as 1 % for the water vapour range from 25 000 ppm down to 7000 ppm, then increasing to 5 % at 50 ppm water vapour. Accuracy at water vapour mole fractions below 50 ppm was difficult to assess, as the reference systems suffered from lack of data availability.

Future deployment of the CRDS system within IAGOS will help to further evaluate the performance, via better statistics and long-term comparison to the MOZAIC humidity device, which is deployed on each IAGOS aircraft. Thus, essential water vapour measurements, including regular in situ data in the sensible UTLS region and vertical profiles of H_2O in the troposphere and lower stratosphere for major parts of the globe, are expected to be delivered for validation of remote sensing based observations from satellites and ground, for the improvement of the performance of climate models and weather forecasts, or for climate trend studies.

3.6 References

Buchholz, B., Kühnreich, B., Smit, H.G.J., and Ebert, V.: Validation of an extractive, airborne, compact TDL spectrometer for atmospheric humidity sensing by blind intercomparison, Appl. Phys. B, 110, 249-262, doi:10.1007/s00340-012-5143-1, 2012.

Buchholz, B., Afchine, A., Klein, A., Schiller, C., Krämer, M., and Ebert, V.: HAI, a new airborne, absolute, twin dual-channel, multi-phase TDLAS-hygrometer: background, design, setup, and first flight data, Atmos. Meas. Tech., 10, 35-57, doi:10.5194/amt-10-35-2017, 2017.

Chen, H., Winderlich, J., Gerbig, C., Hoefer, A., Rella, C. W., Crosson, E. R., Van Pelt, A. D., Steinbach, J., Kolle, O., Beck, V., Daube, B. C., Gottlieb, E. W., Chow, V. Y., Santoni, G. W., and Wofsy, S. C.: High-accuracy continuous airborne measurements of greenhouse gases (CO_2 and CH_4) using the cavity ring-down spectroscopy (CRDS) technique, Atmos. Meas. Tech., 3, 375–386, doi:10.5194/amt-3-375-2010, 2010.

Crosson, E. R.: A cavity ring-down analyser for measuring atmospheric levels of methane, carbon dioxide, and water vapour, Appl. Phys. B, 92, 403–408, doi:10.1007/s00340-008-3135-y, 2008.

Dessler, A. E., Zhang, Z., and Yang, P.: Water-vapour climate feedback inferred from climate fluctuations, 2003–2008, Geophys. Res. Lett., 35, L20704, doi:10.1029/2008GL035333, 2008.

Dirksen, R. J., Sommer, M., Immler, F. J., Hurst, D. F., Kivi, R., and Vömel, H.: Reference quality upper-air measurements: GRUAN data processing for the Vaisala RS92 radiosonde, Atmos. Meas. Tech., 7, 4463–4490, doi:10.5194/amt-7-4463-2014, 2014.

Fahey, D. W., Gao, R.S., Carslaw, K. S. , Kettleborough, J., Popp, P. J., Northway, M. J., Holecek, J. C., Ciciora, S. C., McLaughlin, R. J., Thompson, T. L., Winkler, R. H., Baumgardner, D. G., Gandrud, B., Wennberg, P. O., Dhaniyala, S., Mckinney, K., Peter, Th., Salawitch, R. J., Bui, T. P., Elkins, J.W., Webster, C. R., Atlas, E. L., Jost, H., Wilson, J. C., Herman, R. L., Kleinböhl, A., and von König, M.: The Detection of Large HNO_3-Containing Particles in the Winter Arctic Stratosphere, Science, 291, 1026-1031, 2001.

Fahey, D. W., Gao, R.-S., Möhler, O., Saathoff, H., Schiller, C., Ebert, V., Krämer, M., Peter, T., Amarouche, N., Avallone, L. M., Bauer, R., Bozóki, Z., Christensen, L. E., Davis, S. M., Durry, G., Dyroff, C., Herman, R. L., Hunsmann, S., Khaykin, S. M., Mackrodt, P., Meyer, J., Smith, J. B., Spelten, N., Troy, R. F., Vömel, H., Wagner, S., and Wienhold, F. G.: The AquaVIT-1 Intercomparison of Atmospheric Water Vapour Measurement Techniques, Atmos. Meas. Tech., 7, 3177-3213, doi:10.5194/amt-7-3177-2014, 2014.

Filges, A., Gerbig, C., Chen, H., Franke, H., Klaus, C., and Jordan, A.: The IAGOS-core greenhouse gas package: a measurement system for continuous airborne observations of CO_2, CH_4, H_2O and CO, Tellus B, 67,27989, doi:10.3402/tellusb.v67.27989, 2015.

Forster, P. M. de F. and Shine, K. P.: Assessing the climate impact of trends in stratospheric water vapour, Geophys. Res. Lett., 29(6), 1086, doi:10.1029/2001GL013909, 2002.

Gierens, K., Schumann, U., Helten, M., Smit, H., and Marenco, A.: A distribution law for relative humidity in the upper troposphere and lower stratosphere derived from three years of MOZAIC measurements, Ann. Geophys., 7, 1218-1226, 1999.

Goff, J. A.: Saturation pressure of water on the new Kelvin temperature scale, Transactions of the American society of heating and ventilating engineers, presented at the semi-annual meeting of the American society of heating and ventilating engineers, 347-354, Murray Bay, Que. Canada, 1957.

Hall, E. G., Jordan, A. F., Hurst, D. F., Oltmans, S. J., Vömel, H., Kühnreich, B., and Ebert, V.: Advancements, measurement uncertainties, and recent comparisons of the NOAA frostpoint hygrometer, Atmos. Meas. Tech., 9, 4295-4310, doi:10.5194/amt-9-4295-2016, 2016.

Harries, J. E., Russell, J. M., Tuck, A. F., Gordley, L. L., Purcell, P., Stone, K., Bevilacqua, R. M., Gunson, M., Nedoluha, G., and Traub, W. A.: Validation of measurements of water vapour from the Halogen Occultation Experiment (HALOE), J. Geophys. Res., 101(D6), 10,205-10,216, 1996.

Helten, M., Smit, H. G. J., Straeter, W., Kley, D., Nedelec, P., Zöger, M., and Busen, R.: Calibration and performance of automatic compact instrumentation for the measurement of relative humidity from passenger aircraft, J. Geophys. Res., 103, 25,643–25,652, 1998.

Hurst, D. F., Oltmans, S. J., Vömel, H., Rosenlof, K. H., Davis, S. M., Ray, E. A., Hall, E. G., and Jordan, A. F.: Stratospheric water vapour trends over Boulder, Colorado: Analysis of the 30 year Boulder record, J. Geophys. Res., 116, D02306, doi:10.1029/2010JD015065, 2011.

Kaufmann, S., Voigt, C., Jurkat, T., Thornberry, T., Fahey, D. W., Gao, R.-S., Schlage, R., Schäuble, D., and Zöger, M.: The airborne mass spectrometer AIMS – Part 1: AIMS-H_2O for UTLS water vapour measurements, Atmos. Meas. Tech., 9, 939–953, doi:10.5194/amt-9-939-2016, 2016.

Kiehl, J. T. and Trenberth, K. E.: Earth's annual global mean energy budget, Bull. Am. Meteorol. Soc., 78(2), 197-208, doi:10.1175/1520-0477, 1997.

Kley, D., Russell III, J. M., and Phillips, C., SPARC assessment of upper tropospheric and stratospheric water vapour, World Climate Research Programme Rep. 113, WMO/TD No. 1043, SPARC Rep. No. 2, 324 pp, Geneva, Switzerland, 2000.

Kunz, A., Mueller, R., Homonnai, V., Janosi, I. M., Hurst, D., Rap, A., Forster, P. M., Rohrer, F., Spelten, N., and Riese, M.: Extending water vapour trend observations over Boulder into the tropopause region: trend uncertainties and resulting radiative forcing, J. Geophys. Res. Atmos., 118, 11269-11284, doi:10.1002/jgrd.50831, 2013.

Lambert, A., Read, W., Livesey, N., Santee, M., Manney, G., Froidevaux, L., Wu, D., Schwartz, M., Pumphrey, H., Jimenez, C., Nedoluha, G., Cofield, R., Cuddy, D., Daffer, W., Drouin, B., Fuller, R., Jarnot, R., Knosp, B., Pickett, H., Perun, V., Snyder, W., Stek, P., Thurstans, R., Wagner, P., Waters, J., Jucks, K., Toon, G., Stachnik, R., Bernath, P., Boone, C., Walker, K., Urban, J., Murtagh, D., Elkins, J., and Atlas, E.: Validation of the Aura Microwave Limb Sounder middle atmosphere water vapour and nitrous oxide measurements, J. Geophys. Res., 112, D24S36, doi:10.1029/2007JD008724, 2007.

Marenco, A., Thouret, V., Nédélec, P., Smit, H., Helten, M., Kley, D., Karcher, F., Simon, P., Law, K., Pyle, J., Poschmann, G., Von Wrede, R., Hume, C., and Cook, T.: Measurement of ozone and water vapour by Airbus in-service aircraft: The MOZAIC airborne program, An overview, J. Geophys. Res., 103(D19), 25631–25642, 1998.

May, R. D.: Open-path, near-infrared tunable diode laser spectrometer for atmospheric measurements of H_2O, J. Geophys. Res., 103, 19,161-19,172, 1998.

J. Meyer, J. , Rolf, C., Schiller, C., Rohs, S., Spelten, N., Afchine, A., Zöger, M., Sitnikov, N., Thornberry, T. D., Rollins, A. W., Bozóki, Z., Tátrai, D., Ebert, V., Kühnreich, B., Mackrodt, P., Möhler, O., Saathoff, H., Rosenlof, K. H., and Krämer, M.: Two decades of water vapour measurements with the FISH fluorescence hygrometer: a review, Atmos. Chem. Phys., 15, 8521–8538, doi:10.5194/acp-15-8521-2015, 2015.

Milz, M., von Clarmann, T., Fischer, H., Glatthor, N., Grabowski, U., Höpfner, M., Kellmann, S., Kiefer, M., Linden, A., Mengistu Tsidu, G., Steck, T., Stiller, G. P., Funke, B., López-Puertas, M., and Koukouli, M. E.: Water vapour distributions measured with the Michelson Interferometer for Passive Atmospheric Sounding on board Envisat (MIPAS/Envisat), J. Geophys. Res., 110, D24307, doi:10.1029/2005JD005973, 2005.

Oltmans, S. J., Vömel, H., Hofmann, D. J., Rosenlof, K. H., and Kley, D.: The increase in stratospheric water vapour from balloonborne, frostpoint hygrometer measurements at Washington, D.C., and Boulder, Colorado, Geophys. Res. Lett., 27(21), 3453–3456, doi:10.1029/2000GL012133, 2000.

Petzold A., Thouret, V., Gerbig, C., Zahn, A., Brenninkmeijer, C. A.M., Gallagher, M., Hermann, M., Pontaud, M., Ziereis, H., Boulanger, D., Marshall, J., Nédélec, P., Smit, H. G.J., Friess, U., Flaud, J.-M., Wahner, A., Cammas, J.-P., and Volz-Thomas, A.: Global-scale atmosphere monitoring by in-service aircraft - current achievements and future prospects of the European Research Infrastructure IAGOS, Tellus B, 67, 28452, doi:10.3402/tellusb.v67.28452, 2015.

Read, W. G., Lambert, A., Bacmeister, J., Cofield, R. E., Christensen, L. E., Cuddy, D. T., Daffer, W. H., Drouin, B. J., Fetzer, E., Froidevaux, L., Fuller, R., Herman, R., Jarnot, R. F., Jiang, J. H., Jiang, Y. B., Kelly, K., Knosp, B. W., Kovalenko, L. J., Livesey, N. J., Liu, H.-C., Manney, G. L., Pickett, H. M., Pumphrey, H. C., Rosenlof, K. H., Sabounchi, X., Santee, M. L., Schwartz, M. J., Snyder, W. V., Stek, P. C., Su, H., Takacs, L. L., Thurstans, R. P., Vomel, H., Wagner, P. A., Waters, J. W., Webster,

C. R., Weinstock, E. M., and Wu, D. L.: Aura Microwave Limb Sounder upper tropospheric and lower stratospheric H2O and relative humidity with respect to ice validation, J. Geophys. Res., 112, D24S35, doi:10.1029/2007JD008752, 2007.

Rella, C.W.: Accurate Greenhouse Gas Measurements in Humid Gas Streams Using the Picarro G1301 Carbon Dioxide/Methane/Water Vapour Gas Analyser, Picarro, Inc., Santa Clara, CA, USA, http://www.picarro.com/resources/whitepapers, 2010.

Rella, C. W., Chen, H., Andrews, A. E., Filges, A., Gerbig, C., Hatakka, J., Karion, A., Miles, N. L., Richardson, S. J., Steinbacher, M., Sweeney, C., Wastine, B., and Zellweger, C.: High accuracy measurements of dry mole fractions of carbon dioxide and methane in humid air, Atmos. Meas. Tech., 6, 837-860, doi:10.5194/amt-6-837-2013, 2013.

Reum, F., Gerbig, C., Lavric, J. V., Rella, C. W., Göckede, M.: An improved water correction function for Picarro greenhouse gas analysers, Atmos. Meas. Tech. Discuss., https://doi.org/10.5194/amt-2017-174, 2017.

Riese, M., Ploeger, F., Rap, A., Vogel, B., Konopka, P., Dameris, M., and Forster, P.: Impact of uncertainties in atmospheric mixing on simulated UTLS composition and related radiative effects, J. Geophys. Res., 117, D16305, doi:10.1029/2012JD017751, 2012.

Rind, D., Chiou, E. W., Chu, W., Oltmans, S., Lerner, J., Larsen, J., McCormick, M.P., and McMaster, L.: Overview of the Stratospheric Aerosol and Gase Experiment II water vapour observations: Method, validation, and data characteristics, J. Geophys. Res., 98(D3), 4835-4856, 1993.

Rollins, A. W., Thornberry, T. D., Gao, R. S., Smith, J. B., Sayres, D. S., Sargent, M. R., Schiller, C., Krämer, M., Spelten, N., Hurst, D. F., Jordan, A. F., Hall, E. G., Vömel, H., Diskin, G. S., Podolske, J. R., Christensen, L. E., Rosenlof, K. H., Jensen, E. J., and Fahey, D. W.: Evaluation of UT/LS hygrometer accuracy by intercomparison during the NASA MACPEX mission, J. Geophys. Res., 119, 1915-1935, doi:10.1002/2013JD020817, 2014.

Rozanov, A., Weigel, K., Bovensmann, H., Dhomse, S., Eichmann, K.-U., Kivi, R., Rozanov, V., Vömel, H., Weber, M., and Burrows, J. P.: Retrieval of water vapour vertical distributions in the upper troposphere and the lower stratosphere from SCIAMACHY limb measurements, Atmos. Meas. Tech., 4, 933-954, doi:10.5194/amt-4-933-2011, 2011.

Russell, J. M., Gordley, L. L., Park, J., Drayson, S. R., Tuck, A. F., Harries, J. E., Cicerone, R. J., Crutzen, P. J., and Frederick, J. E.: The Halogen Occultation Experiment, J. Geophys. Res., 98, 10,777-10,797, 1993.

Sayres, D. S., Moyer, E. J., Hanisco, T. F., St. Clair, J. M., Keutsch, F. N., O'Brien, A., Allen, N. T., Lapson, L., Demusz, J. N., Rivero, M., Martin, T., Greenberg, M., Tuozzolo, C., Engel, G. S., Kroll, J. H., Paul, J. B., and Anderson, J. G.: A new cavity based absorption instrument for detection of

water isotopologues in the upper troposphere and lower stratosphere, Rev. Sci. Instrum., 80, 044102, doi:10.1063/1.3117349, 2009.

Schneider, M., Hase, F., and Blumenstock, T.: Water vapour profiles by ground-based FTIR spectroscopy: study for an optimised retrieval and its validation, Atmos. Chem. Phys., 6, 811-830, doi:10.5194/acp-6-811-2006, 2006.

Smit, H. G. J., Volz-Thomas, A., Helten, M., Pätz, H.-W., and Kley, D.: An in-flight Calibration Method for Near-Real-Time Humidity Measurements with the Airborne MOZAIC sensor, Journal of atmospheric and oceanic technology, 25, 656-666, doi:10.1175/2007JTECHA975.1, 2008

Smit, H.G.J., Kivi, R., Vömel, H., and Paukkunen, A.: Thin Film Capacitive Sensors, in: Monitoring Atmospheric Water Vapour: Ground-Based Remote Sensing and In-situ Methods, Kämpfer, N. (Ed.), ISSI Scientific Report Series 10, 11-38, Springer Science+Buisness Media, New York, doi: 10.1007/978-1-4614-3909-7, 2013.

Smith, C. A., Haigh, J. D., and Toumi, R.: Radiative forcing due to trends in stratospheric water vapour, Geophys. Res. Lett., 28, 179-182, 2001.

Solomon, S., Rosenlof, K. H., Portmann, R. W., Daniel, J. S., Davis, S. M., Sanford, T. J., and Plattner, G.-K.: Contributions of stratospheric water vapour to decadal changes in the rate of global warming, Science, 327, 1219-1223, doi:10.1126/science.1182488, 2010.

Tátrai, D., Bozóki, Z., Smit, H., Rolf, C., Spelten, N., Krämer, M., Filges, A., Gerbig, C., Gulyás, G., and Szabó, G.: Dual-channel photoacoustic hygrometer for airborne measurements: background, calibration, laboratory and in-flight intercomparison tests, Atmos. Meas. Tech., 8, 33-42, doi:10.5194/amt-8-33-2015, 2015.

Volz-Thomas, A., Berg, M., Heil, T., Houben, N., Lerner, A., Petrick, W., Raak, D., Pätz, H.-W.: Measurements of total odd nitrogen (NO_y) aboard MOZAIC in-service aircraft: instrument design, operation and performance, Atmos. Chem. Phys., 5(3), 583-595, 2005.

Volz-Thomas, A., Cammas, J.-P., Brenninkmeijer, C. A. M., Machida, T., Cooper, O., Sweeney, C., Waibel, A.: Civil Aviation Monitors Air Quality and Climate, Journal of the Air & Waste Management Association, October 2009, 16-19. 2009.

von Clarmann, T., Höpfner, M., Kellmann, S., Linden, A., Chauhan, S., Funke, B., Grabowski, U., Glatthor, N., Kiefer, M., Schieferdecker, T., Stiller, G. P., and Versick, S.: Retrieval of temperature, H_2O, O_3, HNO_3, CH_4, N_2O, $ClONO_2$ and ClO from MIPAS reduced resolution nominal mode limb emission measurements, Atmos. Meas. Tech., 2, 159-175, doi:10.5194/amt-2-159-2009, 2009.

Vömel, H., David, D. E., and Smith, K.: Accuracy of tropospheric and stratospheric water vapour measurements by the cryogenic frost point hygrometer: Instrumental details and observations, J. Geophys. Res., 112, D08305, doi:10.1029/2006JD007224, 2007.

Vömel, H., Naebert, T., Dirksen, R., and Sommer, M.: An update on the uncertainties of water vapour measurements using cryogenic frost point hygrometers, Atmos. Meas. Tech., 9, 3755-3768, doi:10.5194/amt-9-3755-2016, 2016.

Weigel, K., Rozanov, A., Azam, F., Bramstedt, K., Damadeo, R., Eichmann, K.-U., Gebhardt, C., Hurst, D., Kraemer, M., Lossow, S., Read, W., Spelten, N., Stiller, G. P., Walker, K. A., Weber, M., Bovensmann, H., and Burrows, J. P.: UTLS water vapour from SCIAMACHY limb measurements V3.01 (2002–2012), Atmos. Meas. Tech. , 9, 133-158, doi:10.5194/amt-9-133-2016, 2016.

Weinstock, E. M., Smith, J. B., Sayres, D. S., Pittman, J. V., Spackman, J. R., Hintsa, E. J., Hanisco, T. F., Moyer, E. J., St. Clair, J. M., Sargent, M. R., and Anderson, J. G.: Validation of the Harvard Lyman-a in situ water vapour instrument: Implications for the mechanisms that control stratospheric water vapour, J. Geophys. Res., 114, D23301, doi:10.1029/2009JD012427, 2007.

Winderlich, J., Chen, H., Gerbig, C., Seifert, T., Kolle, O., Lavrič, J. V., Kaiser, C., Höfer, A., and Heimann, M.: Continuous low maintenance CO_2/CH_4/H_2O measurements at the Zotino Tall Tower Observatory (ZOTTO) in Central Siberia, Atmos. Meas. Tech., 3, 1113-1128, doi:10.5194/amt-3-1113-2010, 2010.

World Meteorological Organization (WMO): Guide to Meteorological Instruments and Methods of Observation, 2008 edition, updated in 2010, WMO-No. 8, Geneva, 2012.

Zöger, M., Afchine, A., Eicke, N., Gerhards, M.-T., Klein, E., McKenna, D. S., Mörschel, U., Schmidt, U., Tan, V., Tuitjer, F., Woyke, T., and Schiller, C.: Fast in situ stratospheric hygrometers: A new family of balloon-borne and airborne Lyman-α photofragment fluorescence hygrometers, J. Geophys. Res., 104, 1807-1816, doi:10.1029/1998JD100025, 1999.

4 Test of the IAGOS-Core GHG Package during CHARM-F flights on HALO

4.1 Introduction

Greenhouse gas measurements with the help of aircraft are essential to bridge the gap between in situ measurements on ground and space-born remote sensing products. They provide valuable data from regions of the atmosphere, which are not covered by ground measurements and are also not sufficiently resolved by remote sensing (e.g. the upper troposphere and lower stratosphere). The vertical profile information helps to link remote sensing measurements to calibration scales referenced by the World Meteorological Organization (WMO).

In this context a flight campaign for the validation of CHARM-F (CO_2 and CH_4 Atmospheric Remote Monitoring – Flugzeug), an airborne demonstrator for the upcoming MERLIN (Methane Remote Sensing Lidar Mission) satellite, was planned for 2018. The climate mission MERLIN, focused on methane monitoring, is a collaborative project between Germany and France currently scheduled for launch in 2024 (Ehret et al., 2017; https://merlin.cnes.fr/en). The measurements of atmospheric columns of methane dry-air mole fractions will be conducted with an Integrated Path Differential Absorption (IPDA) Light Detection and Ranging (LIDAR) system. It uses the backscatter of pulsed laser light from the earth surface or clouds to determine the absorption of a trace gas along the light path. The active remote sensing system CHARM-F (Quatrevalet et al., 2010), developed at the Institute of Atmospheric Physics at the German Aerospace Centre (DLR), serves as a technology demonstrator of this observation principle. During the CHARM-F validation mission in 2018 the instrument was tested against passive remote sensing systems, in situ cavity ring-down spectroscopy (CRDS) measurements of CO_2 and CH_4, and air samples.

As preparation for this validation mission first flight tests of the CHARM-F system took place at the German Aerospace Centre in Oberpfaffenhofen (south Germany) in April and May 2015. They were conducted on the German High Altitude and Long Range Research Aircraft (HALO) (http://www.halo.dlr.de). HALO is a modified Gulfstream G550 jet reaching up to 9000 flight kilometers and altitudes of 10-15 km. A total of five flights with a total flight time of 20 hours were used to assess the dependence of the LIDAR signal on different surface characteristics (e.g. land and water surfaces, or mountains) and the ability of the analysers to detect and quantify various methane and CO_2 sources (Amediek et al., 2017). Therefore, destinations like the Po valley with its intensive agriculture and livestock, Silesian coalmines in Poland, the alps, and the Mediterranean Sea were chosen.

During this campaign CHARM-F was complemented by the IAGOS-core Greenhouse Gas (GHG) package (Filges et al., 2015) in order to evaluate the LIDAR measurements with in situ CO_2 and CH_4 observations. The GHG package is based on Cavity Ring-Down Spectroscopy (CRDS) and measures simultaneously CO_2 and CH_4 as well as CO and water vapour. It is originally designed for the operation aboard commercial aircraft within the IAGOS (In-service Aircraft for a Global Observing System) project (Volz-Thomas et al., 2009; Petzold et al., 2015). Deployment of the first GHG package on a passenger aircraft was scheduled in 2017 and it is planned to equip four more aircraft

with the system in the next years. The aim is to provide regular data from climate sensitive regions, like the upper troposphere lower stratosphere (UTLS), and vertical profiles of the trace gases. They will help to validate remote sensing based observations and to improve the understanding of processes which determine the atmospheric abundance of GHGs and thus enhance the performance of regional and global climate models.

The 2015 test mission of CHARM-F was also the first flight test of the IAGOS GHG package prototype in the exact status as it will be deployed within IAGOS. Hence, the campaign allowed for an initial evaluation of the instrument operation and performance, which will be presented in this chapter. The IAGOS GHG system, indicators for the measurement quality, and the calibration strategy are introduced in Section 4.2. An analysis of the instrument performance and the atmospheric data during the CHARM-F test flights in 2015 can be found in Section 4.3. Section 4.4 concludes the evaluation of this first flight test of the IAGOS GHG package.

4.2 Measurement System and Instrument Operation

The general setup and measurement principle of the cavity ring-down spectroscopy (CRDS) based GHG package are described in Filges et al. (2015). Nevertheless, due to specific differences between the IAGOS passenger aircrafts and HALO some small modifications had been necessary. The adjustments concerned mainly the inlet system of the measurement system. Instead of a Rosemount Total Air Temperature (TAT) housing a Trace Gas Inlet (TGI) version 318 was used, which also provides positive ram pressure (~ 80 hPa) and prevents from sampling larger aerosols, ice particles and water droplets, since the inlet line is pointed orthogonal to the air flow through the inlet. However, the air is sampled 25 cm above the aircraft skin, compared to about 9 cm for the Rosemount. Furthermore, the TGI inlet was unfortunately not heated during the campaign, which significantly limited the water vapour measurements due to condensation effects. Due to the instruments rack position in the aircraft the inlet line (OD 3.18 mm, ID 2.18 mm, Fluorinated Ethylene Propylene (FEP)) had to be much longer than for the IAGOS deployment. Including the inlet line part within the TGI inlet the total length adds up to 7.42 m, compared to 60 cm for IAGOS. The exhaust line of the measurement system was connected to a common exhaust line of the aircraft. Ventilation of the instrument was ensured by a ventilation system, specifically designed for the deployment on HALO, but with comparable performance to the IAGOS ventilation system. The sample flow of the GHG package prototype was 104 ml/min (= 104 sccm, standard conditions for all given flows and volumes here and in the following: T = 20 °C, p = 101 kPa).

While the analyser operates fully autonomously during deployment on passenger aircraft it was controlled manually for the test flights. This was necessary due to the missing ‘Weight on Wheel’ signal used on IAGOS aircraft, to switch between flight and ground mode. Moreover, in-flight calibrations ought not to interfere with the specifically planned vertical profile measurements, which are required for the comparison with CHARM-F.

Parameters for the ‘wet-to-dry correction’ of the measurements, which is used to calculate the dry air mole fractions of CO_2, CH_4, and CO from the measured wet air mole fractions, were

determined during laboratory tests in November and December 2014. They are valid for a water vapour range up to 3.5 %.

4.2.1 Sample Cell Pressure

During the CHARM-F test flights HALO flew up to a maximum altitude close to 14 km, which corresponds to an air pressure of 140 hPa. This is considerably higher than it will occur for IAGOS flights, where the maximum altitude of the passenger aircraft is reached at around 12 km. Thus, the HALO flights were perfectly suited to test the limits of the sample cell pressure stability of the instrument. Taking into account the positive ram pressure of around 80 hPa, as well as the pressure drop of about 25 hPa in the 8.22 m long inlet line (7.42 m from the instrument frame to the inlet plus 0.8 m tubing inside the instrument) the inlet pressure dropped to about 195 hPa at ceiling level. This is very close to the sample cell pressure setpoint of 186.65 hPa. Moreover, pressure at the outlet drops to around 60 hPa at the highest altitudes, due to the negative ram pressure at the exhaust. Hence, the question was if the pump can maintain the sample cell pressure and keep the flow stable at 104 ml/min.

The rates of air pressure decrease and increase during ascent and descent of the HALO aircraft are similar to the expected pressure changes during IAGOS deployment: 100 hPa/min at 0-3 km altitude to 10 hPa/min at 9-12 km altitude during ascent, and 20 – 100 hPa/min during descent, respectively. Laboratory experiments, described in Filges et al. (2015), showed only small deviations of the sample cell pressure (<0.03 hPa) for these ranges of air pressure changes. Only for larger changes, especially at low air pressure levels (<300 hPa), the sample cell pressure control is too slow to adapt.

Deviations in sample cell pressure, due to low air pressure conditions at high altitudes or fast air pressure changes, would affect the measurements of CO_2, CH_4, CO, and water vapour. Therefore, adjustment factors have been determined in laboratory experiments to compensate the effect and correct the data (Filges et al., 2015). For CO_2 the correction factor is 0.35 ppm/hPa (at a CO_2 mole fraction level of 390 ppm), for CH_4 6.18 ppb/hPa (at a CH_4 mole fraction level of 1920 ppb), and for CO -2.1 ppb/hPa (at a CO mole fraction level of 150 ppb). For water vapour the correction factor could only be determined for a mole fraction level of about 3 ppm. It amounts to 2.56 ppm/hPa.

4.2.2 Measurement precision

As a measure for the 1-sigma (1 σ) measurement precision of the instrument the standard deviations of the short-periodic parts of the measurement signals are calculated. To obtain the short-periodic part of the measurement data, the 60 s moving average is subtracted from the 0.4 Hz raw signal. Under laboratory conditions the measurement precisions of the CO_2, CH_4 and CO measurements were determined as 0.039 ppm for CO_2, 0.40 ppb for CH_4, and 15 ppb (1.7 ppb for an integration time of 3 minutes) for CO before the HALO flights. Upper limits for the measurement precision of real flight data were so far only determined during test flights of the commercial CRDS analyser in 2011, before it was modified and converted to fit the IAGOS requirements. The results were 0.06 ppm for CO_2, 1 ppb for CH_4, and 10 ppb for CO (Filges et al., 2015). Regarding the water vapour measurements, laboratory results of the measurement

precision, depending on the water vapour mole fraction level, were presented in Filges et al. (2018) and can be seen in Table 4.1. Furthermore, upper limits for the measurement precision of the flight data (0.4 Hz) during the test flights of the commercial CRDS analyser in 2011 were estimated as 4ppm for H_2O <10 ppm, 20 % or 10 ppm (whichever is smaller) for 10 ppm < H_2O < 100 ppm, and 5 % or 30 ppm (whichever is smaller) for water vapour >100 ppm.
The achieved measurement precision of the instrument during the Charm-F tests flights will show if the results of the commercial CRDS analyser can be confirmed or if the results even get closer to the values obtained in the laboratory.

Table 4.1: Measurement precision (1 σ) of the water vapour measurements under laboratory conditions.

Water vapour mole fraction (ppm)	Precision at 2.5 s time resolution (ppm)	Precision at 30 s integration time (ppm)
3	<6	<2
30	<10	<5
5000	<9	<5
8000	<10	<2
12000	<10	<4
19000	<12	<6

4.2.3 Calibrations

Traceability of the CO_2, CH_4 and CO measurements to the WMO primary scales (currently WMO X2007 scale for CO_2, WMO X2004A scale for CH_4, WMO X2014A scale for CO) was ensured by measurements of gas standards before and after the test flights ('pre- and post-deployment calibration') and additional regular measurements of calibration gas during the deployment on HALO ('In-flight calibrations'). To guarantee a good assessment of the calibration procedures and results with regard to future IAGOS deployments, it was tried to stick to the IAGOS calibration equipment and strategy (see Filges et al., 2015) as closely as possible.
Pre- and post-deployment calibrations have been performed at the Max Planck Institute for Biogeochemistry (MPI-BGC) in Jena in March and May 2015. Both times the same three gas tanks ('working standards'), filled with pressurized and dried ambient air at the GasLab of the MPI-BGC, have been used. They covered a range of about 370 to 415 ppm mole fraction for CO_2, 1650 to 2000 ppb for CH_4, and 50 to 200 for CO. The post-deployment calibration was conducted for two times: the second time with swapped pressure regulators of the two in-flight calibration gas cylinders, to allow for an estimation of the impact of different pressure regulators on the measurements. This is important for the IAGOS deployment, since the two pressure regulators can be easily interchanged during transports to the aircraft or back to the MPI-BGC.
The in-flight calibrations, using two compressed gas cylinders (high span and low span), consisted of measurements of calibration gas before, after, and during the flights. Pre-flight calibrations lasted at least six up to ten minutes, while the others lasted only three minutes. The measurement order of the high and low span cylinder was always alternated during the flights. In contrast to the regular frequency of the in-flight calibrations during IAGOS deployment, the in-flight calibrations

during the test flights took place very irregularly, since they were started manually as it fitted the flight plan and did not interfere with the comparison to CHARM-F.
The water vapour measurements were calibrated using a dew point mirror.

4.3 Results and analysis of the test flights

The five flights with HALO all started and ended in Oberpfaffenhofen. The first flight on April 27. was only a short test flight to check for problems with electromagnetic interferences. The second flight on April 29. went to Poland and the Baltic Sea, the third on May 5. to Italy, the fourth on May 11. to North Italy, and the last on May 13. to Poland and Germany.

4.3.1 Calibration

All flight data, which will be shown and discussed in the following, were calibrated according to the pre- and post-deployment calibration at the MPI-BGC. Since these two calibrations took place within only two months and the resulting calibration factors for both calibrations are overlapping within their combined uncertainties, simply the mean of the pre and post calibration factors were chosen for the calibration of the instrument. Table 4.2 shows these mean calibration factors (linearity factor 'a' and offset 'b') and the uncertainties of the calibration in the typical ambient ranges of 380-400 ppm for CO_2, 1700-1950 ppb for CH_4, and 50-175 ppb for CO. The role of the in-flight calibrations in the data processing could not be assessed since the instrument was too stable. Here, a longer deployment period on board aircraft has to be waited for.

Table 4.2: Calibration factors a (slope) and b (offset) for the linear calibration of the IAGOS-core GHG package prototype, together with the uncertainties of the calibrations for the typical ambient ranges (CO_2: 380-400 ppm, CH_4: 1700-1950 ppb, CO: 50-175 ppb).

	a	b	uncertainty
CO_2	0.9999	0.916 ppm	<0.02 ppm
CH_4	0.9885	10.801 ppb	<0.11 ppb
CO	0.9971	5.656 ppb	<1.11 ppb

Swapping the pressure regulators of the two in-flight calibration gas cylinders during a second post-deployment calibration had no significant impact on the calibration of the two gas cylinders and thereby on the measurements of the instrument. The differences were for both cylinders and all species smaller than the uncertainties. Thus, an interchange of the regulators during IAGOS-deployments is not expected to affect the measurements.
The water vapour measurements were offset corrected and calibrated according to a comparison against a dew point mirror in 2013 (Filges et al., 2018).

4.3.2 Sample Cell Pressure

Deviations and instabilities in the sample cell pressure are expected to occur at low air pressure conditions or during fast air pressure changes. To investigate the first aspect, the mean sample cell pressure and its standard deviation were assessed during periods of stable air pressure

conditions in all flights. Table 4.3 shows selected results for the whole altitude range up to 13.8 km. Positively the pump could maintain the sample cell pressure of 186.65 hPa even at this maximum height. This means the additional ram pressure was large enough to bridge the gap between the air pressure of only 146 hPa and the sample cell pressure. But, as can be seen in the standard deviations, at altitudes higher than 13 km the noise of the pressure increases. On ground the standard deviation of the sample cell pressure is around 0.016 hPa. For all heights up to 12.5 km it is only slightly higher (<0.025 hPa), with one exception: at the lowest altitude of 0.8 km it is 0.033 hPa, related to stronger g-forces of the aircraft in the turbulent atmosphere and their effect on the control valve. A sample cell pressure difference of 0.025 hPa to its setpoint at 186.65 hPa corresponds to deviations in CO_2, CH_4, CO, water vapour of 0.01 ppm, 0.2 ppb, 0.06 ppb, and 0.1 ppm. These are small compared to the measurement repeatabilities, and since the deviations are mainly white noise, they are negligible when the data are integrated over time. Hence, during IAGOS-flights, for which the highest altitudes will be around 12.5 km, the slightly higher standard deviations of the sample cell pressure should not affect the measurements considerably.

Table 4.3: Sample cell pressure mean and standard deviation at different altitudes

altitude (km)	air pressure (hPa)	mean of the sample cell pressure (hPa)	standard deviation of the sample cell pressure (hPa)
0.8	919	186.65	0.033
3.7	644	186.65	0.023
4.6	572	186.65	0.017
8.5	329	186.65	0.021
10.1	262	186.65	0.021
10.7	238	186.65	0.016
11.3	216	186.65	0.021
12.5	178	186.65	0.023
13.2	161	186.65	0.050
13.8	146	186.65	0.148

The situation is different when we look at flight periods with changing air pressure. Figure 4.1 shows a typical ascent of the aircraft as it will occur during IAGOS-flights, with air pressure changes from 100 hPa/min at lower altitudes (<3 km) to 10 hPa/min at higher altitudes (>9 km). Up to an altitude of around 8.5 km the sample cell pressure is very stable. Only the mean pressure is shifted by around 0.025 hPa in the beginning. Above 8.5 km the sample cell pressure starts fluctuating and the mean pressure level decreases slowly to 0.05 hPa below the setpoint of 186.65 hPa but is still relatively even and shows no sudden changes. Only after the aircraft reaches 12.5 km the sample cell pressure starts to drop significantly. As the climb ends and the aircraft continues the flight on cruise level the pressure overshoots and the adjustment take around 30 seconds to stabilize the pressure again and another minute to reach the mean pressure level of 186.65 hPa. Analysis of data from all five flights reveals that at altitudes above 9 km air pressure changes larger than 10-15 hPa/min destabilize the sample cell pressure. For slower ascending rates the sample cell pressure is stable as long as the air pressure changes constantly, but already for small changes

in the rate of ascent the adjustment of the sample cell pressure is to slow and it takes around one minute until the pressure recovers again.

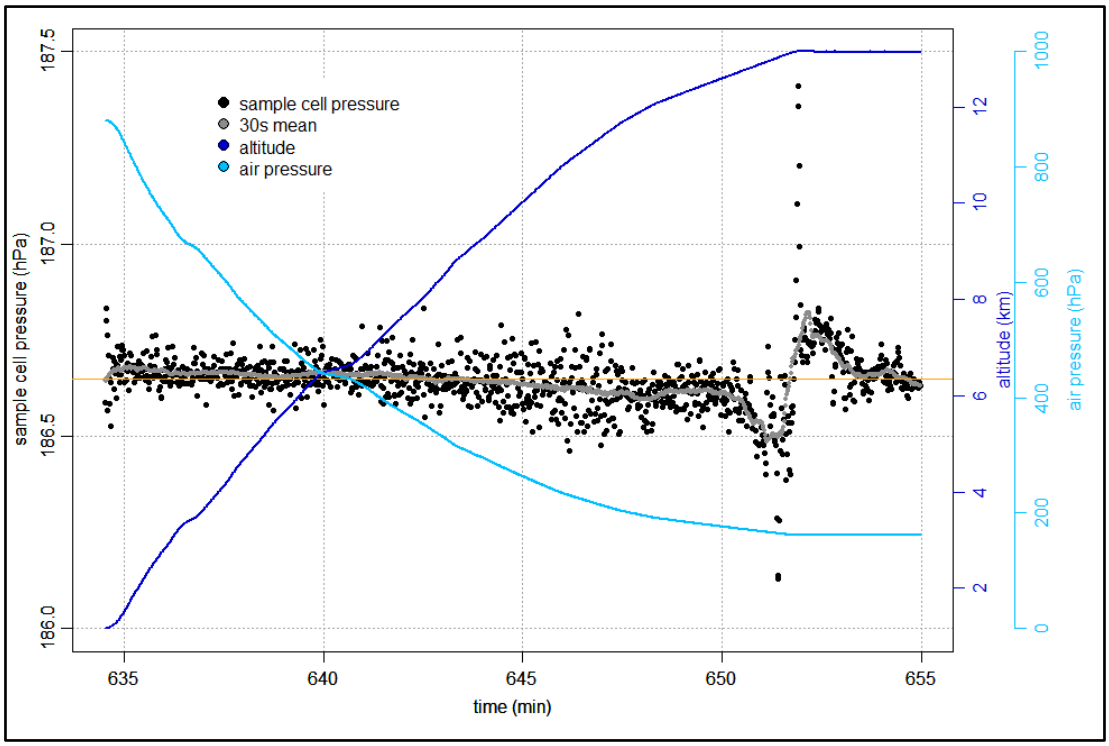

Figure 4.1: Sample cell pressure (black points) and its 30 seconds mean (grey points) during an ascent of the aircraft on the flight on May 13. The thin orange line marks the setpoint of the sample cell pressure at 186,65 hPa. The altitude and corresponding air pressure are shown in blue and light blue.

During descents of the aircraft the sample cell pressure shows a similar behaviour. The pressure responds very sensitive to sudden changes in the rate of descent but stabilizes relatively quickly again in less than 0.5 minutes, as soon as the pressure change rate is constant again. On the other hand, the instrument can handle air pressure change rates up to 25-30 hPa/min at altitudes from 9 to 12.5 km as can be seen in Figure 4.2, which shows the sample cell pressure during a descent from 12.5 km to 0.5 km during the 5th flight. After a peak at the start of the descent the sample cell pressure is stable, while the air pressure changes constantly with 25 hPa/min. Only the mean pressure level is slightly elevated. Unfortunately, the fastest rate of descent during all five flights was only 62 hPa/min. Here, the sample cell pressure showed enhanced noise below 2 km, but the mean was still stable at the setpoint of 186.65 hPa. At minute 735 in Figure 4.2 the sample cell pressure destabilizes without any visible reason in the air pressure. This is most likely due to the fact that the aircraft was exposed to turbulence.

Summarizing, with regard to the IAGOS deployment of the instrument the flights have demonstrated that the adjustment of the sample cell pressure is able to keep the pressure stable at altitudes up to 12.5 km, during ascending rates of 100 hPa/min at 0-3 km altitude to 10 hPa/min at 9-12 km altitude, and during rates of descent from 25 hPa/min at 12 km to around 60 hPa/min at lower altitudes. However, the sample cell pressure is very sensitive to changes in the rate of ascent or descent and takes around 0.5 minutes to adapt after such an event. In some cases, it

may occur that the sample cell pressure is stable, but its mean is shifted. Here, the CO_2, CH_4, CO, and water vapour measurements need to be corrected with the correction factors given in Section 4.2.1. A recent study by Reum et al. (2019) revealed that the sample cell pressure measurement is non-linearly influenced by water vapour for H_2O mole fractions below 0.5 %. This affects not only these pressure correction factors, but also the wet-to-dry-correction of the CO_2, CH_4, and CO measurements. Since the modified laboratory tests to redefine the correction factors for this device have not yet been performed, the effect can only be taken into account by now by increasing the stated uncertainty of the measurement data.

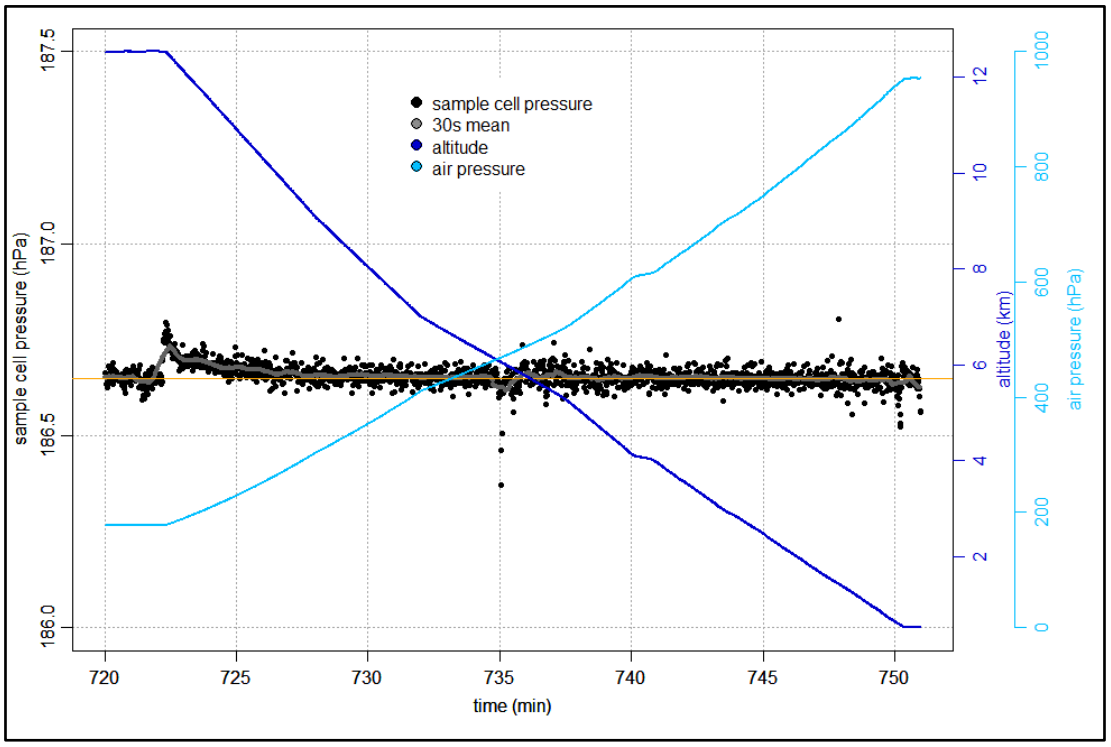

Figure 4.2: Sample cell pressure (black points) and its 30 seconds mean (grey points) during a descent of the aircraft on the flight on May 11. The thin orange line marks the setpoint of the sample cell pressure at 186,65 hPa. The altitude and corresponding air pressure are shown in blue and light blue.

4.3.3 Measurement Precision

For the determination of the measurement repeatability of CO_2, CH_4, and CO the 0.4 Hz raw data of all five flights were 'wet-to-dry' and pressure-corrected, as well as calibrated. The water vapour data were pressure and offset corrected, and calibrated, too. Afterwards, flight periods with stable air pressure and temperature were selected, to minimize the natural variations in the data. Furthermore, periods of time with unstable sample cell pressure were excluded. Finally, the standard deviation (1 σ) of the difference to the 60 s moving average was calculated for remaining data. For CO_2 the mean standard deviation is 0.042 ppm. For CH_4 and CO it is 0.69 ppb and 15 ppb, respectively. Thus, for CO_2 and CH_4 the upper limit of the measurement precision during flight could be reduced by around 0.02 ppm and 0.3 ppb compared to the 2011 flights of the commercial analyser. For CO the flight result confirms the estimates of the laboratory tests on ground. Since the 2011 test flight data were significantly better by 5 ppb, it seems that the settings and

alignment of the CO laser were not sufficient after the rebuilding of the instrument. Shortly after the CHARM-F flight campaign the measurement precision of the CO data actually could be considerably reduced to 6 ppb with the help of some fine-tuning of the laser and an upgrade of the scanning scheme. The measurement precision for water vapour depends on the water level. Figure 4.3 shows the mean standard deviations for different water vapour ranges. The data of the five different flights are indicated by different colours and symbols. Furthermore, the results are weighted according to the number of data points, that were available for the calculation in the corresponding water vapour intervals. Results based on a high number of data are highlighted. Compared to the test flights in 2011 with the commercial analyser the measurement precision estimates of 4 ppm for H_2O <10 ppm and 5 % or 30 ppm (whichever is smaller) for water vapour >100 ppm can be verified. For water vapour between 10 and 100 ppm the estimate of 20 % or 10 ppm (whichever is smaller) seems appropriate for H_2O >20 ppm. Only for water vapour between 10 and 20 ppm the data suggest a higher upper limit of around 30 %, but it must be noted that there are only four data points in this water vapour interval. Here, a more reliable assessment will be possible as soon as enough flight data from IAGOS deployment will be available. Regarding the precision estimates of the laboratory tests the results of the flight data are in good agreement for H_2O <10 ppm, but two to three times larger for water vapour >1000 ppm.

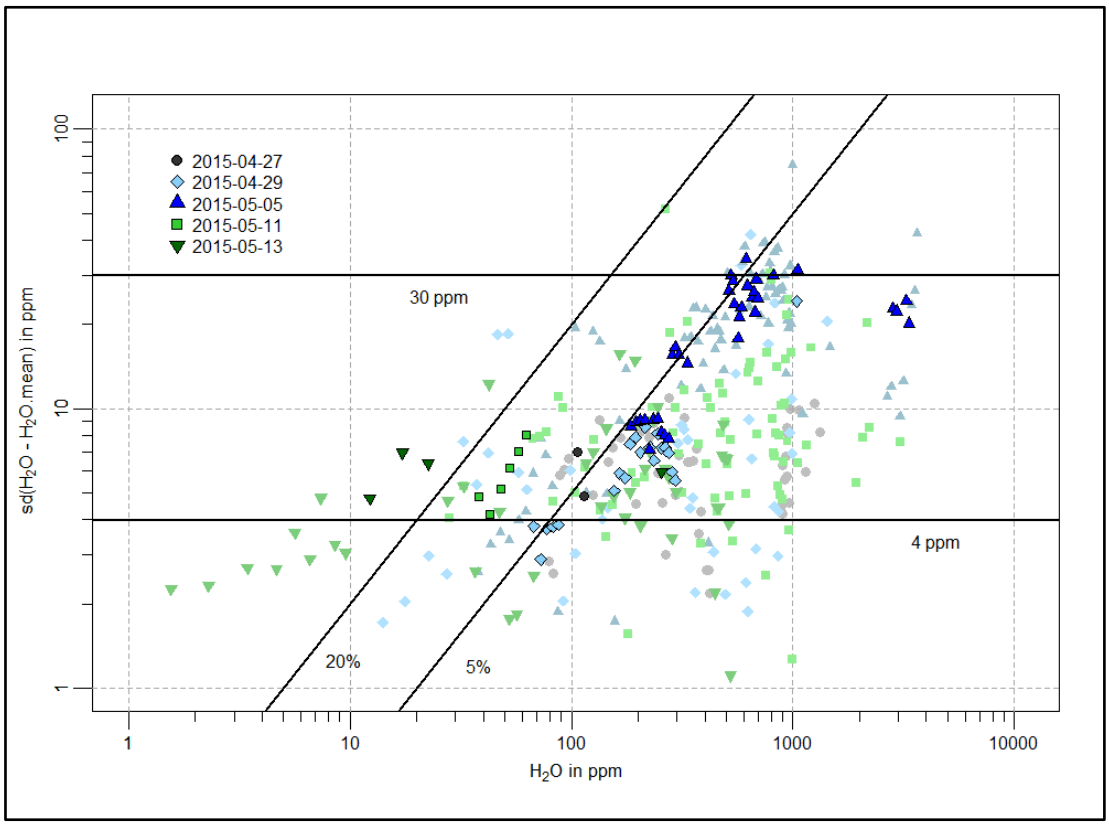

Figure 4.3: Standard deviation of the difference between the 0.4 Hz water vapour data and the 60 s averages, averaged for intervals of 1, 5, 10, and 100 ppm water vapour in the corresponding water vapour ranges of 0–10, 10–100, 100–1000, and 1000–10 000 ppm, respectively. Different colours and symbols indicate the five different flights. Results with higher priority are highlighted with more intense colour. The horizontal and diagonal black lines indicate standard deviations of 4 and 30 ppm, and the ratios of 5% and 20 %, respectively.

4.3.4 Water Vapour Measurements

Unfortunately, the H_2O measurements were strongly affected by icing of the inlet, because the TGI housing was not equipped with a heating system. Figure 4.4 shows the measured water vapour during the whole second flight on April 29. compared to the saturated water vapour. At altitudes higher than 8 km the measured mole fraction is always nearly the same as the mole fraction corresponding to saturation. This indicates that the inlet was frozen during most parts of the flight. Thus, the H_2O measurements allow for no reliable conclusions on the actual atmospheric water vapour for all flights.

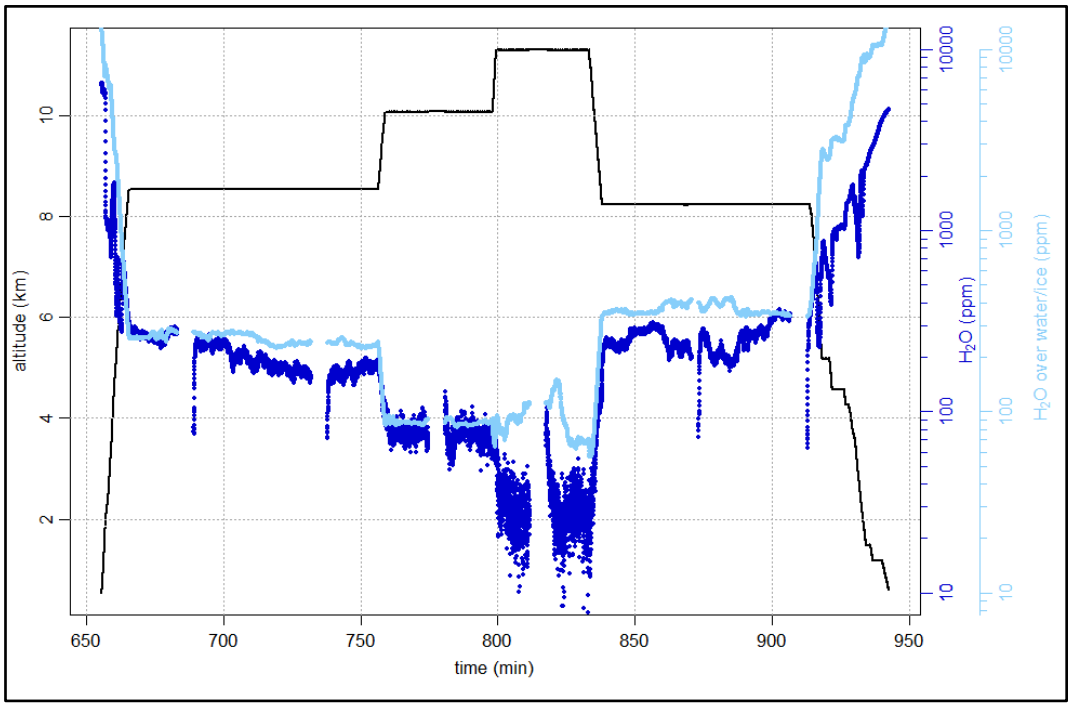

Figure 4.4: Measured water vapour mole fractions (in blue) and the mole fractions corresponding to saturated water vapour (in light blue) at different altitudes (in black) during the second flight on April 29.

4.3.5 CO_2, CH_4, and CO Measurements

The wet-to-dry and pressure corrected, as well as calibrated CO_2, CH_4, and CO measurement data of the second and fifth flight (April 29. and May 13.) can be seen in Figure 4.5 and Figure 4.6 together with the corresponding flight altitudes. For reasons of clarity all calibration periods are skipped and only the 30 seconds mean data are shown for CO. During both flights the aircraft crossed the tropopause: for the second flight around minute 790 at an altitude of 10 km and for the fifth flight at minute 580 and 645 at an altitude of 10.5 km. When the aircraft left the stratosphere again for the second time during the fifth flight at minute 745 the tropopause was slightly higher at around 11.5 km, likely because of a more southern position of the aircraft. While the other crossings took place over northern Germany and mid Poland around latitude 52°, the last one was over southern Germany at a latitude of around 49°. During the third and fourth flight, both to Italy, the aircraft never reached the stratosphere although the highest altitudes were >12 km. The stratospheric levels of CO_2, CH_4, and CO were 5-8 ppm, 100-200 ppb, and 50-90 ppb lower than the ones in the upper troposphere.

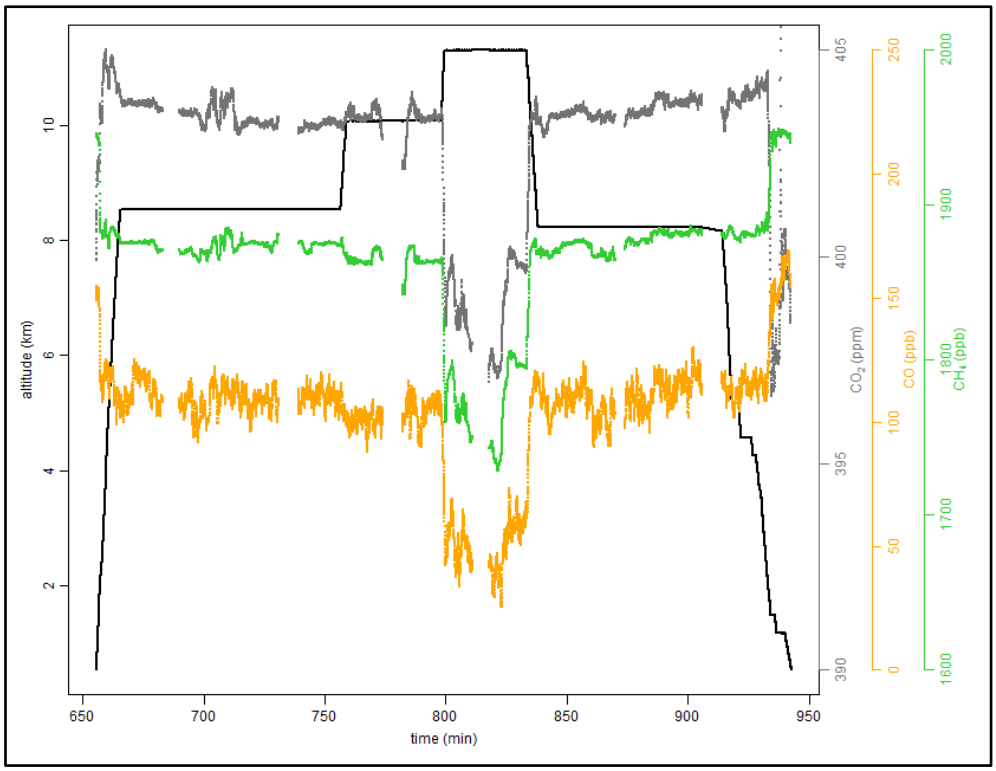

Figure 4.5: CO_2 (in grey), CH_4 (in green), and CO (30 s mean, in orange) mole fractions for the second flight on April 29. together with the corresponding flight altitude (in black). The measurement data are wet-to-dry and pressure corrected, and calibrated.

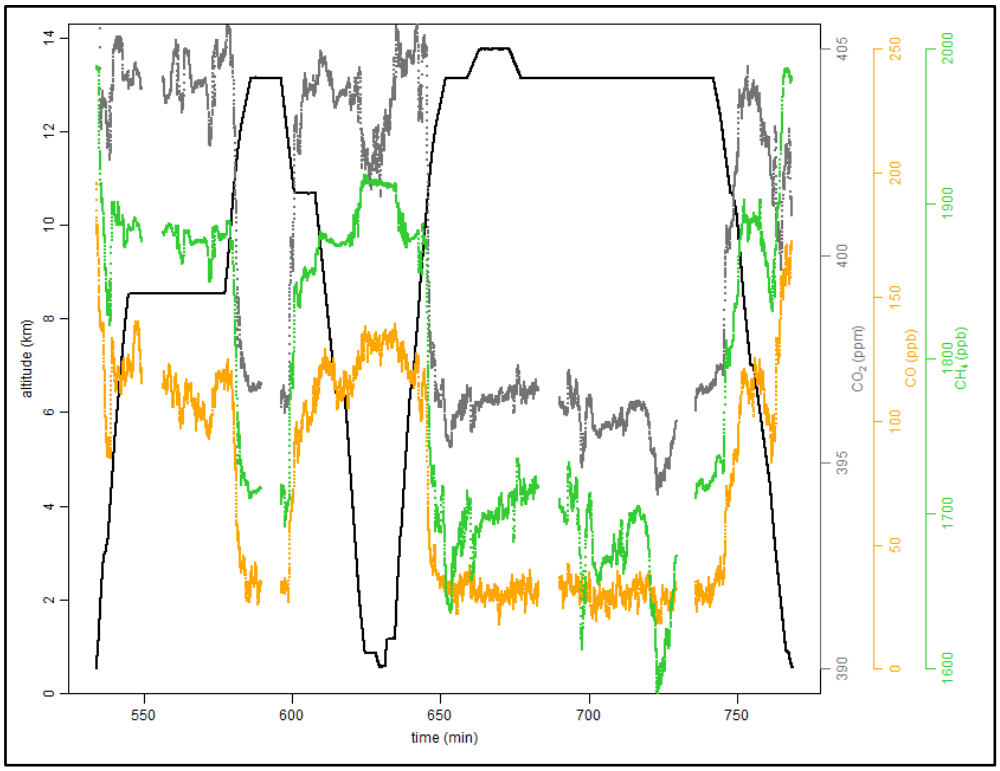

Figure 4.6: CO_2 (in grey), CH_4 (in green), and CO (30 s mean, in orange) mole fractions for the fifths flight on May 13. together with the corresponding flight altitude (in black). The measurement data are wet-to-dry and pressure corrected, and calibrated.

Figure 4.7, Figure 4.8, and Figure 4.9 show profiles of CO_2, CH_4, and CO measured during the fourth (May 11.) and fifth (May 13.) flight over Parma (Italy), the Mediterranean Sea near Corsica, and near Katowice (Poland). For all three one can see the reduced variability of the trace gases in the middle troposphere, with some layering of the atmosphere. Often, CH_4 and CO show a positive correlation, resulting from the fact that both gases have a source at the surface and a sink in the stratosphere, while CO_2 behaves differently due to its photosynthetic sink and emission-related sources, which are both located at the surface. The strong increase in CO_2 and CH_4 mole fractions at around 0.8 km in Figure 4.7 indicates the planetary boundary layer. The high mole fraction levels, caused by the emissions of Parma and the neighbouring agricultural areas of the Po valley, are in clear contrast to the low levels of, in particular, CO_2 over the Sea, which can be seen in Figure 4.8. During the profile flight near Katowice on May 13. the aircraft crossed the tropopause at 10.5 km and the measured mole fractions of CO_2, CH_4, and CO dropped significantly by around 8 ppm, 160 ppb, and 80 ppb.

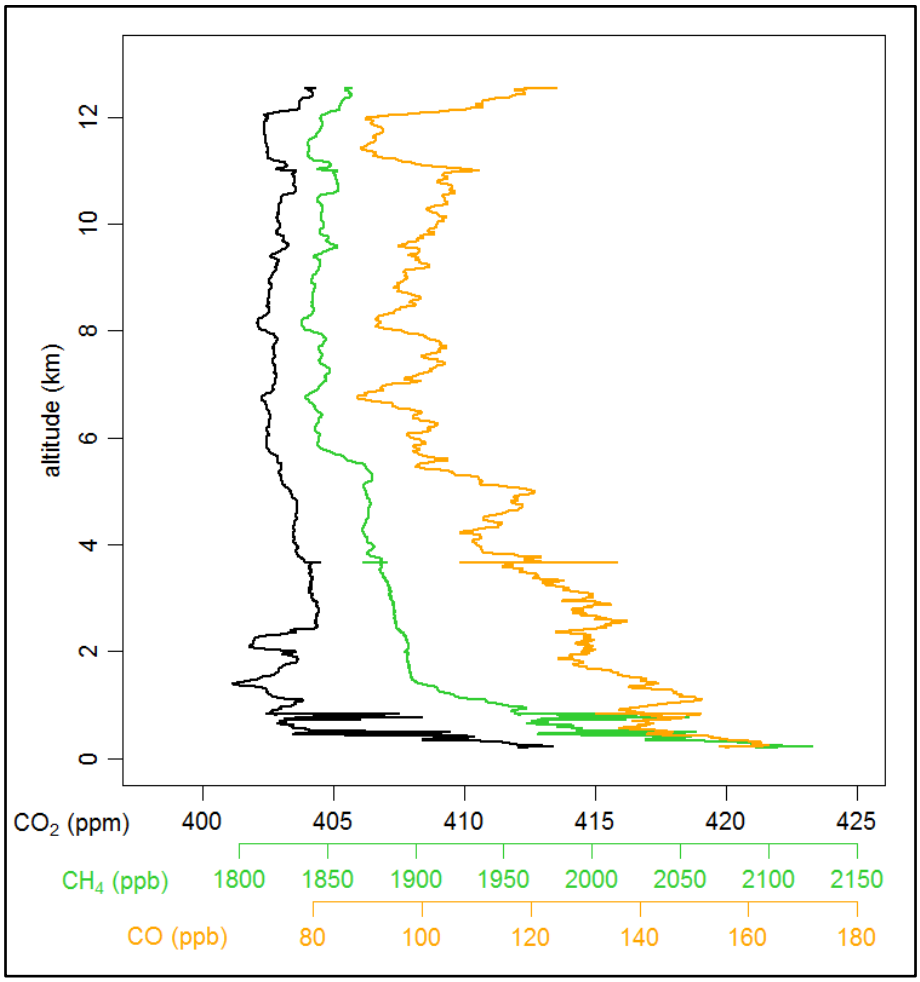

Figure 4.7: Measured profiles of CO_2 (in black), CH_4 (in green), and CO (in orange) during the fourth flight on May 11. around noon time, over Parma in Italy.

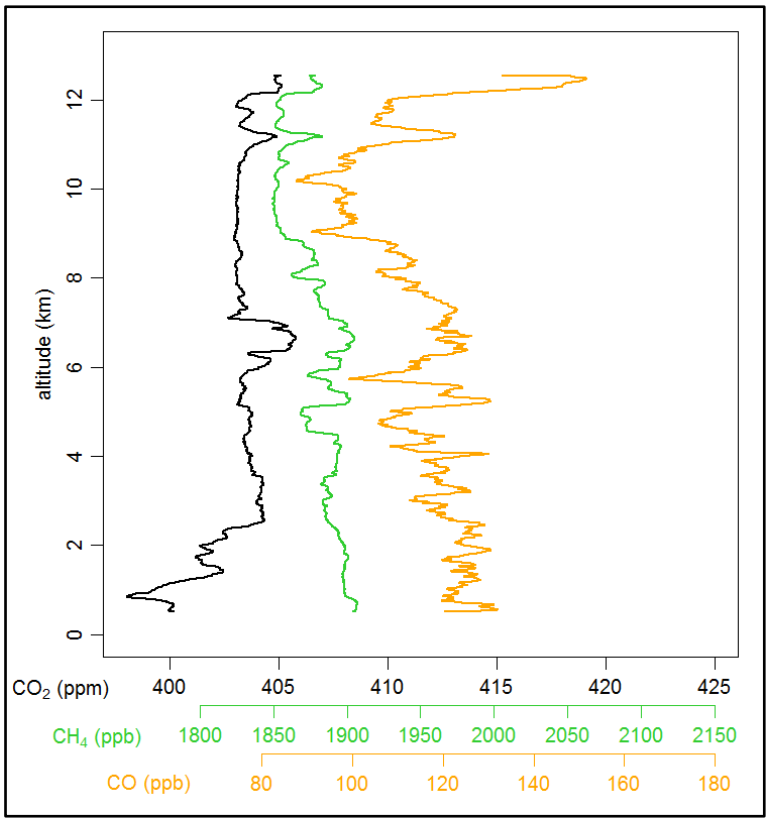

Figure 4.8: Measured profiles of CO_2 (in black), CH_4 (in green), and CO (in orange) during the fourth flight on May 11. around noon time, over the Mediterranean Sea near Corsica.

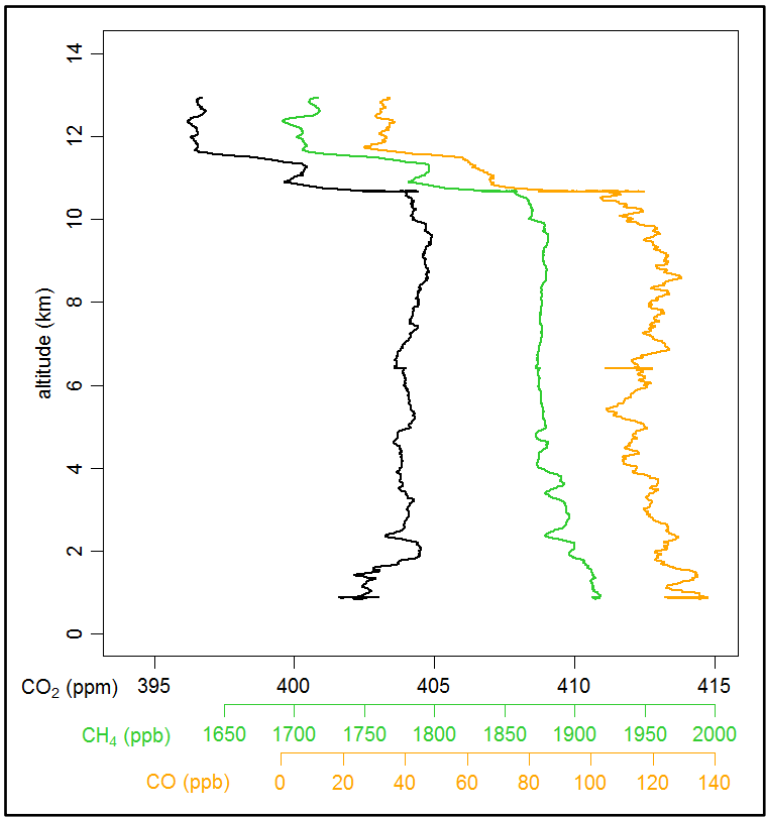

Figure 4.9: Measured profiles of CO_2 (in black), CH_4 (in green), and CO (in orange) during the fifth flight on May 13. around noon time, near Katowice in Poland.

4.4 Conclusions

In spring 2015 five test flights of the IAGOS-core GHG package were carried out on the HALO aircraft as preparation for a later validation mission of the active remote sensing system CHARM-F. The flights went to Germany, mid Poland and Italy. They served as an opportunity to evaluate the GHG device, as the instrument was used in the same setup as for IAGOS. The only difference was another inlet system with a much longer inlet line, which was also not equipped with an inlet heater.

The instrument showed very good performance over the whole flight campaign. The calibrations of the analyser in the laboratory before and after the mission, which were performed two months apart, coincided within their uncertainties. In addition, it could be shown that an exchange of the pressure regulators of the in-flight calibration gas cylinders had no significant impact on the measurements.

Also crucial for the measurements is the sample cell pressure stability. During periods of stable air pressure, i.e. constant flight altitudes, the sample cell pressure was stable even at heights up to 14 km. However, while the standard deviation of the sample cell pressure is 0.016 to 0.025 hPa from ground up to 12.5 km altitude, it considerably increased above 13 km (0.05-0.15 hPa), which in the end has to be accounted for in the uncertainty of the measurements. During ascent and descent of the aircraft the sample cell pressure could be kept stable for ascending rates of 100 hPa/min at 0-3 km altitude to 10 hPa/min at 9-12 km altitude, and for rates of descent from 25 hPa/min at 12 km to around 60 hPa/min at lower altitudes. Larger descending rates than 60 hPa/min did not occur during the five flights and can therefore not be evaluated. In general, the sample cell pressure is strongly affected by changes in the rate of ascent or descent. If the rate of change increases or decreases, it takes around 30 seconds for the sample cell pressure to adapt again. But, as long as the sample cell pressure is stable, even when its mean is shifted relative to the setpoint of 186.65 hPa, the CO_2, CH_4, CO, and water vapour measurements can be corrected for these deviations with the help of pressure correction factors determined in the laboratory. Thus, for IAGOS deployment, where the highest flight altitudes are around 12.5 km and the aircraft flies at constant altitudes or with constant ascending and descending rates for most of the flight, sample cell pressure issues are not expected to have a great impact on the measurements.

The upper limits for the 0.4 Hz measurement precision during flight for CO_2 and CH_4 could be reduced compared to test flights in 2011 to 0.042 ppm and 0.69 ppb. For CO the measurement precision of 15 ppb during the flights was significantly improved by optimizations of the laser setup and alignment after the flight campaign to 6 ppb. For water vapour the results of the 2011 test flights could be by and large confirmed (4 ppm for H_2O <10 ppm, 20 % or 10 ppm (whichever is smaller) for 10 ppm > H_2O < 100 ppm, and 5 % or 30 ppm (whichever is smaller) for water vapour >100 ppm). Only for water vapour between 10 and 20 ppm the upper limit was higher at around 30 %. Here, the larger volume of data, which will be delivered during IAGOS deployments, will very likely help to get more accurate estimates for the precision.

Recently it was found that the measurement of the sample cell pressure is non-linearly influenced by the water vapour in the sample cell for H_2O <0.5 % (Reum et al., 2019). This affects the wet-to-

dry and the sample cell pressure corrections. While there is no subsequent correction of the 2015 flight measurement data so far and the influence of the water vapour-pressure relation can only be considered in an increased uncertainty, the correction formulas should be adjusted and the correction factors new determined for all future deployments of the GHG device.

Due to the missing heating of the inlet system no reliable atmospheric water vapour data could be collected. In contrast, the CO_2, CH_4, and CO measurements, especially the profile data, gave an insight into the different properties of the atmospheric layers flown through and the influences from regional emissions.

In summary the test flights of the GHG package were successful. The system has shown that it fulfils the requirements regarding performance and measurement quality and is ready for deployment aboard passenger aircraft as part of the IAGOS project.

4.5 References

Amediek, A., Ehret, G., Fix, A., Wirth, M., Büdenbender, C., Quatrevalet, M., Kiemle, C., and Gerbig, C.: CHARM-F - a new airborne integrated-path differential-absorption lidar for carbon dioxide and methane observations: measurement performance and quantification of strong point source emissions, Appl. Opt. 56, 5182-5197, https://doi.org/10.1364/AO.56.005182, 2017.

Ehret, G., Bousquet, P., Pierangelo, C., Alpers, M., Millet, B., Abshire, J. B., Bovensmann, H., Burrows, J. P., Chevallier, F., Ciais, P., Crevoisier, C., Fix, A., Flamant, P., Frankenberg, C., Gibert, F., Heim, B., Heimann, M., Houweling, S., Hubberten, H. W., Jöckel, P., Law, K., Löw, A., Marshall, J., Agusti-Panareda, A., Payan, S., Prigent, C., Rairoux, P., Sachs, T., Scholze, M., and Wirth, M.: MERLIN: A French-German Space Lidar Mission Dedicated to Atmospheric Methane, Remote Sens.-Basel, 9, 1052, https://doi.org/10.3390/rs9101052, 2017.

Filges, A., Gerbig, C., Chen, H., Franke, H., Klaus, C., and Jordan, A.: The IAGOS-core greenhouse gas package: a measurement system for continuous airborne observations of CO_2, CH_4, H_2O and CO, Tellus B, 67,27989, doi:10.3402/tellusb.v67.27989, 2015.

Filges, A., Gerbig, C., Rella, C. W., Hoffnagle, J., Smit, H., Krämer, M., Spelten, N., Rolf, C., Bozóki, Z., Buchholz, B., and Ebert, V.: Evaluation of the IAGOS-Core GHG package H_2O measurements during the DENCHAR airborne inter-comparison campaign in 2011, Atmos. Meas. Tech., 11, 5279-5297, https://doi.org/10.5194/amt-11-5279-2018, 2018.

Petzold A., Thouret, V., Gerbig, C., Zahn, A., Brenninkmeijer, C. A.M., Gallagher, M., Hermann, M., Pontaud, M., Ziereis, H., Boulanger, D., Marshall, J., Nédélec, P., Smit, H. G.J., Friess, U., Flaud, J.-M., Wahner, A., Cammas, J.-P., and Volz-Thomas, A.: Global-scale atmosphere monitoring by in-service aircraft - current achievements and future prospects of the European Research Infrastructure IAGOS, Tellus B, 67, 28452, doi:10.3402/tellusb.v67.28452, 2015.

Quatrevalet, M., Amediek, A., Fix, A., Kiemle, C., Wirth, M., Büdenbender, C., Schweyer, S., Ehret, G., Hoffmann, D., Meissner, A., Löhring, J., and Luttmann, J.: CHARM-F: The Airborne Integral Path Differential Absorption Lidar for Simultaneous Measurements of Atmospheric CO_2 and CH_4, 25th International Laser Radar Conference (ILRC), St. Petersburg, Russia, 05.-09. Juli 2010.

Reum, F., Gerbig, C., Lavric, J. V., Rella, C. W., and Göckede, M.: Correcting atmospheric CO_2 and CH_4 mole fractions obtained with Picarro analyzers for sensitivity of cavity pressure to water vapor, Atmos. Meas. Tech., 12, 1013-1027, https://doi.org/10.5194/amt-12-1013-2019, 2019.

Volz-Thomas, A., Cammas, J.-P., Brenninkmeijer, C. A. M., Machida, T., Cooper, O., Sweeney, C., Waibel, A.: Civil Aviation Monitors Air Quality and Climate, Journal of the Air & Waste Management Association, October 2009, 16-19. 2009.

5 Conclusions and outlook

Reliable measurement systems are the basis for investigating the temporal and spatial atmospheric distribution of important GHGs and for understanding their budgets, trends and their connection to global climate change. This thesis presented the 'IAGOS-core Greenhouse Gas package', an instrument for the measurement of CO_2, CH_4, CO, and water vapour, which was developed for deployment aboard commercial aircraft within the frame of the IAGOS infrastructure. It is based on a commercial CRDS analyser which has been modified to meet the specific requirements regarding physical dimensions, automatic and unattended operation and safety issues on board passenger aircraft. The calibration strategy of the system, which ensures the traceability of the CO_2, CH_4 and CO measurements to WMO primary scales, includes, in addition to calibrations of the instrument in the laboratory during pre- and post-operational maintenance, a two-standard calibration system that allows for in-flight and on ground calibrations during each 6-month deployment period. The water vapour measurements can be used to correct dilution and spectroscopic effects of water vapor on the CO_2, CH_4 and CO measurements to obtain dry air mole fractions. Thus, no sample drying is required, which simplifies maintenance considerably.

Various laboratory tests of the prototype instrument regarding stability, sensitivity to pressure changes, the calibration system and airworthiness were successfully conducted and confirmed the great potential of the device. The measurement repeatability of the 0.4 Hz data was determined as 0.039 ppm for CO_2, 0.4 ppb for CH_4 and 15 ppb for CO. Errors due to deviations in sample cell pressure can be corrected by means of specific correction factors without negatively influencing the data quality.

Five test flights of the instrument in the same setup as for IAGOS, except for a slightly different inlet system, took place on the HALO research aircraft. The instrument showed very good performance and measurement quality over the whole flight campaign. The calibration of the analyser was sufficiently stable over the entire two months, so that the in-flight calibrations did not have to be used for reference. Sample cell pressure stability was given even at heights up to 14 km during periods of stable air pressure, and for ascending rates of 100 hPa/min at 0-3 km altitude to 10 hPa/min at 9-12 km altitude and descending rates of 25 hPa/min at 12 km to around 60 hPa/min at lower altitudes. Larger descending rates than 60 hPa/min did not occur during the five flights and could therefore not be evaluated. Changes in the rate of ascent or descent affect the pressure stability strongly and it takes around 30 seconds for the sample cell pressure to adapt again. Since errors in the measurement due to deviations of the sample cell pressure from its setpoint can be corrected as long as the pressure is stable, and since for IAGOS deployment the highest flight altitudes are about 12.5 km and the aircraft flies at constant altitude or with constant climb and sink rates during most of the flight, it is not expected that sample cell pressure issues will strongly influence the measurements. Upper limits for the 0.4 Hz measurement precision during flight were determined as 0.042 ppm for CO_2 and 0.69 ppb for CH_4. For CO the measurement precision was only 15 ppb, due to a less than optimal setup and alignment of the laser but could be improved to 6 ppb by adjusting the laser parameters after the flight campaign.

The measurement precision can be significantly reduced even further by temporal integration of the data.

An estimate of the overall uncertainty of the measurements (1 σ), mainly based on laboratory tests and accounting for uncertainties of the calibration and wet to dry correction and the measurement repeatability, resulted in <0.13 ppm for CO_2, <1.3 ppb for CH_4 and <4 ppb for CO. A less conservative assumption of instrument drift, as suggested by the flight test, reduces the overall uncertainties to <0.10 ppm for CO_2, <1.3 ppb for CH_4 and <3.4 ppb for CO.

Test flights of the instrument on a Learjet during the DENCHAR inter-comparison campaign allowed for an initial validation of the water vapour measurements. Three different calibration methods for the water vapour measurements were tested. Besides the standard comparisons against a dew point mirror and a frost point hygrometer, this was also a newly developed, independent calibration based on the measurement of the dilution effect of water vapour on the CO2 mole fraction. It could be shown that the new method is statistically consistent with the classical calibrations, which allows the method to be considered as a possible calibration not only for H_2O but also for other gas species. During the four DENCHAR flights the CRDS analyser showed a good time response (10 % to 90 % rise and 90 % to 10 % fall times: 6-7 s, recovery time to 99 % of the final water vapour level: 25 s) and long-term stability for the water vapour measurements. An upper limit of the precision (1 σ) was determined as 4 ppm for H_2O <10 ppm, 20 % or 10 ppm (whichever is smaller) for 10 ppm < H_2O < 100 ppm, and 5 % or 30 ppm (whichever is smaller) for water vapour >100 ppm. These results were later by and large confirmed by the experiences of the HALO flight campaign. Only for water vapour between 10 and 20 ppm the upper limit was higher at around 30 %. Accuracy (1 σ) of the analyser was estimated, based on the laboratory calibrations, as 1 % for the water vapour range from 25 000 ppm down to 7000 ppm, then increasing to 5 % at 50 ppm water vapour. Accuracy at water vapour mole fractions below 50 ppm was difficult to assess, as the reference system FISH suffered from lack of data availability during the DENCHAR flights, the response of the reference CR-2 was very slow, a lot of data were affected by clouds, and agreement between the reference instruments FISH and CR-2 was partly poor.

After the positive test and qualification phase the first IAGOS-core GHG package was deployed aboard a passenger aircraft as part of the IAGOS project in 2017. Five more systems are currently assembled and prepared for integration in the next years increasing the fleet to five operationally deployed GHG systems plus a spare instrument. Thus, data from more than 600 flights per year and instrument, and specifically over 6000 vertical profiles per year, will be available. These will help to further evaluate the performance of the instrument and review the uncertainty budgets of the CO_2, CH_4, CO, and water vapour measurements determined in the test phase and update them if necessary. The systems will provide regular and long-term in situ data of the most important GHGs covering major parts of the globe, including unique measurements from the climate sensitive UTLS region, which cannot be sufficiently resolved by satellites. Besides distribution and trend analyses and the use of the data for inverse modelling of GHG fluxes between the surface and the atmosphere, especially the vertical profile measurements are crucial for the validation of remote sensing observations from satellites and from ground. They will help

to trace the remote sensing data back to the same calibration scales as the in situ measurements, generating homogeneous data as input for atmospheric inversions, and thus reduce uncertainties in the estimates of carbon sources and sinks. Furthermore, the data are essential for improving the understanding and quantification of atmospheric transport and chemistry processes, such as stratosphere-troposphere exchange and convection and will thereby help to assess and enhance the predictive capabilities of regional and global climate models. The provision of near real time data through the WMO Information System (WIS) makes the measurements even usable for the evaluation of weather forecast models and the Copernicus Atmospheric Monitoring Services (CAMS).

Acknowledgements

First and foremost, I would like to express my sincere thanks to my supervisors Prof. Wolfgang Weigand and Christoph Gerbig for their guidance, encouragement and patience during my long Ph.D. project. I thank Prof. Weigand for his cooperation, his help with organisational issues, his interest in my work, valuable suggestions and his kindness. I am truly grateful for Christoph's support and advice. His extensive knowledge and experience, his inspiring ideas, enthusiasm and helpful feedback have always been encouraging, especially when we had to face the many difficulties of our project and nothing went according to plan.

My very special thanks go to Reimo Leppert and Stefan Baum for their technical support during the development and tests of the IAGOS instrument. I have benefited a lot from their experience and appreciate all the time and effort they put into the device. I also thank Armin Jordan and the MPI-BGC GasLab team, the workshops and the entire Freiland-Group.

I am indebted to all my colleagues from the BGC-systems department for their support and many fruitful discussions, for everything I learned from them about atmospheric science and the carbon cycle and for providing me the overall picture of my work. I am very thankful to Huilin Chen and Jan Winderlich for helping me getting started with my project and sharing their experiences. I am grateful for the warm and friendly atmosphere in our department through all the years and the wonderful and unforgettable time with so many great people, especially Ulli, Julia, Christian and Thomas, and my fellow Ph.D. students Sung-Bin, Shreeya, Min Jung, Roberto, Veronika, Dhanya, Sabrina, Friedemann, Martina, Johannes, Martin, Ina, Fanny, Gionata, Fabio, Panos and Tonatiuh.

I wish to thank the whole IAGOS team for their support and the nice, productive and motivating meetings. My special thanks are due to Christoph, Harald and the rest of the enviscope team, as well as to our colleagues from Jülich for all their help and assistance.

I am particularly grateful to Chris Rella, John Hoffnagel and the service team from Picarro Inc. for their great cooperation and constant support.

I gratefully acknowledge the financial support that made my Ph.D. work possible. This work was funded by the European Commission [FP6 project IAGOS-DS (contract number 011902-DS), FP7 project IAGOS-ERI (Grant Agreement No. 212128), FP7 project IGAS (grant agreement no. 312311), FP7 project EUFAR], the Bundesministerium für Bildung und Forschung (IAGOS Deutschland), and the German Max Planck Society.

Last but not least, I want to thank my family and friends for all their support, motivation and encouragement, which never let me give up.

Selbständigkeitserklärung

Ich erkläre, dass ich die vorliegende Arbeit selbständig und unter Verwendung der angegebenen Hilfsmittel, persönlichen Mitteilungen und Quellen angefertigt habe.

Ort, Datum Unterschrift der Verfasserin